

A Delocalized Cobaltviologen with Seven Reversibly Accessible Redox States and Highly Tunable Electrochromic Behaviour

Iram F. Mansoor, Derek I. Wozniak, Yilei Wu, Mark C. Lipke*

*Department of Chemistry and Chemical Biology, Rutgers The State University of New Jersey
123 Bevier Road, Piscataway NJ 08854*

Email: ml1353@chem.rutgers.edu

Supporting Information

Table of Contents:

1. General Considerations.....	S2
2. Synthetic Details.....	S3
3. Electrochemical Experiments.....	S5
4. ^1H NMR Characterization and Evans Method Magnetic Moment Measurements.....	S10
5. UV-vis-NIR Spectroscopy and Spectroelectrochemistry.....	S14
6. Establishing the composition of $\mathbf{1}^0$	S20
7. Single-Crystal X-ray Diffraction Analysis.....	S21
8. DFT Calculations.....	S69
9. References.....	S75

1. General Considerations

Sources: Unless otherwise specified, commercially available chemicals and solvents were used as received from (1) Fisher: acetonitrile, chloroform, methanol, and toluene; (2) Acros Organics: tetrabutylammonium hexafluorophosphate, tetrabutylammonium chloride, cobalt(II) chloride hexahydrate, nickel(II) chloride hexahydrate, zinc acetate dihydrate; (3) Alfa-Aesar: ferrocene (Fc), iodomethane; (4) Cambridge Isotopes: acetonitrile-d₃ (D-99.8%) and benzene-d₆ (D-99.5%); (5) Decon Labs Inc.: 200 proof absolute ethanol; (6) Sigma Aldrich: cobaltocene (Cp₂Co) and decamethylcobaltocene (Cp*₂Co). The 4'-(4-pyridyl)-2,2';6',2''-terpyridine ligand precursor was prepared by a literature procedure; The 4'-(N-methyl-4-pyridinio)-2,2';6',2''-terpyridine ligand (MePyTpy) was prepared as its iodide salt by a reported procedure,^{1,2} and then converted to its chloride salt as described below. [(MePyTpy)₂Co^{II}]•4PF₆ (**1**⁴⁺•4PF₆) was prepared by adapting reported procedures,^{3,4} and the complexes [(MePyTpy)₂Zn^{II}]•4PF₆ (**2**•4PF₆) and [(MePyTpy)₂Ni^{II}]•4PF₆ (**3**•4PF₆) were prepared similarly. New and adapted procedures are described below.

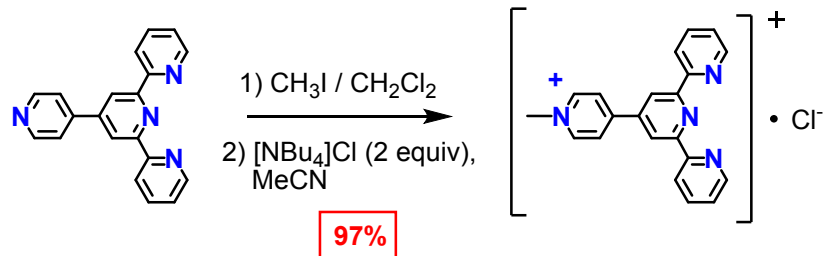
Purification: Dry solvents were obtained by sparging HPLC grade solvents with argon for 1 hour followed by percolation through solvent drying columns supplied by Pure Process Technologies. For electrochemical experiments, acetonitrile was further dried over 3 Å molecular sieves, degassed by three freeze-pump-thaw cycles, distilled via vacuum transfer, and stored under N₂ in flasks sealed with threaded PTFE stoppers. For air-sensitive NMR measurements, NMR solvents were dried over a suitable drying agent (CaH₂ for CD₃CN; NaK alloy for C₆D₆), subjected to three freeze-pump-thaw cycles, distilled by vacuum transfer, and then stored in an N₂ atmosphere glovebox prior to use. Ferrocene was sublimated under static vacuum prior to use. Cobaltocene (Cp₂Co) and decamethyl-cobaltocene (Cp*₂Co) were sublimated under dynamic vacuum and stored at -25 °C in an N₂ atmosphere glovebox prior to use. Tetrabutylammonium hexafluorophosphate (TBAPF₆) was recrystallized three times from absolute ethanol, dried at 125 °C under dynamic vacuum for ≥ 12 hours, and stored in an N₂ atmosphere glovebox prior to use

Air-Sensitive Procedures: All air-sensitive states of the metal complexes were handled in an N₂ atmosphere glovebox (Inert Atmospheres) and spectra were acquired on samples that were sealed under N₂ in NMR tubes or cuvettes using PTFE stoppers.

Physical Measurements: NMR spectra were recorded at 25 °C using a Bruker AVANCE Neo 500 MHz spectrometer or a Varian VNMRS 500 MHz spectrometer. ¹H NMR spectra were referenced to the residual proteo signal of the solvent. Single-crystal X-ray diffraction data was collected on a Bruker diffractometer equipped with a Smart APEX CCD area detector. A CH Instruments 600E potentiostat was used for all electrochemical experiments. UV-vis-NIR spectra were recorded using a Shimadzu UV-2600i spectrophotometer equipped with an ISR-2600Plus integrating sphere detector that provides a 220 – 1400 nm wavelength range for solution absorbance measurements. For wavelengths >1400 nm, a Bruker Vertex 80/80v FTIR spectrometer was utilized, with an effective range of 1250 – 4000 nm. Data from both instruments was combined to provide continuous spectra ranging from 300 – 2500 nm. Additional details of physical measurements are provided in their respective sections below.

2. Synthetic Details

Synthesis of [MePyTpy]Cl.

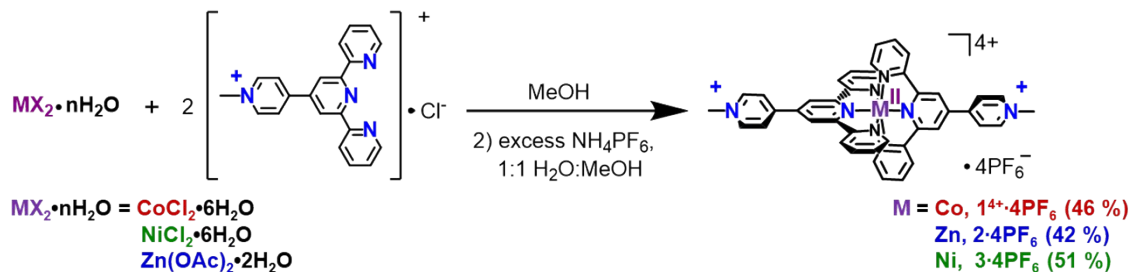


Following a reported procedure,² 4'-(4-pyridyl)-2,2';6',2''-terpyridine (3.605 g, 0.01 mmol) was dissolved in 100 mL of dry dichloromethane under nitrogen and an excess of methyl iodide (7 mL, 0.11 mmol) was added via syringe. The solution was stirred under N₂ for 7 days, during which a yellow precipitate formed. The precipitate was collected by vacuum filtration, washed with dichloromethane, and dried in air to provide the iodide salt of [MePyTpy]⁺ as a fine yellow powder (5.134 g, 98 %).

The iodide salt was poorly soluble in most solvents, hindering reported procedures³ for salt metathesis to the PF₆⁻ salt. However, we found suspensions of the iodide salt converted readily to suspensions of the chloride salt upon stirring or sonication with an excess (ca. 3 equiv) of tetrabutylammonium chloride in acetonitrile. Thus, [MePyTpy]I (5.134 g, 10 mmol) was suspended in 150 mL of acetonitrile and tetrabutylammonium chloride (9.4 g, 34 mmol) was added. Sonication for < 1 min resulted in disappearance of the yellow iodide salt and precipitation of the voluminous white chloride salt. The precipitate was collected by vacuum filtration, washed with acetonitrile and dichloromethane, followed by drying in air to give 4.063 g of [MePyTpy]Cl as an off-white solid (99 % yield). ¹H NMR (500 MHz, D₂O) δ 8.64 (d, J = 6.5 Hz, 2H), 8.26 (d, J = 4.5 Hz, 2H), 7.99 (d, J = 8 Hz, 2H), 7.96 (d, J = 6 Hz, 2H), 7.90 (s, 2H), 7.74 (t, J = 7.5 Hz, 2H), 7.33 (t, J = 10 Hz, 2H), 4.33 (s, 3H).

The combined yield for the two steps was 97 %.

Synthesis of Complexes **1**⁴⁺ · 4PF₆, **2** · 4PF₆, and **3** · 4PF₆.



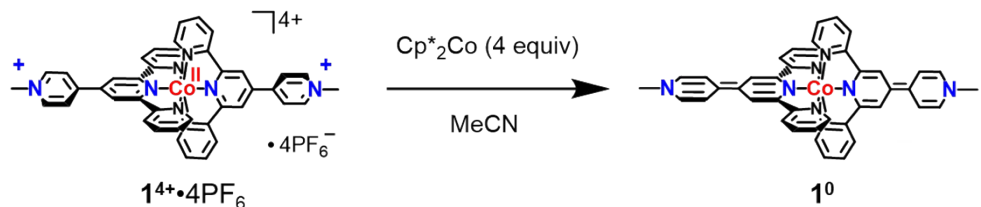
1⁴⁺·4PF₆. [MePyTpy]Cl (1.009 g, 2.8 mmol) was combined with cobalt(II)chloride hexahydrate (0.349 g, 1.4 mmol) in 50 mL of methanol, providing a dark red solution. After stirring for approximately 10 minutes, the solution was combined with a solution of ammonium hexafluorophosphate (1.5 g, 9.2 mmol) in 12 mL of a 1:1 mixture of H₂O:MeOH, resulting in the formation of a red precipitate. The resulting solid was

collected by vacuum filtration and washed with water before drying in air to give **1⁴⁺**·4PF₆ as a red-orange powder (1.663 g, 46 % yield). The ¹H NMR spectrum of the product in CD₃CN matched the reported spectrum,⁴ and we obtained elemental analysis data, which has not previously been reported, to confirm the purity of this complex when prepared by the method described. ¹H NMR (500 MHz, CD₃CN) δ 89.51 (s, 4H), 50.83 (s, 4H), 33.91 (s, 4H), 32.68 (s, 4H), 12.62 (s, 4H), 9.99 (s, 4H), 9.68 (s, 4H), 4.07 (s, 6H). Anal. Calcd for C₄₂H₃₄N₈F₂₄P₄Co (1289.58): C, 39.12; H, 2.66; N, 8.69. Found: C, 38.83; H, 2.48; N, 8.69.

2·4PF₆. This zinc complex was prepared as described for the cobalt analogue and isolated as a white powder (51 % yield). ¹H NMR (500 MHz, CD₃CN) δ 9.06 (s, 4H), 8.96 (d, J= 6.5 Hz, 4H), 8.70 (d, J= 8.5 Hz, 4H), 8.66 (d, J= 6.5 Hz, 4H), 8.19 (dt, J= 1.5, 8 Hz, 4H), 7.86 (d, J= 5 Hz, 4H), 7.43 (m, 4H), 4.47 (s, 6H). Anal. Calcd for C₄₂H₃₄N₈F₂₄P₄Zn (1296.03): C, 38.92; H, 2.64; N, 8.65. Found: C, 38.53; H, 2.58; N, 8.58.

3⁴⁺·4PF₆. This nickel complex was prepared as described for the cobalt analogue and isolated as a tan powder (0.74g, 42 %). ¹H NMR (500 MHz, CD₃CN) δ 131.40 (br), 74.58 (s, 4H), 65.15, (s, 4H), 43.71 (s, 4H), 13.58 (s, 4H), 11.23 (s, 4H), 8.64 (s, 4H), 3.37 (s, 6H).

Synthesis of Complex **1⁰**.



A dark red solution of **1⁴⁺**·4PF₆ (85.0 mg, 0.0659 mmol) in 5 mL of MeCN was added to a suspension of decamethylcobaltocene (86.4 mg, 0.262 mmol) in 1 mL of MeCN, immediately giving a dark blue solution. This mixture was stirred for 20 h, during which the solution took on a dark blackish green color and a fine bluish black precipitate formed. The precipitate was collected on a filter and washed with 15 mL of MeCN, before drying under vacuum to provide **1⁰** as a dark bluish black powder (35.9 mg, 77 % yield). Samples prepared in this manner showed consistent ¹H NMR spectra in which all eight expected resonances could be observed clearly, but satisfactory elemental analysis could not be obtained, which we attribute to the extreme air-sensitivity of **1⁰**. Additional experiments were performed to confirm that **1⁰** is a homoleptic complex of the composition L₂Co. These experiments are described below in Section 6. ¹H NMR (500 MHz, C₆D₆) δ 89.52 (s, 4 H), 78.75 (s, 4 H), 69.72 (s, 4 H), 48.38 (s, 6 H, NCH₃), 38.17 (s, 4 H), 30.18 (s, 4 H), 7.75 (s, 4 H), -24.85 (s, 4 H). Anal. Calcd for C₄₂H₃₄N₈Co (709.72): C, 71.08; H, 4.83; N, 15.79. Found: C, 68.99; H, 4.73; N, 15.90.

3. Electrochemical Experiments

All electrochemical experiments were performed with a CH Instruments 600E potentiostat and 1 mM solutions of analyte in (1) dry MeCN with 0.1 M tetrabutylammonium hexafluorophosphate (TBAPF₆) as the supporting electrolyte, or (2) a pH 7 NaH₂PO₄/Na₂HPO₄ buffer (0.1 M) in water. Cyclic voltammetry was conducted using a 3 mm glassy carbon working electrode, a platinum wire counter electrode, and a silver wire pseudo-reference electrode which was confined in a polypropylene body that provided contact with the analyte solution via a porous zeolite bead or a glass frit. Potentials were referenced to the Fc^{+/-} couple of an internal ferrocene standard or by calibrating the pseudo-reference electrode vs. the Fc^{+/-} couple of an external solution of ferrocene immediately before use. Positive feedback iR compensation was applied during all CV experiments. The 2nd cycle out of three is presented unless otherwise noted. Bulk electrolysis was performed with a platinum mesh working electrode and a platinum wire counter electrode that was confined in a PTFE body that provided contact with the analyte solution via a porous glass frit. A silver wire pseudo-reference electrode was utilized as described for cyclic voltammetry experiments.

The heterogeneous electron transfer rate constants (k°) of the $\mathbf{1}^{n+/(n-1)+}$ ($n = 1 - 4$) redox couples were determined by the Nicholson method as revised by Leddy.^{5,6} Rigorous exclusion of air was required to prevent sample degradation over numerous successive experiments, and the high N₂ flow needed to rigorously exclude air resulted in cooling of the solution by evaporation of MeCN from the sample despite use of a pre-bubbler of MeCN. A temperature of (283 K) was estimated from the minimum peak separation (54 mV) observed for the $\mathbf{1}^{3+/2+}$ redox based on the relationship $\Delta E_p = 2.22RT/F$. The diffusion coefficient of $\mathbf{1}^{n+}$ ($D = [9.45 +/- 0.18] \times 10^{-6} \text{ cm}^2 \cdot \text{s}^{-1}$) was estimated from the Randles-Sevcik equation based on i_p of the $\mathbf{1}^{4+/3+}$ reduction, taking the average of values at scan rates of 1, 2, 4, 6, 8, and 10 V·s⁻¹, which were all in close agreement. Nicholson's equation (Eq. S1) relating the dimensionless electrochemical parameter (ψ) to the heterogeneous electron transfer rate constant (k°) was combined with Leddy's equation (Eq. S2) relating ψ to ΔE_p to provide Eq. S3, which was used to determine k° values based on the slopes obtained from linear fitting of experimental ΔE_p values vs. $v^{1/2}$ in the range of scan rates over which quasireversible behavior is observed (10 – 400 V·s⁻¹, see Figures S1 – 3 below). The values of k° reported in the main text are the average of values determined from two data sets.

Eq. S1.

$$\psi = \frac{k^\circ \left(\frac{D_A}{D_B} \right)^{\alpha}}{\sqrt{\frac{F}{RT} \cdot \pi v D_A}}$$

Eq. S2.

$$\Delta E_p \cdot \left(\frac{nF}{RT} \right) = \frac{M_1}{\psi} + B_1$$

ψ = Dimensionless electrochemical parameter

k° = heterogeneous electron transfer rate constant

D_A = diffusion coefficient for $\mathbf{1}^{n+}$

D_B = diffusion coefficient for $\mathbf{1}^{(n-1)+}$, assumed to equal D_A

α = electron transfer coefficient, assumed here to be 0.5

v = scan rate in V·s⁻¹

M_1 and B_1 are values provided by Leddy for specific values of α .

For an assumed α of 0.5, $M_1 = 0.8248$ and $B_1 = 2.3243$

$$\Delta E_p = \frac{M_1 \sqrt{\nu}}{k^\circ} \cdot \sqrt{\frac{RT\pi D_A}{F}} + B_1 \left(\frac{RT}{F} \right)$$

Eq. S3.

Complex $\mathbf{1}^{4+} \cdot 4\text{PF}_6^-$.

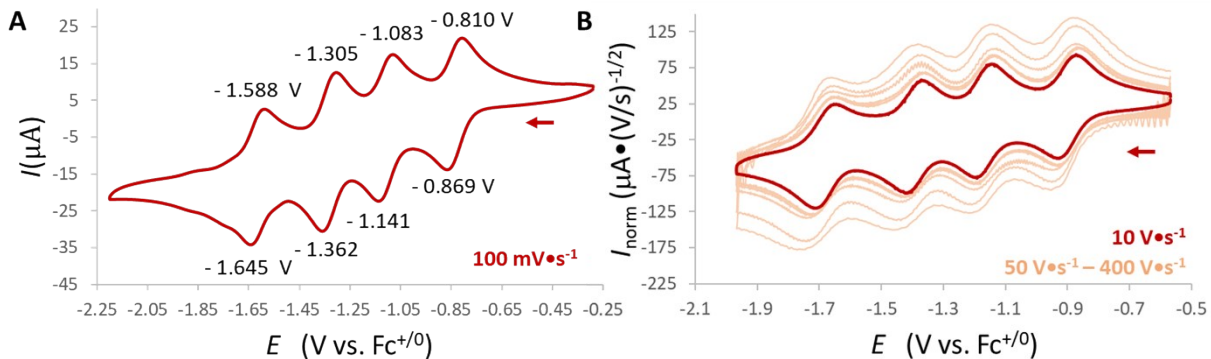


Figure S1: Cyclic voltammograms (CVs) measured from -0.57 V to -1.97 V on a 1.0 mM solution of $\mathbf{1}^{4+} \cdot 4\text{PF}_6^-$ in MeCN containing 0.1 M TBAPF₆ as a supporting electrolyte. (A) CV recorded at a scan rate of 100 mV·s $^{-1}$; (B) CVs recorded at scan rates of 10 V·s $^{-1}$, 50 V·s $^{-1}$, 60 V·s $^{-1}$, 100 V·s $^{-1}$, 200 V·s $^{-1}$, and 400 V·s $^{-1}$, with the current scaled by the square root of the scan rate.

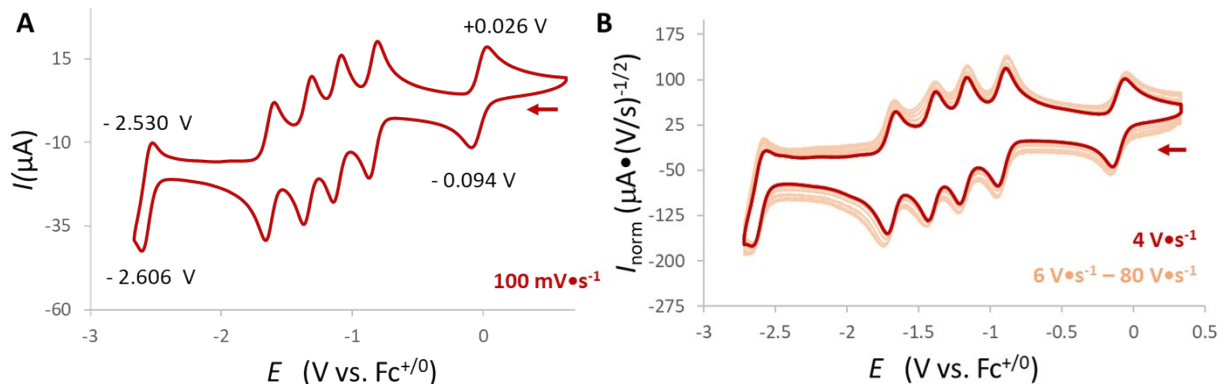


Figure S2: Cyclic voltammograms (CVs) of a 1.0 mM solution of $\mathbf{1}^{4+} \cdot 4\text{PF}_6^-$ in MeCN containing 0.1 M TBAPF₆ as a supporting electrolyte. (A) Measured over a potential window of $+0.64$ V to -2.66 V at a scan rate of 100 mV·s $^{-1}$; (B) Measured over a potential window of $+0.33$ V to -2.72 V at

scan rates of $4 \text{ V}\cdot\text{s}^{-1}$, $6 \text{ V}\cdot\text{s}^{-1}$, $10 \text{ V}\cdot\text{s}^{-1}$, $20 \text{ V}\cdot\text{s}^{-1}$, $40 \text{ V}\cdot\text{s}^{-1}$, $60 \text{ V}\cdot\text{s}^{-1}$, and $80 \text{ V}\cdot\text{s}^{-1}$, with the current scaled by the square root of the scan rate.

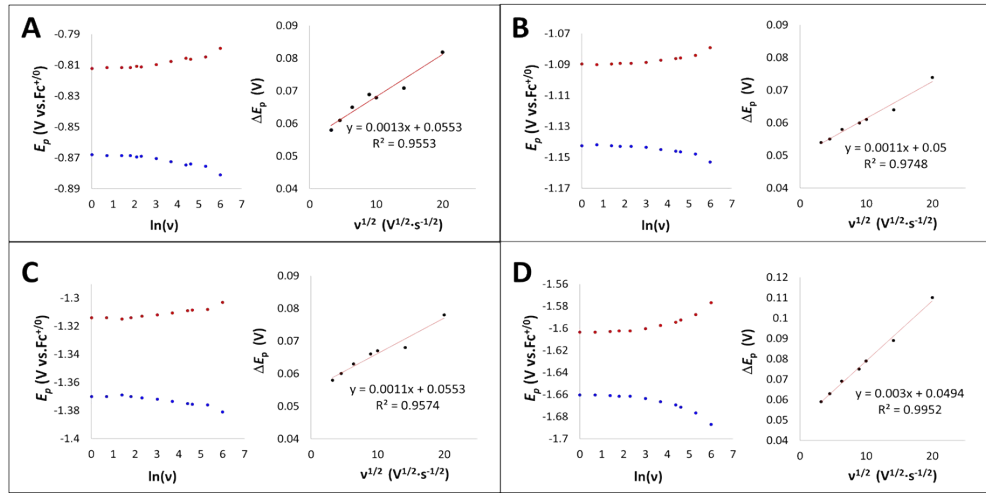


Figure S3. Plots of peak potentials E_{pc} & E_{pa} vs. $\ln(v)$ and plots of ΔE_p vs. $v^{1/2}$ for the redox couples (A) $\mathbf{1}^{4+}/\mathbf{3+}$; (B) $\mathbf{1}^{3+}/\mathbf{2+}$; (C) $\mathbf{1}^{2+}/\mathbf{+}$; and (D) $\mathbf{1}^{+}/\mathbf{0}$ measured over the scan rates $10 - 400 \text{ V}\cdot\text{s}^{-1}$. To clearly depict the increase in peak separations at increasing scan rates, the plots of E_{pc} & E_{pa} vs. $\ln(v)$ were constructed with data that was referenced to maintain $E_{1/2}$ values constant at the potentials determined in CVs immediately after calibrating the pseudo-reference electrode. As described above, slopes of ΔE_p vs. $v^{1/2}$ were used to determine k° values utilizing equation S3.

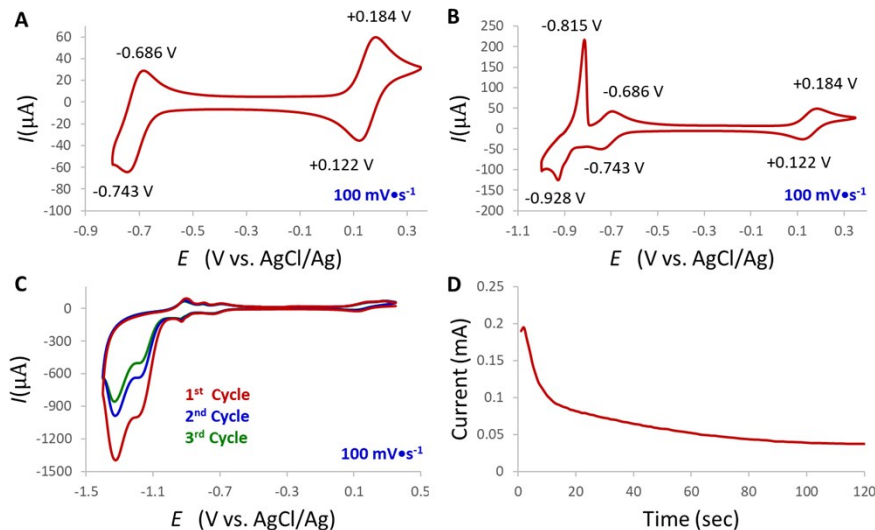


Figure S4. (A) Cyclic voltammogram (CV) measured from $+0.35 \text{ V}$ to -0.80 V on a 2.0 mM solution of $\mathbf{1}^{4+}\cdot\mathbf{4Cl}$ in a pH 7.2 $\text{NaH}_2\text{PO}_4/\text{Na}_2\text{HPO}_4$ buffer (0.1 M) in water, recorded at a scan rate of $100 \text{ mV}\cdot\text{s}^{-1}$; (B) CV measured from $+0.35 \text{ V}$ to -1.0 V on a 1.0 mM solution of $\mathbf{1}^{4+}\cdot\mathbf{4Cl}$ in a pH 7.2 $\text{NaH}_2\text{PO}_4/\text{Na}_2\text{HPO}_4$ buffer (0.1 M) in water, recorded at a scan rate of $100 \text{ mV}\cdot\text{s}^{-1}$; (C) CV measured from $+0.35 \text{ V}$ to -1.4 V on a 1.0 mM solution of $\mathbf{1}^{4+}\cdot\mathbf{4Cl}$ in a pH 7.2 $\text{NaH}_2\text{PO}_4/\text{Na}_2\text{HPO}_4$ buffer (0.1 M) in water, recorded at a scan rate of $100 \text{ mV}\cdot\text{s}^{-1}$. The large increase in current with an onset at ca. -1.0 V is attributed to H^+ reduction activity, and

changes of the CVs over multiple cycles suggest $\mathbf{1}^{\text{n}+}$ is unstable under these conditions; (D) Controlled potential electrolysis of a stirred 1.0 mM solution of $\mathbf{1}^{4+}\cdot\text{4Cl}$ in a pH 7.2 $\text{NaH}_2\text{PO}_4/\text{Na}_2\text{HPO}_4$ buffer (0.1 M) in water at -1.15 V. The rapid decrease in current indicates $\mathbf{1}^{\text{n}+}$ is unstable under these conditions.

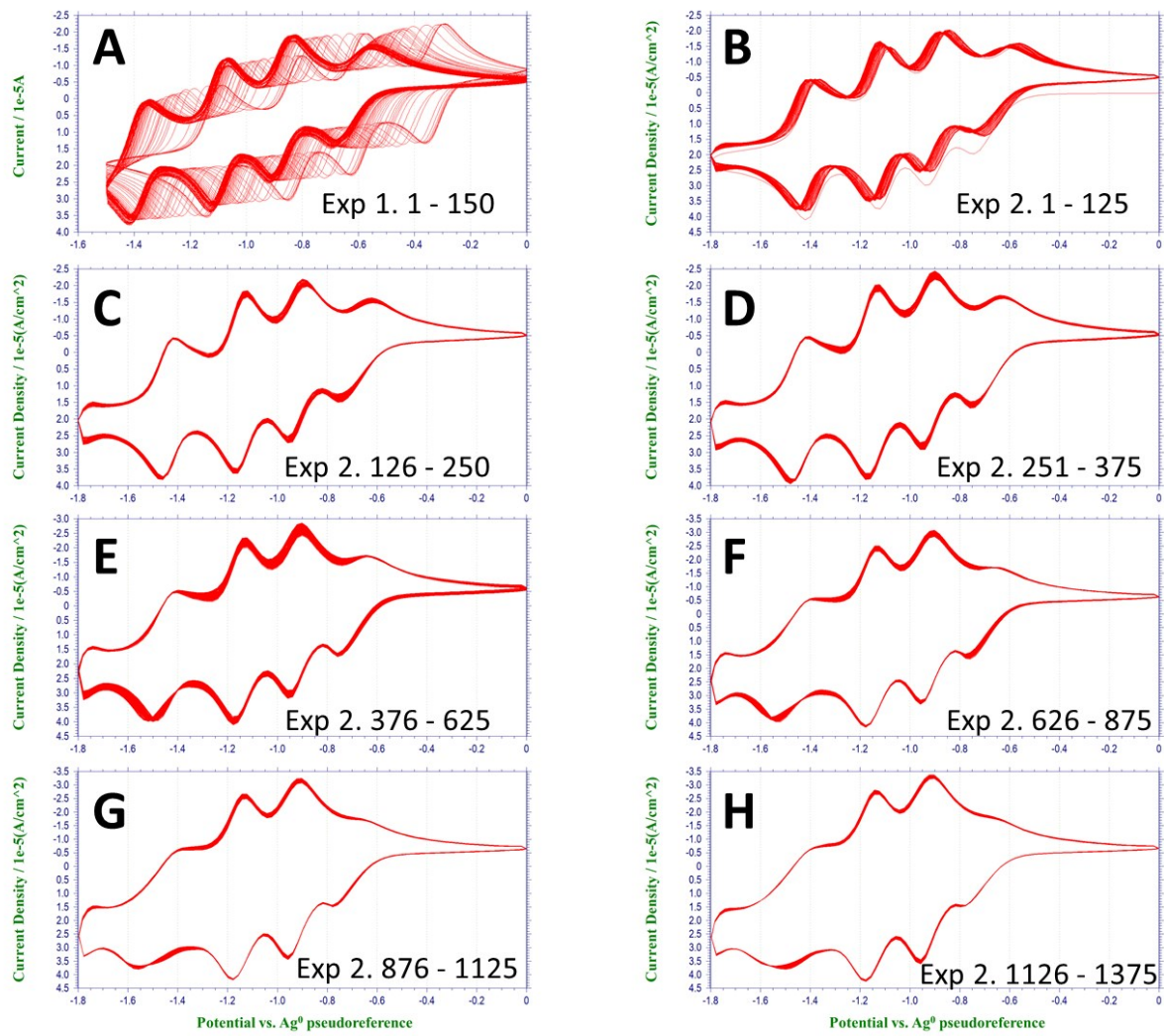


Figure S5. The stability of $\mathbf{1}^{\text{n}+}$ during extended redox cycling was examined by cyclic voltammetry recorded at a scan rate of $0.1 \text{ V}\cdot\text{s}^{-1}$ with a glassy carbon working electrode, a platinum mesh counter electrode, and a silver wire pseudo-reference electrode. The reference electrode was not isolated from the analyte solution and showed considerable drift during initial scans. Potentials are those directly measured against this pseudo-reference electrode. (A) In an initial experiment (Exp 1), 150 cycles were recorded while the potential of the pseudo-reference electrode stabilized. Once stabilized, the pseudo-reference electrode maintained a potential about 200 mV negative of the $\text{Fc}^{+/-}$ redox couple, shifting the measured redox potentials positive by about 200 mV relative to those reported in our other CVs. Aside from the drift of the reference electrode, the only other change to the CVs recorded in this experiment was a broadening of the reoxidation wave of the most positive redox couple, which is attributed to changes to the working electrode surface. (B – H) A second experiment recorded 1375 continuous cycles, finding that the first and fourth redox couples slowly broaden, while the middle two redox couples remain well defined. These

results indicate **1⁴⁺** remains intact, though the electrode becomes fouled somewhat as evident from the quasireversible behavior of two of the redox couples. Some degradation of **1⁴⁺** is indicated by the growth of a small wave near the negative extreme of the CV, as clearly evident in C to H.

Complex **2·4PF₆**.

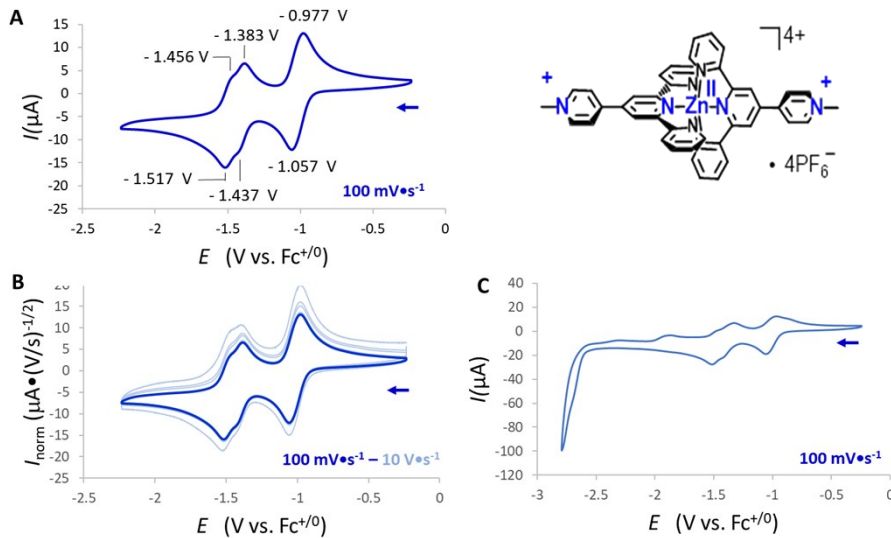


Figure S6: Cyclic voltammograms measured on a 1.0 mM solution of **2·4PF₆** in MeCN containing 0.1 M TBAPF₆ as a supporting electrolyte. (A) Measured over a potential window of -0.23 V to -2.23 V at a scan rate of 100 mV·s⁻¹; (B) Measured over a potential window of -0.23 V to -2.23 V at scan rates of 100 mV·s⁻¹, 200 mV·s⁻¹, 500 mV·s⁻¹, 1 V·s⁻¹, and 10 V·s⁻¹, with the current scaled by the square root of the scan rate. (C) Measured from +0.78 V to -2.72 V at a scan rate of 100 mV·s⁻¹.

Complex **3·4PF₆**.

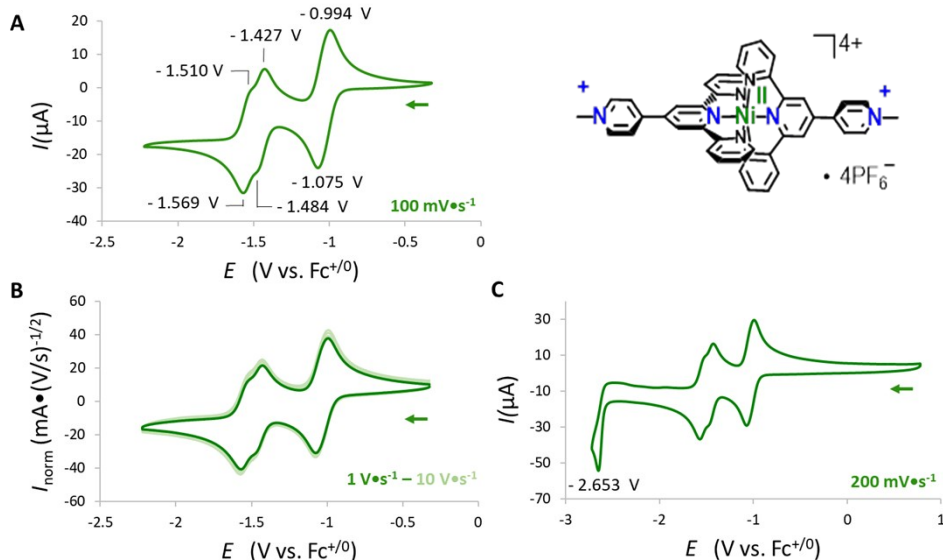


Figure S7: Cyclic voltammograms measured on a 1.0 mM solution of **3·4PF₆** in MeCN containing 0.1 M TBAPF₆ as a supporting electrolyte. (A) Measured over a potential window of -0.32 V to -2.22 V at a scan

rate of $100 \text{ mV}\cdot\text{s}^{-1}$; (B) Measured over a potential window of -0.32 V to -2.22 V at scan rates of $1 \text{ V}\cdot\text{s}^{-1}$, $2 \text{ V}\cdot\text{s}^{-1}$, $5 \text{ V}\cdot\text{s}^{-1}$, and $10 \text{ V}\cdot\text{s}^{-1}$, with the current scaled by the square root of the scan rate. (C) Measured from $+0.78 \text{ V}$ to -2.72 V at a scan rate of $200 \text{ mV}\cdot\text{s}^{-1}$.

4. ^1H NMR Spectroscopy and Evans Method Magnetic Moment

Instrumentation: Nuclear magnetic resonance (NMR) spectra were measured using a Bruker AVANCE Neo spectrometer or a Varian VNMR spectrometer, both with a 500 MHz working frequency for ^1H nuclei. ^1H NMR spectra were referenced to the residual proteo signal of the solvent ($^1\text{H} \delta 1.94 \text{ ppm}$ for CD_2HCN in CD_3CN). Internal ferrocene capillary standards (Fc) were made of 80 mM ferrocene in acetonitrile. ^1H NMR spectra of paramagnetic species were acquired at 64 or 128 scans.

Sample Preparation: Reduced states of the complexes were prepared in an N_2 atmosphere glovebox by *in situ* by addition of 1 – 3 equivalents of Cp_2^*Co to a solution of $\mathbf{1}^{4+}\cdot 4\text{PF}_6^-$ in CD_3CN , or 2 equivalents of Cp_2Co to a solution of $\mathbf{2}\cdot 4\text{PF}_6^-$ or $\mathbf{3}\cdot 4\text{PF}_6^-$ in CD_3CN . The NMR samples were sealed from air using threaded PTFE stoppers on J-Young type NMR tubes. For samples of $\mathbf{1}^{n+}$ ($n = 3, 2, 1$), some resonances were occasionally observed as very broad or flattened completely, which is attributed to electron self-exchange between the desired oxidation state and small amounts of the higher or lower state. Even the use of a semi-micro balance for measuring quantities of $\mathbf{1}^{4+}\cdot 4\text{PF}_6^-$ and Cp_2^*Co was insufficient for consistently obtaining exact stoichiometries. However, very well resolved spectra were consistently obtained by first adding slightly less than 1, 2, or 3 equivalents of Cp_2^*Co to solutions of $\mathbf{1}^{4+}\cdot 4\text{PF}_6^-$, followed by iterative additions of very small quantities (i.e. too small to measure by mass) of Cp_2^*Co with the tip of a fine spatula until well resolved spectra were observed. The sharp signals in these spectra confirm the presence of a single oxidation state of $\mathbf{1}^{n+}$ in these samples.

Evans method: Solution magnetic moment measurements were performed on 20 mM samples of $\mathbf{1}^{4+}$, $\mathbf{1}^{3+}$, and $\mathbf{1}^{2+}$ in CD_3CN , while a 5 mM concentration of $\mathbf{1}^+$ was employed due to its lower solubility in CD_3CN . A 5 mM concentration of ferrocene was included in the analyte solution and a sealed capillary containing ca. $50 \mu\text{L}$ of an 80 mM concentration ferrocene solution in CD_3CN was included as a reference inside the NMR tube. The difference in chemical shift between the ferrocene resonances in the paramagnetic and diamagnetic environment was recorded and used to calculate the magnetic moments of each oxidation state of $\mathbf{1}^{n+}$,⁷ providing values of:

$\mathbf{1}^{4+}$: $3.1 \mu\text{B}$ (note: this results from a mixture of the $S = 1/2$ and $S = 3/2$ states)

$\mathbf{1}^{3+}$: $3.1 \mu\text{B}$ ($S = 1$)

$\mathbf{1}^{2+}$: $3.7 \mu\text{B}$ ($S = 3/2$)

1⁺: 4.8 μB ($S = 2$)

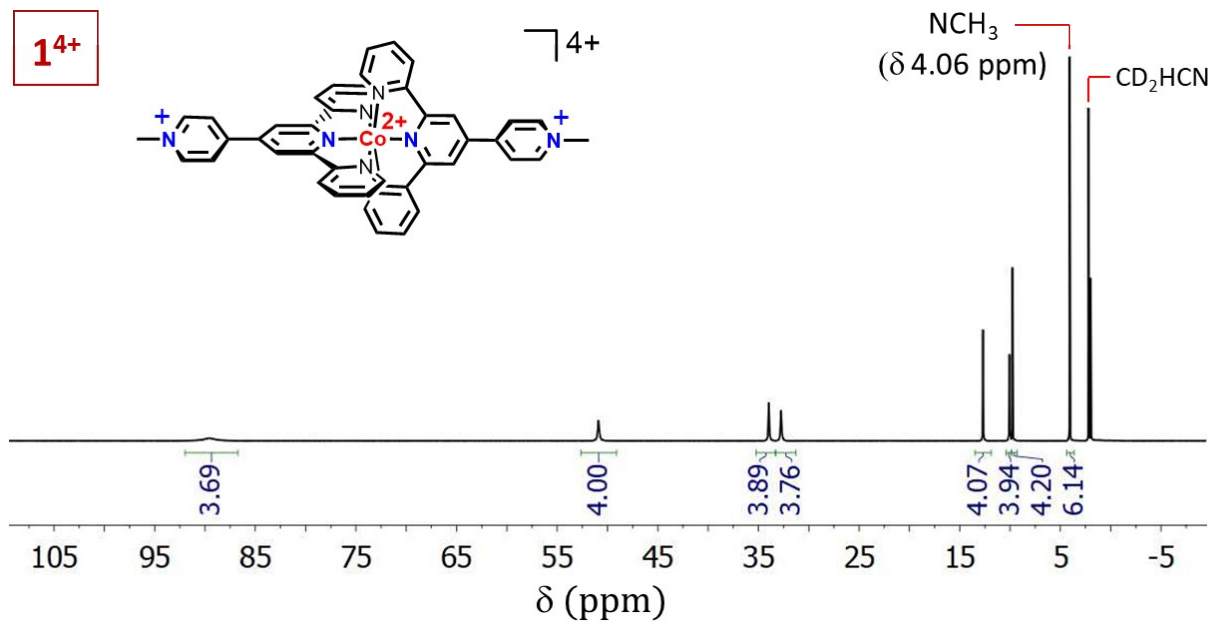


Figure S8. ^1H NMR spectrum (CD₃CN, 500 MHz, 298 K) of **1⁴⁺·4PF₆**.

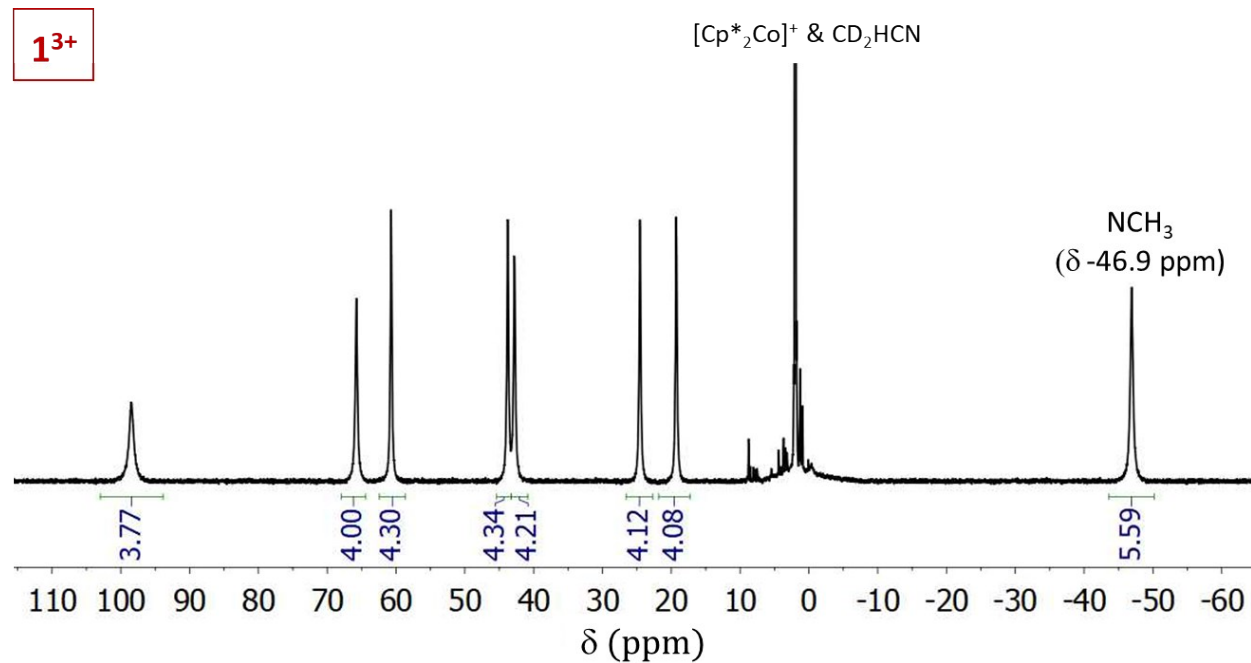


Figure S9. ^1H NMR spectrum (CD_3CN , 500 MHz, 298 K) of $\mathbf{1}^{3+}$ generated in situ from $\mathbf{1}^{4+}\cdot 4\text{PF}_6^-$ and 1 equiv of Cp^*_2Co .

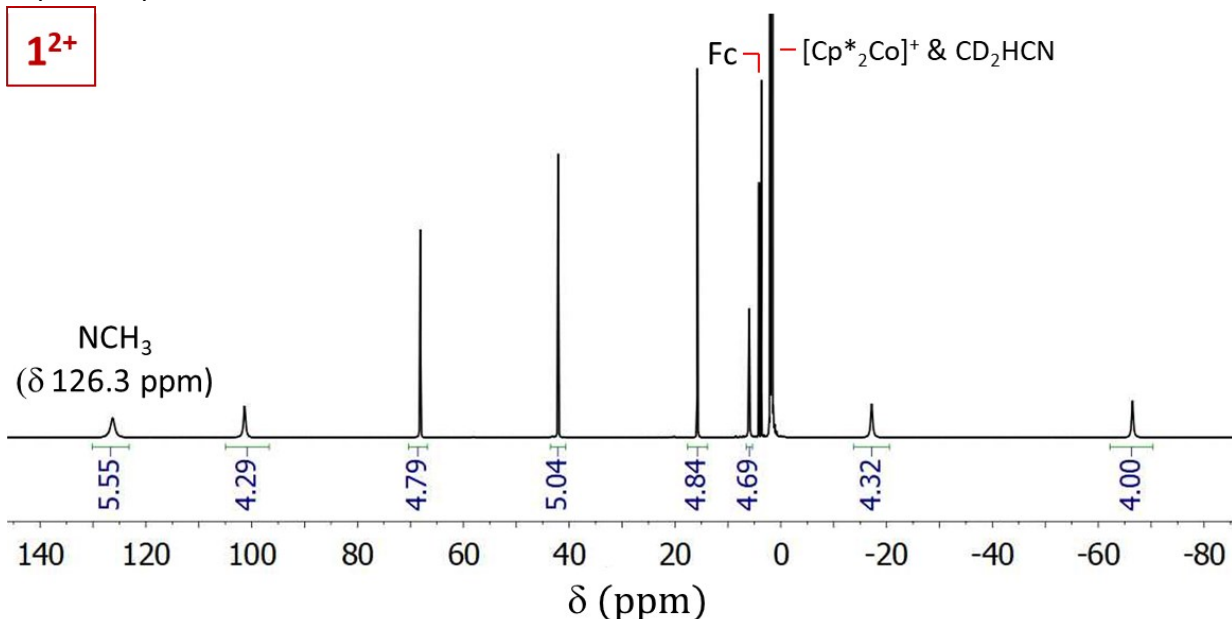


Figure S10. ^1H NMR spectrum (CD_3CN , 500 MHz, 298 K) of $\mathbf{1}^{2+}$ generated in situ from $\mathbf{1}^{4+}\cdot 4\text{PF}_6^-$ and 2 equiv of Cp^*_2Co .

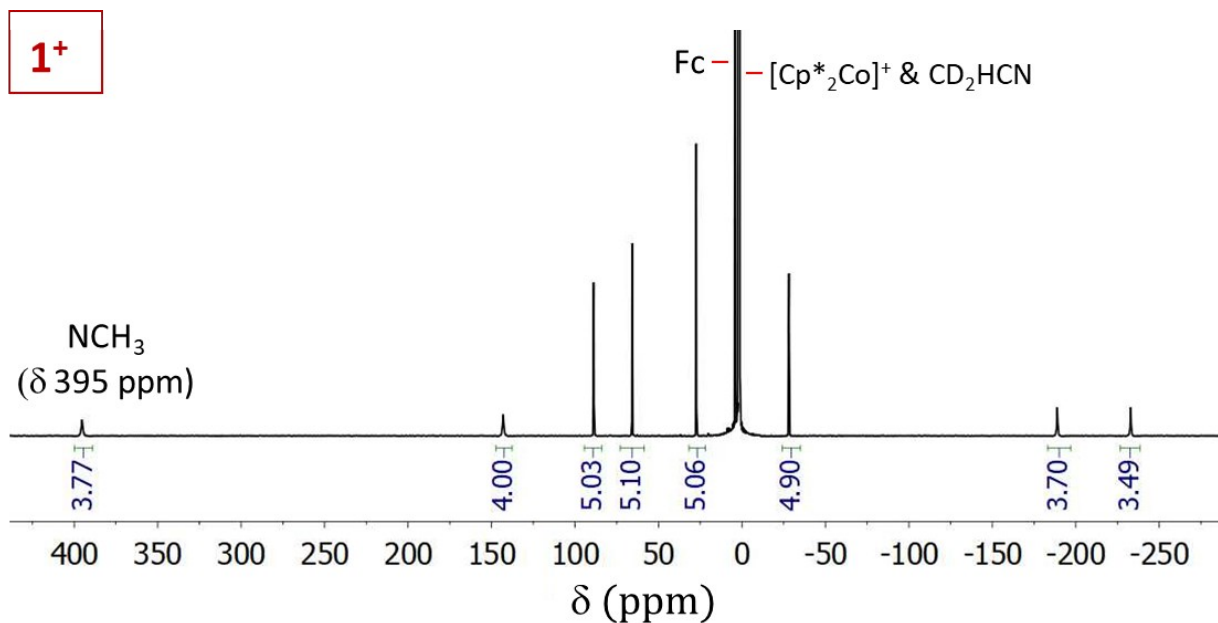


Figure S11. ^1H NMR spectrum (CD_3CN , 500 MHz, 298 K) of $\mathbf{1}^+$ generated in situ from $\mathbf{1}^{4+}\cdot 4\text{PF}_6^-$ and 3 equiv of Cp^*_2Co .

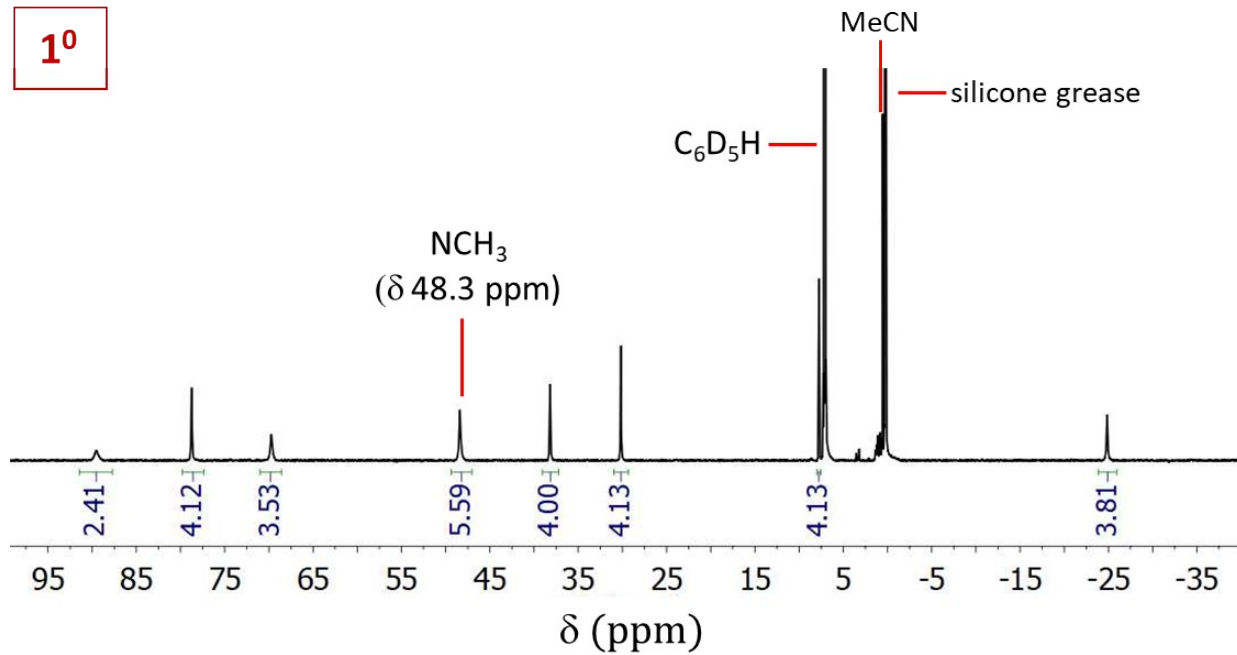


Figure S12. ^1H NMR spectrum (C_6D_6 , 500 MHz, 298 K) of isolated $\mathbf{1}^0$. Note that the silicone grease impurity was present in the NMR solvent from drying and distillation.

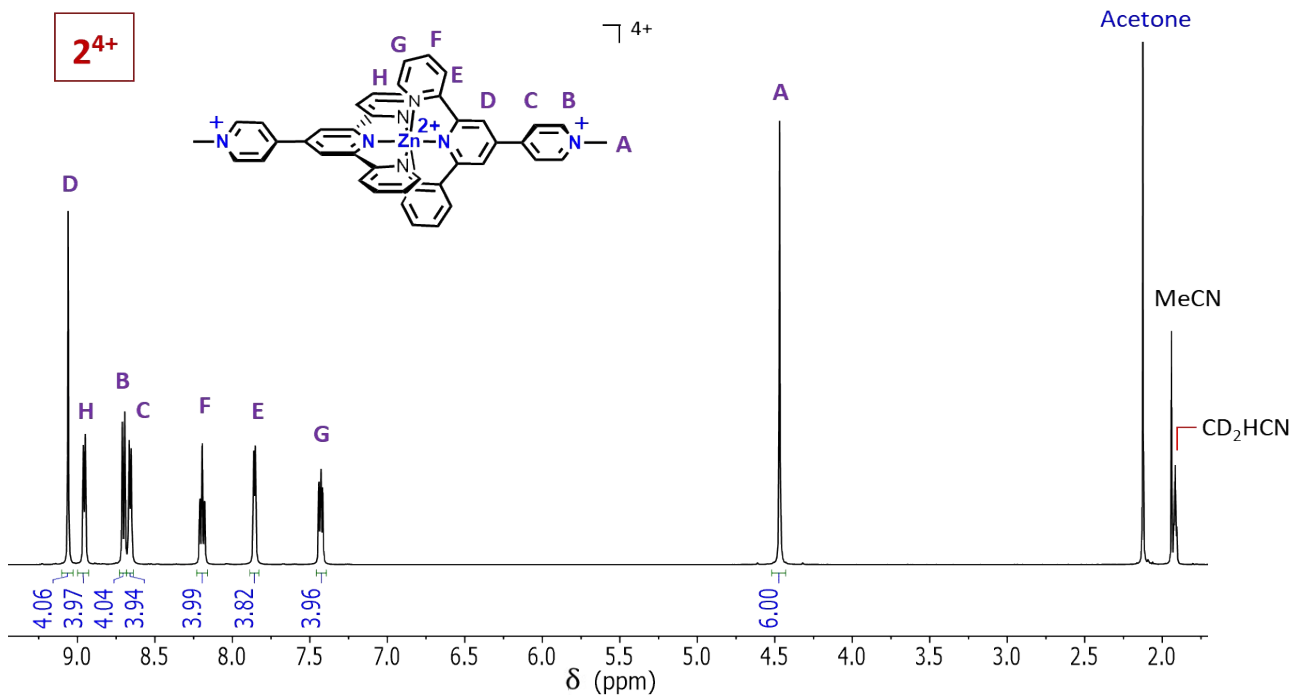


Figure S13. ^1H NMR spectrum (CD_3CN , 500 MHz, 298 K) of **2**· 4PF_6 .

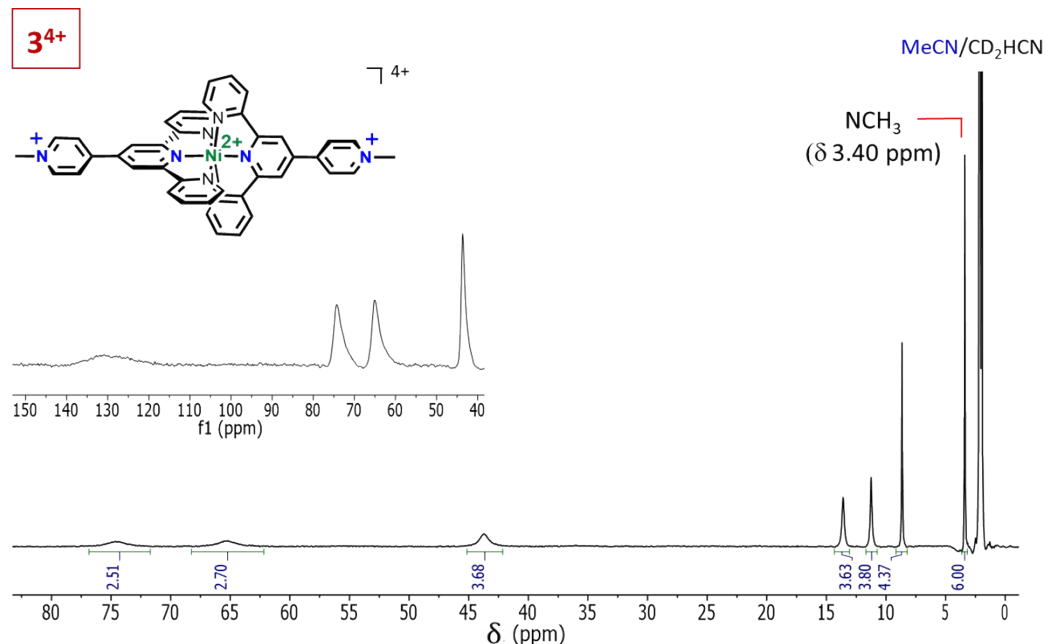


Figure S14. ^1H NMR spectrum (CD_3CN , 500 MHz, 298 K) of **3**· 4PF_6 .

5. UV-vis-NIR Spectroscopy and Spectroelectrochemistry

Sample preparation: All UV-vis-NIR spectra were recorded in 1mm path length quartz cuvettes. Samples of 0.5 mM concentration of **1³⁺**, **1²⁺**, and **1⁺** in MeCN were prepared by three methods (1) Reduction of 0.5 mM solutions of **1⁴⁺·4PF₆** by addition of 1, 2, or 10 equivalents of Cp₂Co (note: excess Cp₂Co is needed to fully access the **1⁺** state since the **1²⁺/1⁺** reduction potential is comparable to that of Cp₂Co^{+/-}); (2) Dilution of NMR samples of **1³⁺**, **1²⁺**, and **1⁺** that were prepared as described above; and (3) Controlled-potential electrochemical reduction of a stirred solution of **1⁴⁺·4PF₆** (0.5 mM in a 0.1 M solution of TBAPF₆ in MeCN) in an N₂ atmosphere glovebox using a platinum mesh working electrode and a platinum-wire counter electrode separated from the bulk sample by a glass frit. Good agreement was seen between all three methods for all oxidation states. Spectra are presented for sample prepared by the third method. Samples of **2²⁺** were prepared by reduction of a 0.5 mM solution of **2·4PF₆** with sequential additions of 4 x 0.5 equivalent additions of Cp₂Co.

Spectroelectrochemistry (SEC): Spectroelectrochemistry experiments were conducted in a 1 mm path length Quartz SEC-C Thin Layer spectroelectrochemistry cell from ALS Co. Ltd. on 0.5 mM solutions of **1⁴⁺·4PF₆**, **2·4PF₆**, or **3·4PF₆** in dry MeCN with 0.1 M tetrabutylammonium hexafluorophosphate (TBAPF₆) as the supporting electrolyte. Samples were electrochemically reduced using a platinum mesh working electrode, a platinum wire counter electrode, and a silver wire pseudo-reference electrode. The counter and reference electrodes were housed in individual PTFE bodies that were separated from the analyte solution using porous glass frits. The pseudo-reference electrode was calibrated prior to use by performing CVs on a solution of ferrocene, and a CV scan of each analyte was taken in the SEC cell to confirm the external calibration of the pseudo-reference electrode prior to applying the appropriate potential to access the desired reduced state of the complexes. For **1ⁿ⁺** (n = 3, 2, 1), **2²⁺**, and **3²⁺**, the reductions were monitored visually, and digital photographs were recorded of each state against a plain white background. A time lapse video (71x playback speed) of the sequential reductions of **1⁴⁺** is presented as additional ESI. The SEC cell was also used to acquire the UV-vis spectrum of **3²⁺**.

Complex **1⁴⁺·4PF₆**

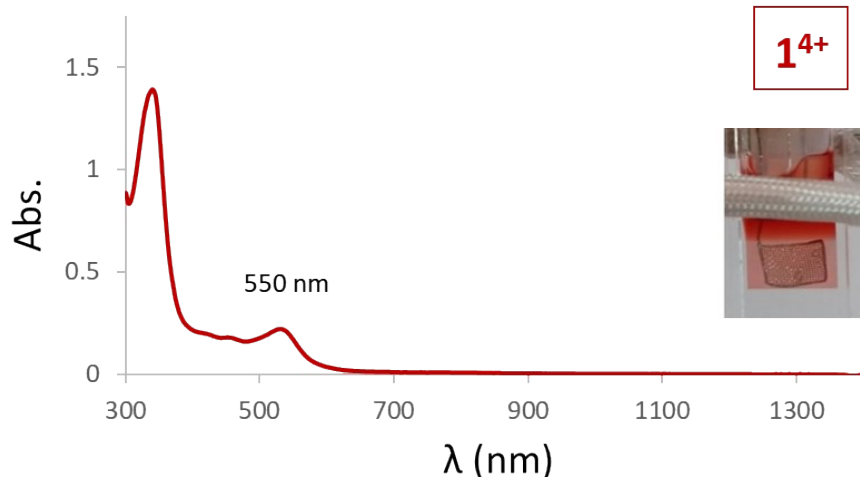


Figure S15. UV-Vis-NIR spectrum (1 mm path) of a 0.5 mM concentration solution of **1⁴⁺** in MeCN containing 0.1 M TBAPF₆. Inset shows a red solution of **1⁴⁺** in an SEC cell with no potential applied.

Complex **1³⁺**

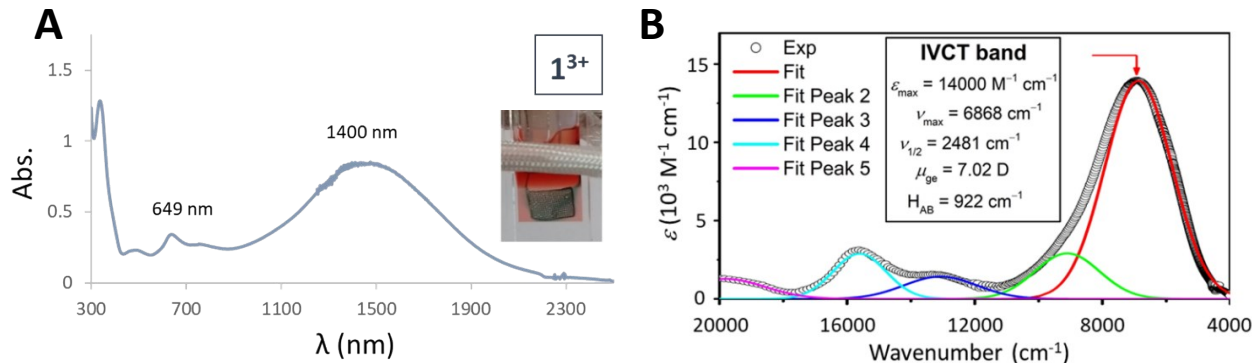


Figure S16. (A) Superimposed UV-vis-NIR (300 nm – 1400 nm) and FTIR (1300 nm – 2500 nm) spectra of a 0.5 mM concentration solution of **1³⁺** in MeCN containing 0.1 M TBAPF₆. The sample of **1³⁺** was prepared from a 0.5 mM solution of **1⁴⁺·4PF₆** by applying a potential of -0.96 V (vs. Fc^{+/-}) for 15 minutes with stirring, followed by transferring the reduced solution to a 1 mm path cuvette. Relative to the spectrum of **1⁴⁺**, the maximum change in the visible region of **1³⁺** corresponds to λ_{maxVis} at 649 nm ($\varepsilon_{649\text{nm}} = 8020 \text{ M}^{-1} \text{ cm}^{-1}$), a wavelength where **1⁴⁺** shows negligible absorptivity. The visible region minimum λ_{minVis} occurs at 544 nm ($\varepsilon_{544\text{nm}} = 4040 \text{ M}^{-1} \text{ cm}^{-1}$). The inset shows the blue-green color of **1³⁺** while applying a potential of -0.96 V at platinum mesh electrode in an SEC cell. (B) Fitting of the vis-NIR portion of the spectrum to Gaussian curves and quantification of electronic delocalization by analysis of the IVCT band.

Complex **1²⁺**

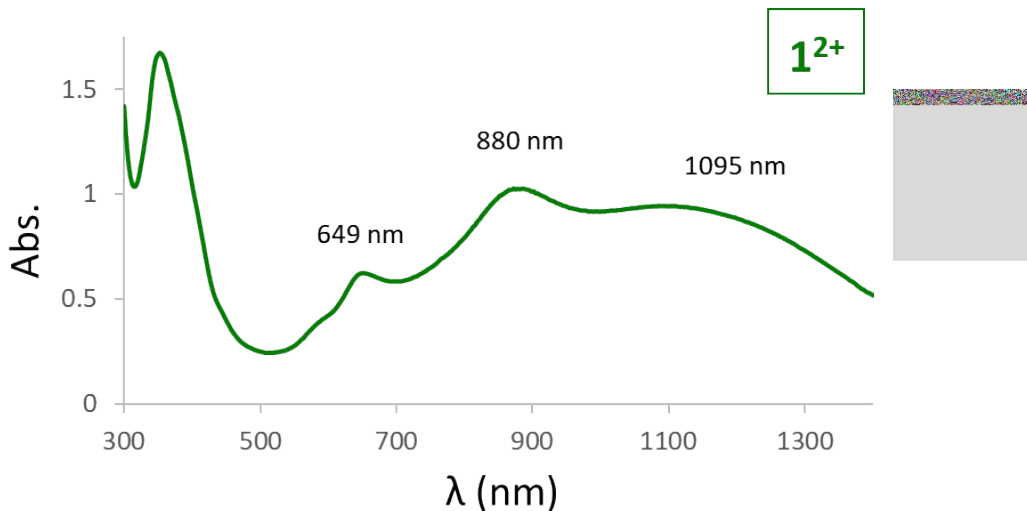


Figure S17. UV-Vis-NIR spectrum of a 0.5 mM concentration solution of **1²⁺** in MeCN containing 0.1 M TBAPF₆. The sample of **1²⁺** was prepared from a 0.5 mM solution of **1⁴⁺·4PF₆** by applying a potential of -1.22 V (vs. Fc^{+/-}) for 15 minutes with stirring, followed by transferring the reduced solution to a 1 mm path cuvette. Relative to the spectrum of **1⁴⁺**, the maximum change in the visible region of **1²⁺** corresponds to λ_{maxVis} at 649 nm ($\varepsilon_{649\text{nm}} = 12980 \text{ M}^{-1} \text{ cm}^{-1}$), a wavelength where **1⁴⁺** shows negligible absorptivity. The visible region minimum λ_{minVis} occurs at 509 nm ($\varepsilon_{509\text{nm}} = 5320 \text{ M}^{-1} \text{ cm}^{-1}$). Inset shows the green color of **1²⁺** while applying a potential of -1.22 V at platinum mesh electrode in an SEC cell.

Complex $\mathbf{1}^+\cdot\mathbf{4PF}_6$

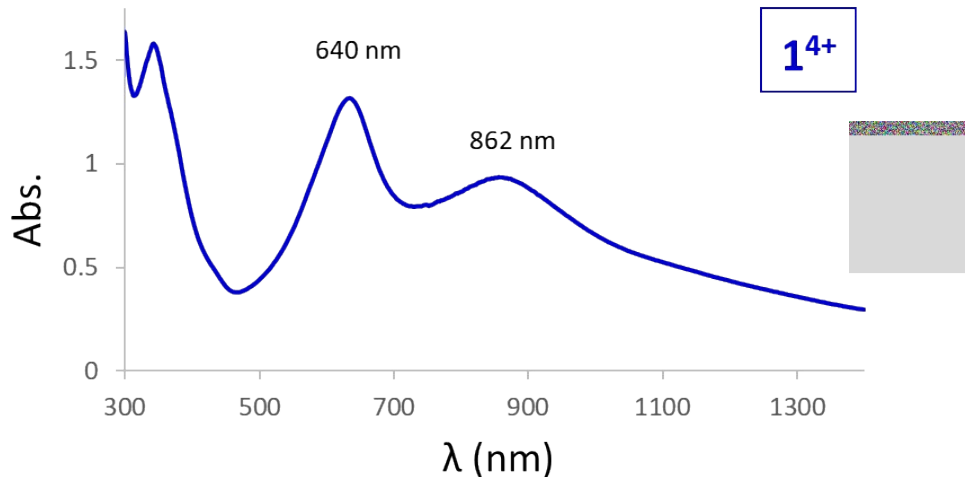


Figure S18. UV-Vis-NIR spectrum of a 0.5 mM concentration solution of $\mathbf{1}^+$ in MeCN containing 0.1 M TBAPF₆. The sample of $\mathbf{1}^+$ was prepared from a 0.5 mM solution of $\mathbf{1}^{4+}\cdot\mathbf{4PF}_6$ by applying a potential of -1.47 V (vs. Fc^{+/-}) for 15 minutes with stirring, followed by transferring the reduced solution to a 1 mm path cuvette. Relative to the spectrum of $\mathbf{1}^{4+}$, the maximum change in the visible region of $\mathbf{1}^+$ corresponds to λ_{maxVis} at 640 nm ($\epsilon_{640\text{nm}} = 24980 \text{ M}^{-1} \text{ cm}^{-1}$), a wavelength where $\mathbf{1}^{4+}$ shows negligible absorptivity. The visible region minimum λ_{minVis} occurs at 467 nm ($\epsilon_{467\text{nm}} = 7600 \text{ M}^{-1} \text{ cm}^{-1}$). Inset shows the blue color of $\mathbf{1}^+$ while applying a potential of -1.47 V at platinum mesh electrode in an SEC cell.

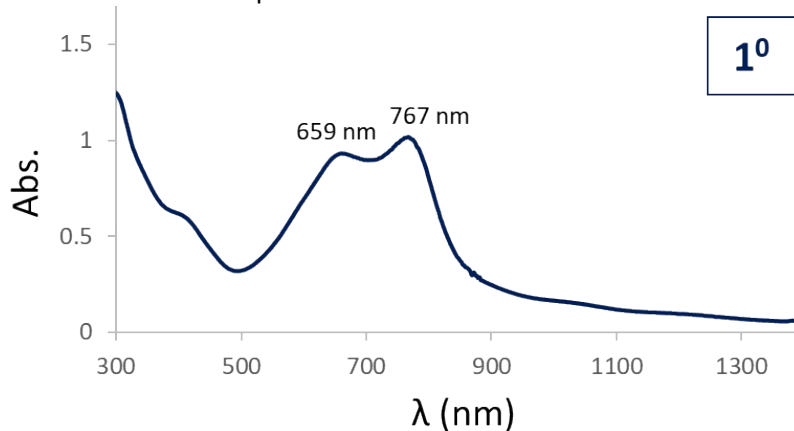


Figure S19. UV-Vis-NIR spectrum (1 mm path) of a 0.5 mM concentration solution of $\mathbf{1}^0$ in toluene.

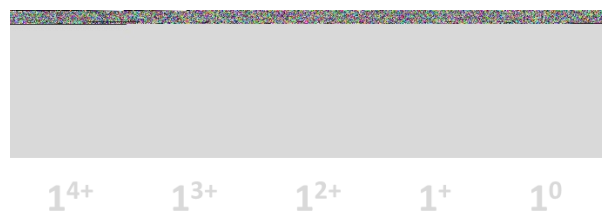


Figure S20. Color changes occurring during sequential electrochemical reductions of a 0.5 mM concentration solution of $\mathbf{1}^{4+}\cdot\mathbf{4PF}_6$ in MeCN containing 0.1 M TBAPF₆ at platinum mesh electrode in an SEC

cell. Oxidation states **1³⁺**, **1²⁺**, **1⁺**, and **1⁰** were obtained by applying potentials of -0.96 V, -1.22V, -1.47 V, and -1.80 V to the sample, respectively. Color changes were observed starting from red (**1⁴⁺**), to blue-green (**1³⁺**), to green (**1²⁺**), to blue (**1⁺**), to a darker blue (**1⁰**).

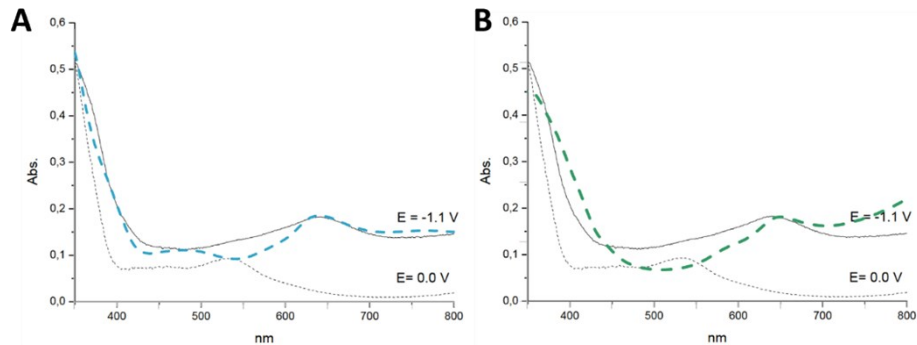


Figure S21. Comparison between a reported aqueous spectrum of a reduced state of a $[(\text{RPyTpy})_2\text{Co}^{\text{II}}]^{n+}$ coordination polymer⁸ (solid gray line) accessed by applying a potential of -1.1 V vs. AgCl/Ag and (A) the spectrum of **1³⁺** in MeCN (dashed blue-green line); or (B) the spectrum of **1²⁺** in MeCN (dashed green line). The spectra of **1³⁺** and **1²⁺** were both scaled so their peaks near 650 nm are equal in height to that of the reported spectrum, revealing that the reported spectrum better matches that of the **1³⁺** state rather than the **1²⁺** state even though the applied potential (-1.1 V vs. AgCl/Ag) for the reported spectrum should access the second reduced state of the coordination polymer. Note: The dotted gray line is the reported spectrum of the air-stable state of the coordination polymer. The spectra of the coordination polymer were reproduced from reference 8 with permission from the Royal Society of Chemistry.

Complex **2⁴⁺·4PF₆**

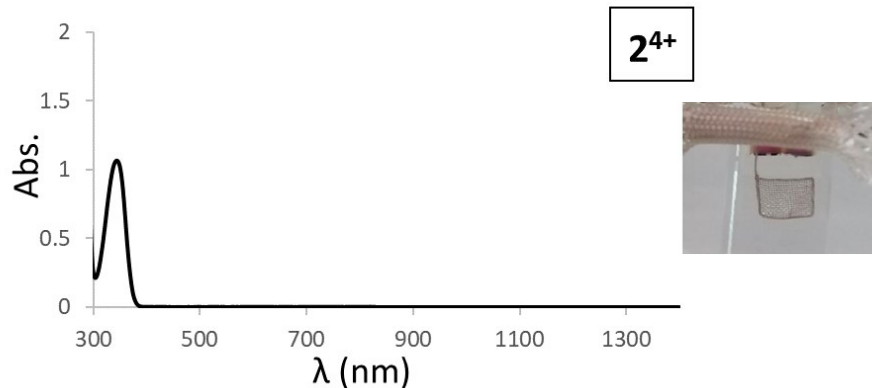


Figure S22. UV-vis-NIR spectrum (1 mm path) of a 0.5 mM concentration solution of **2·4PF₆** in MeCN. Inset shows a colorless solution of **2·4PF₆** in MeCN containing 0.1 M TBAPF₆ in an SEC cell with no potential applied.

Complex **2²⁺**

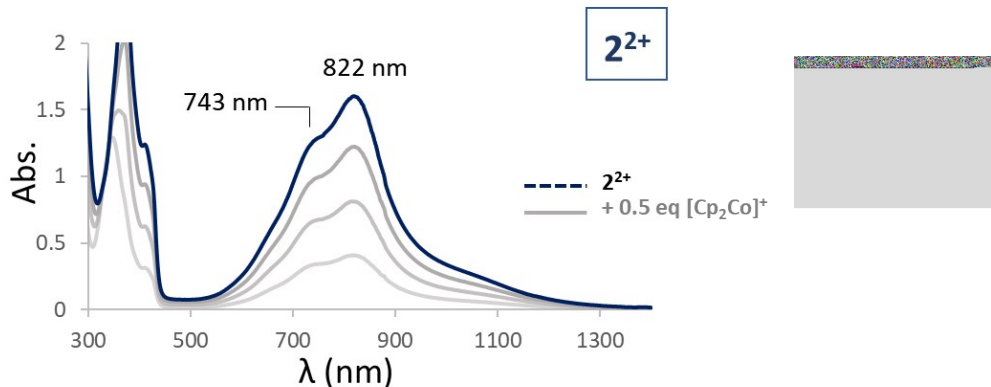


Figure S23. UV-vis-NIR spectrum of a 0.5 mM solution of $\mathbf{2}^{2+}$ in MeCN, which was prepared *in situ* in a 1 mm path cuvette by four sequential additions of 0.5 equiv of Cp₂Co to a 0.5 mM solution of $\mathbf{2}\cdot\text{PF}_6^-$. Further changes of the spectrum were not observed upon further addition of Cp₂Co. Inset shows the blue-green color of $\mathbf{2}^{2+}$ while applying a potential of -1.2 V at platinum mesh electrode in an SEC cell.

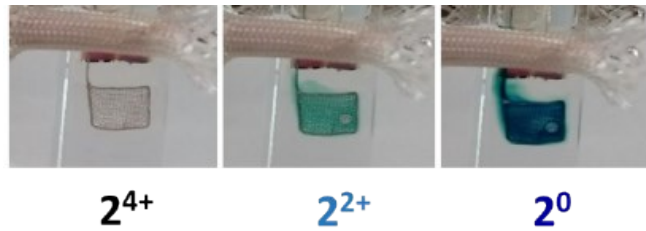


Figure S24. Color changes occurring during sequential electrochemical reductions of a 0.5 mM solution of $\mathbf{2}\cdot\text{PF}_6^-$ in MeCN containing 0.1 M TBAPF₆ at platinum mesh electrode in an SEC cell. Oxidation states $\mathbf{2}^{2+}$ and $\mathbf{2}^0$ were obtained by applying potentials of -1.20 V and -1.80 V to the sample, respectively. Color changes were observed from colorless to blue-green ($\mathbf{2}^{2+}$) to deep blue ($\mathbf{2}^0$).

Complex $\mathbf{3}^{4+}\cdot\text{PF}_6^-$

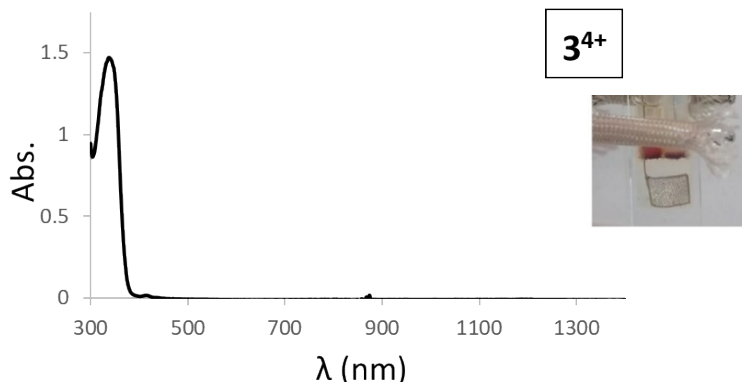


Figure S25. UV-vis-NIR spectrum (1 mm path) of a 0.5 mM concentration solution of $\mathbf{3}\cdot\text{PF}_6^-$ in MeCN. Inset shows a colorless solution of $\mathbf{3}\cdot\text{PF}_6^-$ in MeCN containing 0.1 M TBAPF₆ in an SEC cell with no potential applied.

Complex $\mathbf{3}^{2+}$

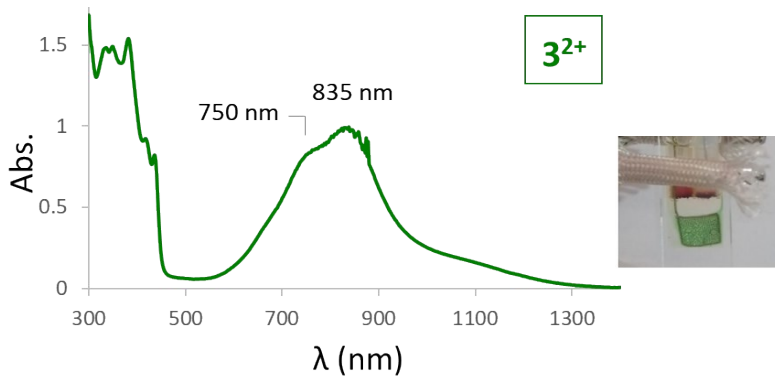


Figure S26. UV-Vis-NIR spectrum of a 0.5 mM concentration solution of $\mathbf{3}^{2+}$ in MeCN containing 0.1 M TBAPF₆. The sample of $\mathbf{3}^{2+}$ was prepared from a 0.5 mM solution of $\mathbf{3}\cdot\text{4PF}_6$ by applying a potential of -1.29 V (vs. Fc^{+/-}) for 2 minutes in an SEC cell. Inset shows the green color of $\mathbf{3}^{2+}$ while applying a potential of -1.29 V at platinum mesh electrode in an SEC cell.

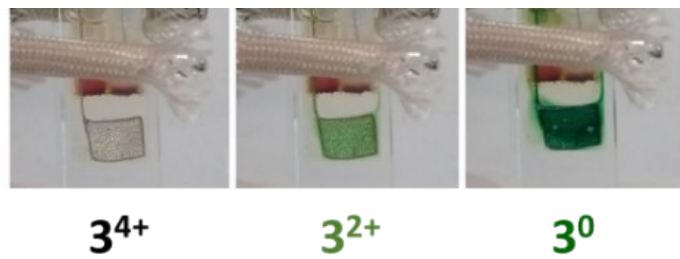


Figure S27. Inset shows color changes occurring during the sequential electrochemical reduction of a 0.5 mM concentration solution of $\mathbf{3}\cdot\text{4PF}_6$ in MeCN containing 0.1 M TBAPF₆ at platinum mesh electrode in an SEC cell. Oxidation states $\mathbf{3}^{2+}$ and $\mathbf{3}^0$ were obtained by applying potentials of -1.29 V and -1.80 V to the sample, respectively. Color changes were observed from colorless to light green ($\mathbf{3}^{2+}$) to dark green ($\mathbf{3}^0$).

6. Establishing the composition of $\mathbf{1}^0$.

As noted in the synthetic details, satisfactory elemental analysis could not be obtained for $\mathbf{1}^0$, which can be attributed to the extreme sensitivity of this complex to oxidation, resulting in the presence of small amounts of higher oxidation states even when handled with great care to exclude oxygen or water. For similar reasons, the reduced states of organic viologen radicals are rarely, if ever, isolated and characterized as bulk samples. However, since coordination bonds are potentially labile, we sought to confirm that $\mathbf{1}^0$ maintains a composition of one cobalt center ligated by two [MePyTpy]ⁿ ligands. Thus, a sample of isolated $\mathbf{1}^0$ (0.93 mg, 0.0013 mmol) was suspended in 0.65 mL of CD₃CN and an excess of AgPF₆ (4 mg, 0.016 mmol) was added, upon which $\mathbf{1}^0$ rapidly dissolved to give a hazy red solution. The ¹H NMR spectrum of this solution was obtained (Figure S27), revealing signals matching those of isolated $\mathbf{1}^{4+}\cdot\text{4PF}_6$. New signals corresponding to a diamagnetic impurity were also observed, but accounted for only ca. 6 % of the analyte that was observable by ¹H NMR spectroscopy. The sample was diluted with MeCN to $\frac{1}{4}$ its initial concentration, providing an estimated 0.5 mM concentration of $\mathbf{1}^{4+}$ based on the initial amount of $\mathbf{1}^0$ used. This solution was filtered through a 0.22 μm syringe filter and its UV-vis spectrum was obtained (Figure S28), matching that of a 0.5 mM sample of pure $\mathbf{1}^{4+}\cdot\text{4PF}_6$. The ability to regenerate $\mathbf{1}^{4+}$ by oxidation of isolated $\mathbf{1}^0$ confirms that $\mathbf{1}^0$ retains two equivalents of the reduced ligand per cobalt center. By

extension, the intermediate oxidation states **1⁺** to **1³⁺** must also retain both ligands, differing from **1⁴⁺** only with respect to the redox state of the ligands and possibly the cobalt center.

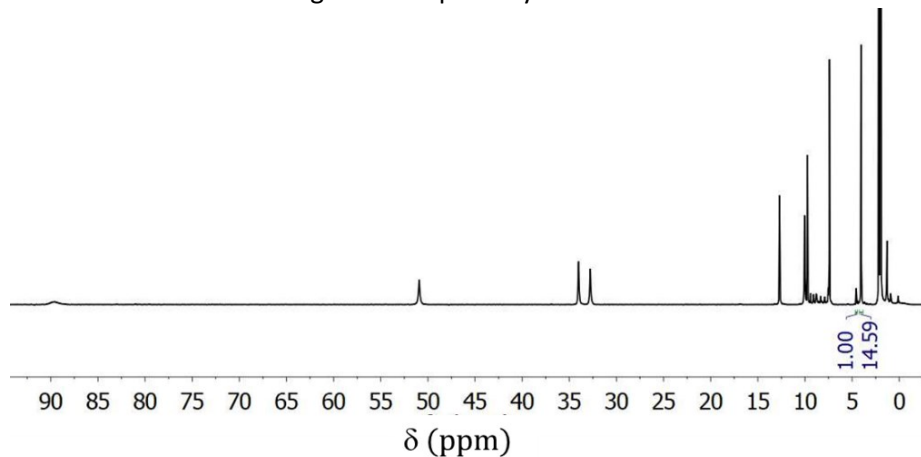


Figure S28. ^1H NMR spectrum of a sample of **1⁴⁺** generated by oxidation of **1⁰** with an excess of AgPF_6 in CD_3CN . The integrated signals compare the NCH_3 resonance of **1⁴⁺** with that of an unidentified impurity.

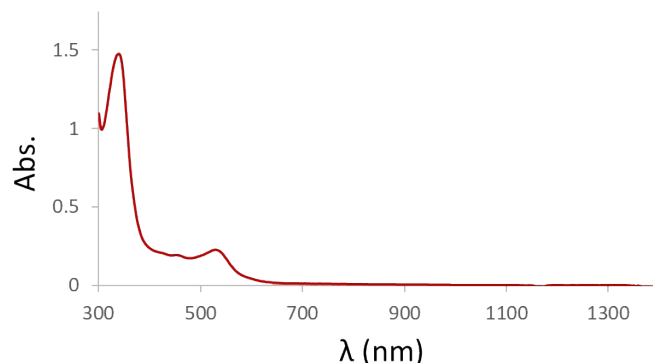


Figure S29. UV-vis-NIR spectrum of a 0.5 mM sample of **1⁴⁺** prepared by oxidation of **1⁰** with AgPF_6 .

7. Single-crystal X-ray Diffraction Analysis

Sample preparation, data collection, and analysis:

1⁴⁺·4PF₆. Dark red crystals of **1⁴⁺·4PF₆** were grown over several days at room temperature by vapor diffusion of Et_2O into an MeCN solution of **1⁴⁺·4PF₆**. A suitable crystal was selected and mounted on a glass loop using Paratone oil. Diffraction data were collected at 120 K on a Bruker Smart APEX CCD diffractometer with graphite monochromatized Mo K α radiation ($\lambda = 0.71073\text{\AA}$). The X-ray data for **1⁴⁺** were corrected for Lorenz effects, polarization, and absorption, the latter by a numerical method (SADABS).⁹ The structure of **1⁴⁺·4PF₆** was solved by an intrinsic phasing method (SHELXT)¹¹ revealing two independent molecules of **1⁴⁺** in the asymmetric unit. All non-hydrogen atoms were refined (SHELXL)¹⁰ based upon $(F_{\text{obs}})^2$ as a two-component inversion twin (twin law 100 010 00-1). All hydrogen atom coordinates were calculated with idealized geometries (SHELXL).¹⁰ Scattering factors (f_0 , f' , f'') are as described in SHELXL.¹⁰ Crystallographic data and final R indices for **1⁴⁺** are given below in Tables S1 – S6.

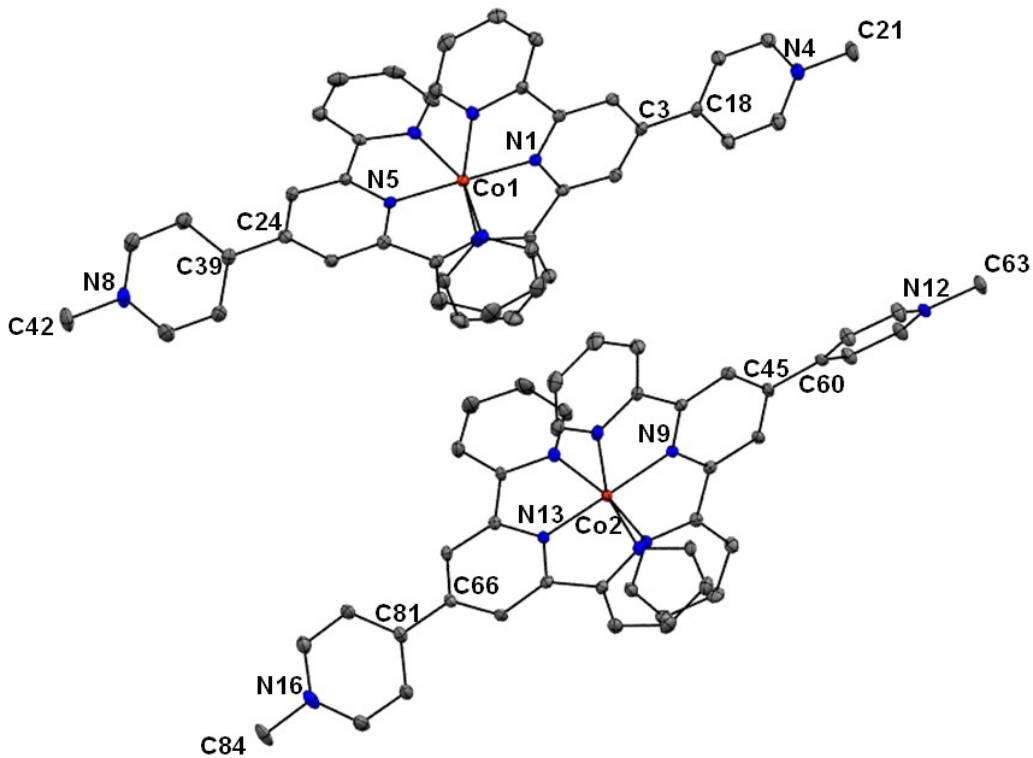


Figure S30: Asymmetric unit of the solid-state structure of $\mathbf{1}^{3+}\cdot\mathbf{4PF}_6$. Ellipsoids are shown at 50% probability. Hydrogen atoms, solvent (MeCN), and PF_6^- anions are omitted for clarity.

$\mathbf{1}^{3+}\cdot\mathbf{4PF}_6$. In an N_2 atmosphere glovebox, a 20 mL vial was charged with 39 mg (0.03 mmol) $\mathbf{1}^{3+}$, $\mathbf{4PF}_6$ and 5 mL dry MeCN, resulting in a dark red solution that was then added to a 20 mL vial containing 13 mg of $\text{Cr}(\text{C}_6\text{H}_6)_2$ (0.0625 mmol). Upon addition, the solution immediately became a dark blue-green color. The mixture was stirred for 20 h, after which the solvent was removed under reduced pressure. The dark residue was triturated under 10 mL of benzene and then repeatedly under ca. 1 mL amounts of THF to remove $[\text{Cr}(\text{C}_6\text{H}_6)_2]\text{PF}_6$ before drying in vacuo. The ^1H NMR spectrum of the dark solid indicated the presence of both $\mathbf{1}^{3+}$ and $\mathbf{1}^{2+}$. The solid was dissolved in MeCN and vapor diffusion of $^i\text{Pr}_2\text{O}$ into this solution at room temperature resulted in growth of X-ray quality greenish-blue crystals of $\mathbf{1}^{3+}\cdot\mathbf{3PF}_6$ over several days. The crystals were coated in Paratone oil on a slide in the glovebox and sealed in a jar which was removed from the glovebox. A single crystal was quickly selected under ambient atmosphere and mounted on a glass loop. Data for $\mathbf{1}^{3+}$ were collected on a Bruker Smart APEX CCD diffractometer with graphite monochromatized Mo $\text{K}\alpha$ radiation ($\lambda = 0.71073\text{\AA}$) at 120K. The X-ray data for $\mathbf{1}^{3+}$ were corrected for Lorenz effects and polarization, and absorption, the latter by a multi-scan (SADABS)⁹ method. The structure of $\mathbf{1}^{3+}$ was solved by an intrinsic phasing method (SHELXT).¹¹ All non-hydrogen atoms were refined (SHELXL)¹⁰ based upon $(\text{F}_{\text{obs}})^2$. All hydrogen atom coordinates were calculated with idealized geometries (SHELXL).¹⁰ Scattering

factors (f_0 , f' , f'') are as described in SHELXL.¹⁰ Crystallographic data and final R indices for $\mathbf{1}^{3+}$ are given below in Tables S7 – S12.

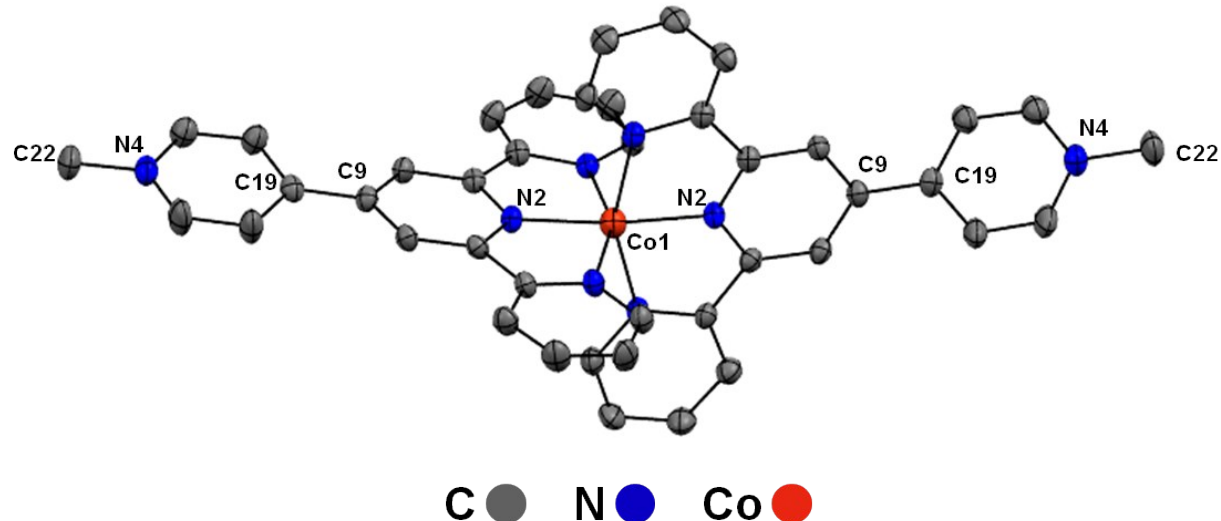


Figure S31: Solid-state structure of $\mathbf{1}^{3+}\cdot\mathbf{3PF}_6$. Ellipsoids are shown at 50% probability. Hydrogen atoms, solvent (MeCN), and PF_6^- anions are omitted for clarity.

Table S1. Crystal data and structure refinement for $\mathbf{1}^{4+}\cdot\mathbf{4PF}_6$.

Identification code	1
Empirical formula	C44 H37 Co F24 N9 P4
Formula weight	1330.63
Temperature	120(2) K
Wavelength	0.71073 Å
Crystal system	Monoclinic
Space group	P2 ₁ /c
Unit cell dimensions	a = 12.9089(14) Å α = 90°. b = 31.053(3) Å β = 90.106(2)°. c = 25.429(3) Å γ = 90°.

Volume 10193.5(19) Å³
Z 8
Density (calculated) 1.734 Mg/m³
Absorption coefficient 0.596 mm⁻¹
F(000) 5336
Crystal size 0.34 x 0.30 x 0.09 mm³
Theta range for data collection 1.537 to 30.507°.
Index ranges -18<=h<=18, -43<=k<=44, -36<=l<=36
Reflections collected 131496
Independent reflections 31114 [R(int) = 0.0636]
Completeness to theta = 25.242° 100.0 %
Absorption correction Numerical
Max. and min. transmission 0.95671 and 0.85564
Refinement method Full-matrix least-squares on F²
Data / restraints / parameters 31114 / 2508 / 1484
Goodness-of-fit on F² 1.076
Final R indices [I>2sigma(I)] R1 = 0.0527, wR2 = 0.1100
R indices (all data) R1 = 0.0691, wR2 = 0.1174
Extinction coefficient n/a
Largest diff. peak and hole 0.968 and -0.590 e.Å⁻³

Table S2. Atomic coordinates (x 104) and equivalent isotropic displacement parameters (Å² x 103) for **1⁴⁺·4PF₆**. U(eq) is defined as one third of the trace of the orthogonalized Uij tensor.

	x	y	z	U(eq)
Co(1)	-134(1)	2361(1)		6327(1)
N(1)	127(1)	1768(1)		6320(1)
N(2)	1320(2)		2366(1)	6628(1)
N(3)	-1509(2)		2155(1)	6037(1)
N(4)	976(2)	-462(1)	6481(1)	14(1)
N(5)	-383(1)	2967(1)		6322(1)
N(6)	436(2)	2520(1)		5573(1)
N(7)	-803(2)	2443(1)		7085(1)
N(8)	-935(2)	5199(1)		6416(1)
C(1)	1052(2)		1620(1)	6487(1)
C(2)	1259(2)		1182(1)	6500(1)
C(3)	503(2)	890(1)	6327(1)	10(1)
C(4)	-438(2)	1055(1)		6138(1)
C(5)	-607(2)	1496(1)		6146(1)
C(6)	1757(2)		1967(1)	6654(1)
C(7)	2765(2)		1905(1)	6823(1)
C(8)	3342(2)		2260(1)	6981(1)
C(9)	2894(2)		2665(1)	6965(1)
C(10)	1887(2)		2707(1)	6786(1)
C(11)	-1571(2)		1719(1)	5994(1)
C(12)	-2465(2)		1513(1)	5830(1)
C(13)	-3331(2)		1757(1)	5703(1)
				17(1)

C(14)	-3267(2)	2201(1)	5745(1)	18(1)
C(15)	-2350(2)	2389(1)	5913(1)	16(1)
C(16)	1770(2)	-192(1) 6558(1)		16(1)
C(17)	1643(2)	247(1) 6500(1)		15(1)
C(18)	676(2) 416(1)	6366(1)		11(1)
C(19)	-133(2) 124(1)	6286(1)		15(1)
C(20)	37(2) -309(1)	6349(1)		15(1)
C(21)	1120(2)	-934(1) 6527(1)		21(1)
C(22)	-58(2) 3204(1)	5909(1)		10(1)
C(23)	-187(2) 3647(1)	5906(1)		11(1)
C(24)	-696(2) 3844(1)	6321(1)		12(1)
C(25)	-1060(2)	3593(1)	6737(1)	12(1)
C(26)	-859(2) 3155(1)	6735(1)		10(1)
C(27)	404(2) 2951(1)	5479(1)		12(1)
C(28)	760(2) 3128(1)	5013(1)		19(1)
C(29)	1121(2)	2851(1)	4622(1)	26(1)
C(30)	1140(2)	2413(1)	4715(1)	26(1)
C(31)	798(2) 2262(1)	5196(1)		19(1)
C(32)	-1092(2)	2856(1)	7175(1)	11(1)
C(33)	-1527(2)	2986(1)	7645(1)	14(1)
C(34)	-1669(2)	2681(1)	8039(1)	19(1)
C(35)	-1375(2)	2259(1)	7951(1)	19(1)
C(36)	-953(2) 2153(1)	7468(1)		17(1)
C(37)	-62(2) 5017(1)	6240(1)		22(1)
C(38)	21(2) 4579(1)	6196(1)		19(1)
C(39)	-809(2) 4318(1)	6340(1)		13(1)
C(40)	-1713(2)	4516(1)	6517(1)	17(1)

C(41)	-1757(2)	4957(1)	6549(1)	18(1)
C(42)	-995(2)5675(1)	6464(1)	26(1)	
Co(2)	4851(1)	2649(1)	3891(1)	9(1)
N(9)	4633(1)	2036(1)	3898(1)	9(1)
N(10)	3339(2)	2609(1)	3536(1)	12(1)
N(11)	6305(2)	2427(1)	4216(1)	11(1)
N(12)	4123(2)	-198(1)3681(1)	12(1)	
N(13)	5042(1)	3242(1)	3878(1)	9(1)
N(14)	4219(2)	2795(1)	4584(1)	12(1)
N(15)	5512(2)	2694(1)	3183(1)	11(1)
N(16)	5765(2)	5467(1)	3673(1)	16(1)
C(43)	3729(2)	1873(1)	3724(1)	10(1)
C(44)	3556(2)	1433(1)	3705(1)	12(1)
C(45)	4343(2)	1154(1)	3871(1)	10(1)
C(46)	5267(2)	1328(1)	4056(1)	10(1)
C(47)	5399(2)	1771(1)	4064(1)	9(1)
C(48)	2976(2)	2199(1)	3535(1)	10(1)
C(49)	1984(2)	2099(1)	3359(1)	16(1)
C(50)	1359(2)	2431(1)	3171(1)	20(1)
C(51)	1735(2)	2848(1)	3164(1)	20(1)
C(52)	2733(2)	2924(1)	3350(1)	16(1)
C(53)	6361(2)	1992(1)	4231(1)	10(1)
C(54)	7255(2)	1774(1)	4377(1)	14(1)
C(55)	8127(2)	2010(1)	4514(1)	17(1)
C(56)	8074(2)	2456(1)	4502(1)	17(1)
C(57)	7155(2)	2651(1)	4353(1)	14(1)
C(58)	3650(2)	64(1)	3333(1)	17(1)

C(59)	3694(2)	504(1)	3396(1)	16(1)
C(60)	4231(2)	680(1)	3821(1)	11(1)
C(61)	4697(2)	400(1)	4177(1)	14(1)
C(62)	4636(2)	-36(1)	4098(1)	16(1)
C(63)	4085(2)	-670(1)	3596(1)	19(1)
C(64)	4675(2)	3488(1)	4275(1)	10(1)
C(65)	4801(2)	3931(1)	4271(1)	11(1)
C(66)	5350(2)	4119(1)	3857(1)	10(1)
C(67)	5727(2)	3860(1)	3452(1)	11(1)
C(68)	5540(2)	3422(1)	3466(1)	10(1)
C(69)	4175(2)	3225(1)	4683(1)	10(1)
C(70)	3720(2)	3388(1)	5136(1)	16(1)
C(71)	3333(2)	3100(1)	5505(1)	20(1)
C(72)	3395(2)	2663(1)	5410(1)	21(1)
C(73)	3837(2)	2522(1)	4944(1)	16(1)
C(74)	5784(2)	3104(1)	3054(1)	10(1)
C(75)	6204(2)	3208(1)	2568(1)	14(1)
C(76)	6360(2)	2881(1)	2204(1)	17(1)
C(77)	6090(2)	2462(1)	2333(1)	16(1)
C(78)	5670(2)	2381(1)	2825(1)	14(1)
C(79)	4907(2)	5321(1)	3916(1)	18(1)
C(80)	4760(2)	4885(1)	3995(1)	15(1)
C(81)	5498(2)	4593(1)	3820(1)	12(1)
C(82)	6393(2)	4757(1)	3584(1)	16(1)
C(83)	6507(2)	5194(1)	3515(1)	18(1)
C(84)	5916(2)	5935(1)	3582(1)	24(1)
P(1)	1469(1)	1059(1)	2454(1)	17(1)

P(2)	3603(1)	1248(1)	5434(1)	16(1)
P(3)	3554(1)	4201(1)	2575(1)	28(1)
P(4)	2171(1)	4509(1)	5049(1)	26(1)
F(1)	2128(1)	625(1) 2399(1)	33(1)	
F(2)	1492(1)	1121(1)	1829(1)	35(1)
F(3)	2528(1)	1329(1)	2505(1)	29(1)
F(4)	820(1) 1497(1)	2513(1)	28(1)	
F(5)	1458(1)	1003(1)	3085(1)	21(1)
F(6)	417(1) 792(1) 2412(1)	26(1)		
F(7)	4458(1)	880(1) 5354(1)	30(1)	
F(8)	3089(1)	1118(1)	4889(1)	38(1)
F(9)	4358(1)	1579(1)	5133(1)	30(1)
F(10)	2765(2)	1622(1)	5514(1)	43(1)
F(11)	4139(1)	1380(1)	5978(1)	35(1)
F(12)	2875(1)	916(1) 5737(1)	34(1)	
F(13)	4048(2)	3730(1)	2629(1)	38(1)
F(14)	3605(1)	4159(1)	1947(1)	30(1)
F(15)	4679(1)	4408(1)	2591(1)	37(1)
F(16)	3040(2)	4666(1)	2520(1)	56(1)
F(17)	3483(1)	4239(1)	3203(1)	43(1)
F(18)	2420(1)	3985(1)	2562(1)	52(1)
F(19)	2380(2)	4140(1)	4616(1)	56(1)
F(20)	3383(1)	4510(1)	5178(1)	33(1)
F(21)	2307(2)	4864(1)	4615(1)	64(1)
F(22)	1962(1)	4860(1)	5491(1)	35(1)
F(23)	956(2) 4478(1)	4932(1)	61(1)	
F(24)	2025(2)	4136(1)	5484(1)	43(1)

P(5)	6200(1)	1050(1)	2612(1)	17(1)
P(6)	7575(1)	482(1) 4906(1)		15(1)
P(7)	8363(1)	4153(1)	2522(1)	19(1)
P(8)	6739(1)	3553(1)	5452(1)	24(1)
F(25)	5844(1)	708(1) 2181(1)		37(1)
F(26)	7383(1)	889(1) 2546(1)		24(1)
F(27)	6391(2)	1402(1)	2165(1)	36(1)
F(28)	6587(1)	1394(1)	3046(1)	28(1)
F(29)	5039(1)	1216(1)	2685(1)	34(1)
F(30)	6041(1)	704(1) 3069(1)		28(1)
F(31)	8524(1)	205(1) 4688(1)		26(1)
F(32)	7277(1)	626(1) 4318(1)		26(1)
F(33)	8327(1)	895(1) 4952(1)		27(1)
F(34)	6630(1)	768(1) 5124(1)		24(1)
F(35)	7869(1)	352(1) 5501(1)		30(1)
F(36)	6835(1)	76(1) 4863(1)		30(1)
F(37)	8048(1)	3803(1)	2084(1)	29(1)
F(38)	9531(1)	3988(1)	2494(1)	44(1)
F(39)	8569(2)	4496(1)	2069(1)	44(1)
F(40)	8654(2)	4494(1)	2967(1)	43(1)
F(41)	7173(1)	4310(1)	2546(1)	24(1)
F(42)	8110(1)	3804(1)	2970(1)	34(1)
F(43)	7826(1)	3317(1)	5361(1)	32(1)
F(44)	6717(1)	3680(1)	4842(1)	37(1)
F(45)	7330(2)	3991(1)	5585(1)	54(1)
F(46)	5650(2)	3794(1)	5525(1)	48(1)
F(47)	6763(2)	3413(1)	6051(1)	59(1)

F(48)	6142(1)	3116(1)	5313(1)	31(1)
N(17)	634(3)	1391(1)	4377(1)	48(1)
C(85)	794(2)	1081(1)	4604(1)	29(1)
C(86)	980(2)	683(1)	4889(1)	31(1)
N(18)	9143(4)	3424(1)	4055(2)	70(1)
C(87)	8924(3)	3732(1)	4244(2)	56(1)
C(88)	8678(4)	4139(2)	4510(2)	85(2)

Table S3. Bond lengths [\AA] and angles [$^\circ$] for $\mathbf{1}^{4+}\cdot\mathbf{4PF}_6$.

Co(1)-N(1)	1.8730(18)	C(1)-C(6)	1.473(3)
Co(1)-N(5)	1.9090(18)	C(2)-C(3)	1.402(3)
Co(1)-N(3)	2.0250(19)	C(2)-H(2)	0.9500
Co(1)-N(2)	2.025(2)	C(3)-C(4)	1.403(3)
Co(1)-N(6)	2.113(2)	C(3)-C(18)	1.491(3)
Co(1)-N(7)	2.130(2)	C(4)-C(5)	1.387(3)
N(1)-C(5)	1.342(3)	C(4)-H(4)	0.9500
N(1)-C(1)	1.346(3)	C(5)-C(11)	1.474(3)
N(2)-C(10)	1.347(3)	C(6)-C(7)	1.384(3)
N(2)-C(6)	1.364(3)	C(7)-C(8)	1.390(3)
N(3)-C(15)	1.344(3)	C(7)-H(7)	0.9500
N(3)-C(11)	1.360(3)	C(8)-C(9)	1.385(4)
N(4)-C(16)	1.340(3)	C(8)-H(8)	0.9500
N(4)-C(20)	1.343(3)	C(9)-C(10)	1.383(4)
N(4)-C(21)	1.481(3)	C(9)-H(9)	0.9500
N(5)-C(26)	1.350(3)	C(10)-H(10)	0.9500
N(5)-C(22)	1.352(3)	C(11)-C(12)	1.383(3)
N(6)-C(31)	1.337(3)	C(12)-C(13)	1.389(3)
N(6)-C(27)	1.359(3)	C(12)-H(12)	0.9500
N(7)-C(36)	1.342(3)	C(13)-C(14)	1.384(3)
N(7)-C(32)	1.355(3)	C(13)-H(13)	0.9500
N(8)-C(37)	1.340(3)	C(14)-C(15)	1.387(3)
N(8)-C(41)	1.346(3)	C(14)-H(14)	0.9500
N(8)-C(42)	1.486(3)	C(15)-H(15)	0.9500
C(1)-C(2)	1.387(3)	C(16)-C(17)	1.381(3)

C(16)-H(16)	0.9500	C(32)-C(33)	1.381(3)
C(17)-C(18)	1.395(3)	C(33)-C(34)	1.391(3)
C(17)-H(17)	0.9500	C(33)-H(33)	0.9500
C(18)-C(19)	1.399(3)	C(34)-C(35)	1.384(4)
C(19)-C(20)	1.372(3)	C(34)-H(34)	0.9500
C(19)-H(19)	0.9500	C(35)-C(36)	1.383(4)
C(20)-H(20)	0.9500	C(35)-H(35)	0.9500
C(21)-H(21A)	0.9800	C(36)-H(36)	0.9500
C(21)-H(21B)	0.9800	C(37)-C(38)	1.370(3)
C(21)-H(21C)	0.9800	C(37)-H(37)	0.9500
C(22)-C(23)	1.386(3)	C(38)-C(39)	1.391(3)
C(22)-C(27)	1.474(3)	C(38)-H(38)	0.9500
C(23)-C(24)	1.386(3)	C(39)-C(40)	1.394(3)
C(23)-H(23)	0.9500	C(40)-C(41)	1.373(3)
C(24)-C(25)	1.396(3)	C(40)-H(40)	0.9500
C(24)-C(39)	1.481(3)	C(41)-H(41)	0.9500
C(25)-C(26)	1.386(3)	C(42)-H(42A)	0.9800
C(25)-H(25)	0.9500	C(42)-H(42B)	0.9800
C(26)-C(32)	1.483(3)	C(42)-H(42C)	0.9800
C(27)-C(28)	1.385(3)	Co(2)-N(13)	1.8580(18)
C(28)-C(29)	1.396(4)	Co(2)-N(9)	1.9239(18)
C(28)-H(28)	0.9500	Co(2)-N(14)	1.9948(19)
C(29)-C(30)	1.379(4)	Co(2)-N(15)	1.9997(19)
C(29)-H(29)	0.9500	Co(2)-N(10)	2.153(2)
C(30)-C(31)	1.383(4)	Co(2)-N(11)	2.1629(19)
C(30)-H(30)	0.9500	N(9)-C(43)	1.348(3)
C(31)-H(31)	0.9500	N(9)-C(47)	1.352(3)

N(10)-C(52)	1.338(3)	C(49)-H(49)	0.9500
N(10)-C(48)	1.354(3)	C(50)-C(51)	1.381(4)
N(11)-C(57)	1.344(3)	C(50)-H(50)	0.9500
N(11)-C(53)	1.355(3)	C(51)-C(52)	1.394(4)
N(12)-C(62)	1.345(3)	C(51)-H(51)	0.9500
N(12)-C(58)	1.348(3)	C(52)-H(52)	0.9500
N(12)-C(63)	1.481(3)	C(53)-C(54)	1.388(3)
N(13)-C(64)	1.351(3)	C(54)-C(55)	1.388(3)
N(13)-C(68)	1.353(3)	C(54)-H(54)	0.9500
N(14)-C(73)	1.343(3)	C(55)-C(56)	1.387(3)
N(14)-C(69)	1.360(3)	C(55)-H(55)	0.9500
N(15)-C(78)	1.346(3)	C(56)-C(57)	1.384(3)
N(15)-C(74)	1.361(3)	C(56)-H(56)	0.9500
N(16)-C(83)	1.341(3)	C(57)-H(57)	0.9500
N(16)-C(79)	1.348(3)	C(58)-C(59)	1.376(3)
N(16)-C(84)	1.485(3)	C(58)-H(58)	0.9500
C(43)-C(44)	1.385(3)	C(59)-C(60)	1.394(3)
C(43)-C(48)	1.484(3)	C(59)-H(59)	0.9500
C(44)-C(45)	1.398(3)	C(60)-C(61)	1.392(3)
C(44)-H(44)	0.9500	C(61)-C(62)	1.373(3)
C(45)-C(46)	1.390(3)	C(61)-H(61)	0.9500
C(45)-C(60)	1.484(3)	C(62)-H(62)	0.9500
C(46)-C(47)	1.387(3)	C(63)-H(63A)	0.9800
C(46)-H(46)	0.9500	C(63)-H(63B)	0.9800
C(47)-C(53)	1.479(3)	C(63)-H(63C)	0.9800
C(48)-C(49)	1.392(3)	C(64)-C(65)	1.387(3)
C(49)-C(50)	1.394(3)	C(64)-C(69)	1.472(3)

C(65)-C(66)	1.397(3)	C(81)-C(82)	1.400(3)
C(65)-H(65)	0.9500	C(82)-C(83)	1.374(3)
C(66)-C(67)	1.395(3)	C(82)-H(82)	0.9500
C(66)-C(81)	1.486(3)	C(83)-H(83)	0.9500
C(67)-C(68)	1.382(3)	C(84)-H(84A)	0.9800
C(67)-H(67)	0.9500	C(84)-H(84B)	0.9800
C(68)-C(74)	1.474(3)	C(84)-H(84C)	0.9800
C(69)-C(70)	1.388(3)	P(1)-F(6)	1.5949(16)
C(70)-C(71)	1.388(3)	P(1)-F(1)	1.5990(17)
C(70)-H(70)	0.9500	P(1)-F(2)	1.6020(18)
C(71)-C(72)	1.382(3)	P(1)-F(4)	1.6049(17)
C(71)-H(71)	0.9500	P(1)-F(3)	1.6081(17)
C(72)-C(73)	1.387(3)	P(1)-F(5)	1.6126(16)
C(72)-H(72)	0.9500	P(2)-F(8)	1.5883(18)
C(73)-H(73)	0.9500	P(2)-F(12)	1.5940(17)
C(74)-C(75)	1.386(3)	P(2)-F(11)	1.5992(18)
C(75)-C(76)	1.390(3)	P(2)-F(10)	1.6010(18)
C(75)-H(75)	0.9500	P(2)-F(7)	1.6012(17)
C(76)-C(77)	1.386(3)	P(2)-F(9)	1.6110(17)
C(76)-H(76)	0.9500	P(3)-F(15)	1.589(2)
C(77)-C(78)	1.389(3)	P(3)-F(16)	1.594(2)
C(77)-H(77)	0.9500	P(3)-F(13)	1.602(2)
C(78)-H(78)	0.9500	P(3)-F(17)	1.6041(19)
C(79)-C(80)	1.379(3)	P(3)-F(14)	1.6043(18)
C(79)-H(79)	0.9500	P(3)-F(18)	1.611(2)
C(80)-C(81)	1.391(3)	P(4)-F(21)	1.570(2)
C(80)-H(80)	0.9500	P(4)-F(22)	1.5904(18)

P(4)-F(20)	1.5975(18)	P(7)-F(42)	1.6047(18)
P(4)-F(23)	1.599(2)	P(7)-F(37)	1.6080(17)
P(4)-F(19)	1.611(2)	P(7)-F(41)	1.6124(16)
P(4)-F(24)	1.614(2)	P(8)-F(47)	1.586(2)
P(5)-F(25)	1.5930(18)	P(8)-F(45)	1.595(2)
P(5)-F(29)	1.5957(17)	P(8)-F(48)	1.5985(18)
P(5)-F(27)	1.5958(17)	P(8)-F(44)	1.599(2)
P(5)-F(30)	1.5981(17)	P(8)-F(43)	1.6017(18)
P(5)-F(28)	1.6132(17)	P(8)-F(46)	1.604(2)
P(5)-F(26)	1.6160(16)	N(17)-C(85)	1.139(4)
P(6)-F(36)	1.5867(17)	C(85)-C(86)	1.454(4)
P(6)-F(31)	1.5964(16)	C(86)-H(86A)	0.9800
P(6)-F(32)	1.6076(16)	C(86)-H(86B)	0.9800
P(6)-F(34)	1.6082(16)	C(86)-H(86C)	0.9800
P(6)-F(35)	1.6102(16)	N(18)-C(87)	1.110(6)
P(6)-F(33)	1.6115(17)	C(87)-C(88)	1.466(7)
P(7)-F(39)	1.5927(19)	C(88)-H(88A)	0.9800
P(7)-F(38)	1.5942(19)	C(88)-H(88B)	0.9800
P(7)-F(40)	1.5942(18)	C(88)-H(88C)	0.9800

N(1)-Co(1)-N(5)	178.90(8)	N(5)-Co(1)-N(6)	79.76(8)
N(1)-Co(1)-N(3)	80.98(8)	N(3)-Co(1)-N(6)	92.90(8)
N(5)-Co(1)-N(3)	99.29(8)	N(2)-Co(1)-N(6)	91.00(8)
N(1)-Co(1)-N(2)	81.08(8)	N(1)-Co(1)-N(7)	101.53(8)
N(5)-Co(1)-N(2)	98.66(8)	N(5)-Co(1)-N(7)	79.54(8)
N(3)-Co(1)-N(2)	162.03(8)	N(3)-Co(1)-N(7)	90.59(7)
N(1)-Co(1)-N(6)	99.16(8)	N(2)-Co(1)-N(7)	91.93(8)

N(6)-Co(1)-N(7)	159.31(8)	C(2)-C(1)-C(6) 126.3(2)
C(5)-N(1)-C(1)	120.99(19)	C(1)-C(2)-C(3) 119.4(2)
C(5)-N(1)-Co(1)	119.56(15)	C(1)-C(2)-H(2) 120.3
C(1)-N(1)-Co(1)	119.46(15)	C(3)-C(2)-H(2) 120.3
C(10)-N(2)-C(6)	118.3(2)	C(2)-C(3)-C(4) 118.3(2)
C(10)-N(2)-Co(1)	128.45(17)	C(2)-C(3)-C(18) 120.7(2)
C(6)-N(2)-Co(1)	113.20(15)	C(4)-C(3)-C(18) 120.9(2)
C(15)-N(3)-C(11)	118.3(2)	C(5)-C(4)-C(3) 119.5(2)
C(15)-N(3)-Co(1)	128.39(16)	C(5)-C(4)-H(4) 120.3
C(11)-N(3)-Co(1)	113.27(15)	C(3)-C(4)-H(4) 120.3
C(16)-N(4)-C(20)	120.3(2)	N(1)-C(5)-C(4) 120.9(2)
C(16)-N(4)-C(21)	120.8(2)	N(1)-C(5)-C(11) 112.81(19)
C(20)-N(4)-C(21)	118.9(2)	C(4)-C(5)-C(11) 126.3(2)
C(26)-N(5)-C(22)	120.77(19)	N(2)-C(6)-C(7) 122.1(2)
C(26)-N(5)-Co(1)	119.89(15)	N(2)-C(6)-C(1) 113.33(19)
C(22)-N(5)-Co(1)	119.33(15)	C(7)-C(6)-C(1) 124.6(2)
C(31)-N(6)-C(27)	118.3(2)	C(6)-C(7)-C(8) 118.8(2)
C(31)-N(6)-Co(1)	129.33(17)	C(6)-C(7)-H(7) 120.6
C(27)-N(6)-Co(1)	112.37(14)	C(8)-C(7)-H(7) 120.6
C(36)-N(7)-C(32)	118.3(2)	C(9)-C(8)-C(7) 119.3(2)
C(36)-N(7)-Co(1)	129.45(16)	C(9)-C(8)-H(8) 120.3
C(32)-N(7)-Co(1)	112.19(15)	C(7)-C(8)-H(8) 120.3
C(37)-N(8)-C(41)	120.8(2)	C(10)-C(9)-C(8) 119.1(2)
C(37)-N(8)-C(42)	119.5(2)	C(10)-C(9)-H(9) 120.5
C(41)-N(8)-C(42)	119.7(2)	C(8)-C(9)-H(9) 120.5
N(1)-C(1)-C(2)	120.9(2)	N(2)-C(10)-C(9) 122.4(2)
N(1)-C(1)-C(6)	112.83(19)	N(2)-C(10)-H(10) 118.8

C(9)-C(10)-H(10)	118.8	C(18)-C(19)-H(19)	120.0
N(3)-C(11)-C(12)	122.2(2)	N(4)-C(20)-C(19)	121.3(2)
N(3)-C(11)-C(5)	113.33(19)	N(4)-C(20)-H(20)	119.4
C(12)-C(11)-C(5)	124.4(2)	C(19)-C(20)-H(20)	119.4
C(11)-C(12)-C(13)	119.2(2)	N(4)-C(21)-H(21A)	109.5
C(11)-C(12)-H(12)	120.4	N(4)-C(21)-H(21B)	109.5
C(13)-C(12)-H(12)	120.4	H(21A)-C(21)-H(21B)	109.5
C(14)-C(13)-C(12)	118.6(2)	N(4)-C(21)-H(21C)	109.5
C(14)-C(13)-H(13)	120.7	H(21A)-C(21)-H(21C)	109.5
C(12)-C(13)-H(13)	120.7	H(21B)-C(21)-H(21C)	109.5
C(13)-C(14)-C(15)	119.6(2)	N(5)-C(22)-C(23)	120.5(2)
C(13)-C(14)-H(14)	120.2	N(5)-C(22)-C(27)	114.37(19)
C(15)-C(14)-H(14)	120.2	C(23)-C(22)-C(27)	125.1(2)
N(3)-C(15)-C(14)	122.1(2)	C(22)-C(23)-C(24)	119.4(2)
N(3)-C(15)-H(15)	118.9	C(22)-C(23)-H(23)	120.3
C(14)-C(15)-H(15)	118.9	C(24)-C(23)-H(23)	120.3
N(4)-C(16)-C(17)	120.8(2)	C(23)-C(24)-C(25)	119.4(2)
N(4)-C(16)-H(16)	119.6	C(23)-C(24)-C(39)	120.7(2)
C(17)-C(16)-H(16)	119.6	C(25)-C(24)-C(39)	119.8(2)
C(16)-C(17)-C(18)	120.3(2)	C(26)-C(25)-C(24)	118.8(2)
C(16)-C(17)-H(17)	119.9	C(26)-C(25)-H(25)	120.6
C(18)-C(17)-H(17)	119.9	C(24)-C(25)-H(25)	120.6
C(17)-C(18)-C(19)	117.3(2)	N(5)-C(26)-C(25)	120.9(2)
C(17)-C(18)-C(3)	121.5(2)	N(5)-C(26)-C(32)	114.13(19)
C(19)-C(18)-C(3)	121.2(2)	C(25)-C(26)-C(32)	125.0(2)
C(20)-C(19)-C(18)	120.0(2)	N(6)-C(27)-C(28)	122.1(2)
C(20)-C(19)-H(19)	120.0	N(6)-C(27)-C(22)	113.95(19)

C(28)-C(27)-C(22)	123.9(2)	C(35)-C(36)-H(36)	118.6
C(27)-C(28)-C(29)	118.5(2)	N(8)-C(37)-C(38)	120.9(2)
C(27)-C(28)-H(28)	120.7	N(8)-C(37)-H(37)	119.5
C(29)-C(28)-H(28)	120.7	C(38)-C(37)-H(37)	119.5
C(30)-C(29)-C(28)	119.3(2)	C(37)-C(38)-C(39)	119.7(2)
C(30)-C(29)-H(29)	120.4	C(37)-C(38)-H(38)	120.2
C(28)-C(29)-H(29)	120.4	C(39)-C(38)-H(38)	120.2
C(29)-C(30)-C(31)	118.9(2)	C(38)-C(39)-C(40)	118.4(2)
C(29)-C(30)-H(30)	120.6	C(38)-C(39)-C(24)	119.6(2)
C(31)-C(30)-H(30)	120.6	C(40)-C(39)-C(24)	122.0(2)
N(6)-C(31)-C(30)	122.9(2)	C(41)-C(40)-C(39)	119.5(2)
N(6)-C(31)-H(31)	118.6	C(41)-C(40)-H(40)	120.3
C(30)-C(31)-H(31)	118.6	C(39)-C(40)-H(40)	120.3
N(7)-C(32)-C(33)	122.3(2)	N(8)-C(41)-C(40)	120.7(2)
N(7)-C(32)-C(26)	114.15(19)	N(8)-C(41)-H(41)	119.6
C(33)-C(32)-C(26)	123.5(2)	C(40)-C(41)-H(41)	119.6
C(32)-C(33)-C(34)	118.6(2)	N(8)-C(42)-H(42A)	109.5
C(32)-C(33)-H(33)	120.7	N(8)-C(42)-H(42B)	109.5
C(34)-C(33)-H(33)	120.7	H(42A)-C(42)-H(42B)	109.5
C(35)-C(34)-C(33)	119.5(2)	N(8)-C(42)-H(42C)	109.5
C(35)-C(34)-H(34)	120.2	H(42A)-C(42)-H(42C)	109.5
C(33)-C(34)-H(34)	120.2	H(42B)-C(42)-H(42C)	109.5
C(36)-C(35)-C(34)	118.5(2)	N(13)-Co(2)-N(9)	179.12(8)
C(36)-C(35)-H(35)	120.8	N(13)-Co(2)-N(14)	81.06(8)
C(34)-C(35)-H(35)	120.8	N(9)-Co(2)-N(14)	98.99(8)
N(7)-C(36)-C(35)	122.8(2)	N(13)-Co(2)-N(15)	81.86(8)
N(7)-C(36)-H(36)	118.6	N(9)-Co(2)-N(15)	98.06(8)

N(14)-Co(2)-N(15)	162.87(8)	C(69)-N(14)-Co(2)	113.88(15)
N(13)-Co(2)-N(10)	99.82(7)	C(78)-N(15)-C(74)	118.3(2)
N(9)-Co(2)-N(10)	79.30(7)	C(78)-N(15)-Co(2)	128.55(16)
N(14)-Co(2)-N(10)	90.67(8)	C(74)-N(15)-Co(2)	113.12(14)
N(15)-Co(2)-N(10)	90.84(8)	C(83)-N(16)-C(79)	120.7(2)
N(13)-Co(2)-N(11)	101.96(7)	C(83)-N(16)-C(84)	118.6(2)
N(9)-Co(2)-N(11)	78.92(7)	C(79)-N(16)-C(84)	120.7(2)
N(14)-Co(2)-N(11)	95.23(8)	N(9)-C(43)-C(44)	121.5(2)
N(15)-Co(2)-N(11)	89.68(7)	N(9)-C(43)-C(48)	114.53(18)
N(10)-Co(2)-N(11)	158.06(7)	C(44)-C(43)-C(48)	123.96(19)
C(43)-N(9)-C(47)	120.36(18)	C(43)-C(44)-C(45)	118.9(2)
C(43)-N(9)-Co(2)	119.73(15)	C(43)-C(44)-H(44)	120.6
C(47)-N(9)-Co(2)	119.88(15)	C(45)-C(44)-H(44)	120.6
C(52)-N(10)-C(48)	119.0(2)	C(46)-C(45)-C(44)	118.97(19)
C(52)-N(10)-Co(2)	129.33(16)	C(46)-C(45)-C(60)	119.82(19)
C(48)-N(10)-Co(2)	111.60(14)	C(44)-C(45)-C(60)	121.1(2)
C(57)-N(11)-C(53)	117.82(19)	C(47)-C(46)-C(45)	119.7(2)
C(57)-N(11)-Co(2)	129.90(15)	C(47)-C(46)-H(46)	120.2
C(53)-N(11)-Co(2)	111.97(14)	C(45)-C(46)-H(46)	120.2
C(62)-N(12)-C(58)	120.82(19)	N(9)-C(47)-C(46)	120.7(2)
C(62)-N(12)-C(63)	120.0(2)	N(9)-C(47)-C(53)	114.86(18)
C(58)-N(12)-C(63)	119.1(2)	C(46)-C(47)-C(53)	124.45(19)
C(64)-N(13)-C(68)	120.82(18)	N(10)-C(48)-C(49)	121.9(2)
C(64)-N(13)-Co(2)	120.05(15)	N(10)-C(48)-C(43)	114.55(19)
C(68)-N(13)-Co(2)	119.13(15)	C(49)-C(48)-C(43)	123.5(2)
C(73)-N(14)-C(69)	118.5(2)	C(48)-C(49)-C(50)	118.4(2)
C(73)-N(14)-Co(2)	127.60(16)	C(48)-C(49)-H(49)	120.8

C(50)-C(49)-H(49)	120.8	C(59)-C(58)-H(58)	119.8
C(51)-C(50)-C(49)	119.7(2)	C(58)-C(59)-C(60)	120.1(2)
C(51)-C(50)-H(50)	120.2	C(58)-C(59)-H(59)	120.0
C(49)-C(50)-H(50)	120.2	C(60)-C(59)-H(59)	120.0
C(50)-C(51)-C(52)	118.6(2)	C(61)-C(60)-C(59)	118.2(2)
C(50)-C(51)-H(51)	120.7	C(61)-C(60)-C(45)	121.5(2)
C(52)-C(51)-H(51)	120.7	C(59)-C(60)-C(45)	120.3(2)
N(10)-C(52)-C(51)	122.4(2)	C(62)-C(61)-C(60)	119.8(2)
N(10)-C(52)-H(52)	118.8	C(62)-C(61)-H(61)	120.1
C(51)-C(52)-H(52)	118.8	C(60)-C(61)-H(61)	120.1
N(11)-C(53)-C(54)	122.5(2)	N(12)-C(62)-C(61)	120.9(2)
N(11)-C(53)-C(47)	114.19(19)	N(12)-C(62)-H(62)	119.6
C(54)-C(53)-C(47)	123.29(19)	C(61)-C(62)-H(62)	119.6
C(55)-C(54)-C(53)	118.9(2)	N(12)-C(63)-H(63A)	109.5
C(55)-C(54)-H(54)	120.6	N(12)-C(63)-H(63B)	109.5
C(53)-C(54)-H(54)	120.6	H(63A)-C(63)-H(63B)	109.5
C(56)-C(55)-C(54)	118.9(2)	N(12)-C(63)-H(63C)	109.5
C(56)-C(55)-H(55)	120.5	H(63A)-C(63)-H(63C)	109.5
C(54)-C(55)-H(55)	120.5	H(63B)-C(63)-H(63C)	109.5
C(57)-C(56)-C(55)	119.0(2)	N(13)-C(64)-C(65)	121.0(2)
C(57)-C(56)-H(56)	120.5	N(13)-C(64)-C(69)	111.57(18)
C(55)-C(56)-H(56)	120.5	C(65)-C(64)-C(69)	127.4(2)
N(11)-C(57)-C(56)	122.9(2)	C(64)-C(65)-C(66)	118.6(2)
N(11)-C(57)-H(57)	118.5	C(64)-C(65)-H(65)	120.7
C(56)-C(57)-H(57)	118.5	C(66)-C(65)-H(65)	120.7
N(12)-C(58)-C(59)	120.3(2)	C(67)-C(66)-C(65)	119.63(19)
N(12)-C(58)-H(58)	119.8	C(67)-C(66)-C(81)	118.52(19)

C(65)-C(66)-C(81)	121.8(2)	C(76)-C(75)-H(75)	120.6
C(68)-C(67)-C(66)	119.1(2)	C(77)-C(76)-C(75)	119.3(2)
C(68)-C(67)-H(67)	120.4	C(77)-C(76)-H(76)	120.3
C(66)-C(67)-H(67)	120.4	C(75)-C(76)-H(76)	120.3
N(13)-C(68)-C(67)	120.7(2)	C(76)-C(77)-C(78)	118.9(2)
N(13)-C(68)-C(74)	112.08(19)	C(76)-C(77)-H(77)	120.6
C(67)-C(68)-C(74)	127.2(2)	C(78)-C(77)-H(77)	120.6
N(14)-C(69)-C(70)	122.0(2)	N(15)-C(78)-C(77)	122.5(2)
N(14)-C(69)-C(64)	113.25(19)	N(15)-C(78)-H(78)	118.7
C(70)-C(69)-C(64)	124.8(2)	C(77)-C(78)-H(78)	118.7
C(71)-C(70)-C(69)	118.6(2)	N(16)-C(79)-C(80)	120.7(2)
C(71)-C(70)-H(70)	120.7	N(16)-C(79)-H(79)	119.6
C(69)-C(70)-H(70)	120.7	C(80)-C(79)-H(79)	119.6
C(72)-C(71)-C(70)	119.6(2)	C(79)-C(80)-C(81)	119.9(2)
C(72)-C(71)-H(71)	120.2	C(79)-C(80)-H(80)	120.1
C(70)-C(71)-H(71)	120.2	C(81)-C(80)-H(80)	120.1
C(71)-C(72)-C(73)	118.9(2)	C(80)-C(81)-C(82)	117.7(2)
C(71)-C(72)-H(72)	120.6	C(80)-C(81)-C(66)	122.5(2)
C(73)-C(72)-H(72)	120.6	C(82)-C(81)-C(66)	119.7(2)
N(14)-C(73)-C(72)	122.4(2)	C(83)-C(82)-C(81)	120.2(2)
N(14)-C(73)-H(73)	118.8	C(83)-C(82)-H(82)	119.9
C(72)-C(73)-H(73)	118.8	C(81)-C(82)-H(82)	119.9
N(15)-C(74)-C(75)	122.2(2)	N(16)-C(83)-C(82)	120.6(2)
N(15)-C(74)-C(68)	113.62(19)	N(16)-C(83)-H(83)	119.7
C(75)-C(74)-C(68)	124.1(2)	C(82)-C(83)-H(83)	119.7
C(74)-C(75)-C(76)	118.8(2)	N(16)-C(84)-H(84A)	109.5
C(74)-C(75)-H(75)	120.6	N(16)-C(84)-H(84B)	109.5

H(84A)-C(84)-H(84B)	109.5	F(11)-P(2)-F(7) 89.69(10)
N(16)-C(84)-H(84C)	109.5	F(10)-P(2)-F(7) 178.92(11)
H(84A)-C(84)-H(84C)	109.5	F(8)-P(2)-F(9) 90.04(10)
H(84B)-C(84)-H(84C)	109.5	F(12)-P(2)-F(9) 178.89(11)
F(6)-P(1)-F(1)	90.56(10)	F(11)-P(2)-F(9) 89.15(10)
F(6)-P(1)-F(2)	90.75(9)	F(10)-P(2)-F(9) 90.38(10)
F(1)-P(1)-F(2)	90.24(10)	F(7)-P(2)-F(9) 88.73(9)
F(6)-P(1)-F(4)	90.09(9)	F(15)-P(3)-F(16) 90.91(13)
F(1)-P(1)-F(4)	179.27(10)	F(15)-P(3)-F(13) 90.23(10)
F(2)-P(1)-F(4)	90.07(10)	F(16)-P(3)-F(13) 178.86(13)
F(6)-P(1)-F(3)	179.26(10)	F(15)-P(3)-F(17) 89.94(10)
F(1)-P(1)-F(3)	89.70(10)	F(16)-P(3)-F(17) 89.78(11)
F(2)-P(1)-F(3)	89.94(9)	F(13)-P(3)-F(17) 90.29(11)
F(4)-P(1)-F(3)	89.64(9)	F(15)-P(3)-F(14) 91.08(10)
F(6)-P(1)-F(5)	90.12(9)	F(16)-P(3)-F(14) 90.29(10)
F(1)-P(1)-F(5)	90.13(9)	F(13)-P(3)-F(14) 89.62(10)
F(2)-P(1)-F(5)	179.05(10)	F(17)-P(3)-F(14) 178.98(12)
F(4)-P(1)-F(5)	89.56(9)	F(15)-P(3)-F(18) 179.18(13)
F(3)-P(1)-F(5)	89.19(8)	F(16)-P(3)-F(18) 89.88(13)
F(8)-P(2)-F(12)	90.67(10)	F(13)-P(3)-F(18) 88.98(12)
F(8)-P(2)-F(11)	179.04(10)	F(17)-P(3)-F(18) 89.88(11)
F(12)-P(2)-F(11)	90.14(10)	F(14)-P(3)-F(18) 89.11(10)
F(8)-P(2)-F(10)	90.84(11)	F(21)-P(4)-F(22) 92.03(12)
F(12)-P(2)-F(10)	90.46(10)	F(21)-P(4)-F(20) 91.82(12)
F(11)-P(2)-F(10)	89.69(11)	F(22)-P(4)-F(20) 91.15(10)
F(8)-P(2)-F(7)	89.77(10)	F(21)-P(4)-F(23) 91.20(14)
F(12)-P(2)-F(7)	90.42(10)	F(22)-P(4)-F(23) 90.28(11)

F(20)-P(4)-F(23)	176.60(13)	F(31)-P(6)-F(32)	90.51(9)
F(21)-P(4)-F(19)	89.99(14)	F(36)-P(6)-F(34)	90.37(9)
F(22)-P(4)-F(19)	177.98(13)	F(31)-P(6)-F(34)	179.05(10)
F(20)-P(4)-F(19)	88.67(10)	F(32)-P(6)-F(34)	89.22(9)
F(23)-P(4)-F(19)	89.78(12)	F(36)-P(6)-F(35)	90.36(9)
F(21)-P(4)-F(24)	178.70(14)	F(31)-P(6)-F(35)	90.66(9)
F(22)-P(4)-F(24)	89.16(10)	F(32)-P(6)-F(35)	178.34(10)
F(20)-P(4)-F(24)	88.68(11)	F(34)-P(6)-F(35)	89.59(9)
F(23)-P(4)-F(24)	88.26(13)	F(36)-P(6)-F(33)	179.80(11)
F(19)-P(4)-F(24)	88.82(12)	F(31)-P(6)-F(33)	89.48(9)
F(25)-P(5)-F(29)	91.43(10)	F(32)-P(6)-F(33)	89.39(9)
F(25)-P(5)-F(27)	90.60(11)	F(34)-P(6)-F(33)	89.61(9)
F(29)-P(5)-F(27)	90.53(10)	F(35)-P(6)-F(33)	89.44(9)
F(25)-P(5)-F(30)	90.85(10)	F(39)-P(7)-F(38)	91.24(12)
F(29)-P(5)-F(30)	90.60(9)	F(39)-P(7)-F(40)	91.67(12)
F(27)-P(5)-F(30)	178.14(11)	F(38)-P(7)-F(40)	91.33(11)
F(25)-P(5)-F(28)	178.70(10)	F(39)-P(7)-F(42)	177.79(12)
F(29)-P(5)-F(28)	89.86(9)	F(38)-P(7)-F(42)	90.55(11)
F(27)-P(5)-F(28)	89.23(10)	F(40)-P(7)-F(42)	89.58(11)
F(30)-P(5)-F(28)	89.29(9)	F(39)-P(7)-F(37)	89.57(10)
F(25)-P(5)-F(26)	89.55(9)	F(38)-P(7)-F(37)	89.41(10)
F(29)-P(5)-F(26)	179.02(11)	F(40)-P(7)-F(37)	178.55(11)
F(27)-P(5)-F(26)	89.45(10)	F(42)-P(7)-F(37)	89.17(10)
F(30)-P(5)-F(26)	89.40(9)	F(39)-P(7)-F(41)	89.15(10)
F(28)-P(5)-F(26)	89.16(9)	F(38)-P(7)-F(41)	178.79(11)
F(36)-P(6)-F(31)	90.55(9)	F(40)-P(7)-F(41)	89.80(10)
F(36)-P(6)-F(32)	90.81(9)	F(42)-P(7)-F(41)	89.03(9)

F(37)-P(7)-F(41)	89.45(9)	F(43)-P(8)-F(46)	178.42(12)
F(47)-P(8)-F(45)	91.16(13)	N(17)-C(85)-C(86)	178.9(3)
F(47)-P(8)-F(48)	89.29(12)	C(85)-C(86)-H(86A)	109.5
F(45)-P(8)-F(48)	179.52(12)	C(85)-C(86)-H(86B)	109.5
F(47)-P(8)-F(44)	178.34(12)	H(86A)-C(86)-H(86B)	109.5
F(45)-P(8)-F(44)	90.21(12)	C(85)-C(86)-H(86C)	109.5
F(48)-P(8)-F(44)	89.34(10)	H(86A)-C(86)-H(86C)	109.5
F(47)-P(8)-F(43)	89.78(12)	H(86B)-C(86)-H(86C)	109.5
F(45)-P(8)-F(43)	90.09(11)	N(18)-C(87)-C(88)	177.3(5)
F(48)-P(8)-F(43)	90.09(9)	C(87)-C(88)-H(88A)	109.5
F(44)-P(8)-F(43)	89.30(10)	C(87)-C(88)-H(88B)	109.5
F(47)-P(8)-F(46)	91.80(13)	H(88A)-C(88)-H(88B)	109.5
F(45)-P(8)-F(46)	89.80(11)	C(87)-C(88)-H(88C)	109.5
F(48)-P(8)-F(46)	90.01(10)	H(88A)-C(88)-H(88C)	109.5
F(44)-P(8)-F(46)	89.13(11)	H(88B)-C(88)-H(88C)	109.5

Table S4. Anisotropic displacement parameters ($\text{\AA}^2 \times 103$) for $\mathbf{1}^{4+}$. The anisotropic displacement factor exponent takes the form: $-2\pi^2 [h_2 a^* 2U_{11} + \dots + 2 h_k a^* b^* U_{12}]$

	U11	U22	U33	U23	U13	U12
Co(1)	9(1)	11(1)	10(1)	-2(1)	0(1)	0(1)
N(1)	10(1)	10(1)	10(1)	0(1)	1(1)	0(1)
N(2)	13(1)	13(1)	14(1)	-3(1)	2(1)	-1(1)
N(3)	13(1)	10(1)	11(1)	-1(1)	1(1)	-1(1)
N(4)	18(1)	11(1)	14(1)	-1(1)	0(1)	1(1)

N(5)	7(1)	11(1)	11(1)	-1(1)	0(1)	1(1)
N(6)	12(1)	12(1)	16(1)	-3(1)	1(1)	1(1)
N(7)	11(1)	11(1)	16(1)	-2(1)	-1(1)	-2(1)
N(8)	26(1)	11(1)	16(1)	-1(1)	1(1)	5(1)
C(1)	8(1)	13(1)	10(1)	-1(1)	-1(1)	-1(1)
C(2)	11(1)	13(1)	11(1)	-2(1)	0(1)	2(1)
C(3)	11(1)	12(1)	9(1)	-1(1)	1(1)	1(1)
C(4)	10(1)	13(1)	11(1)	-2(1)	0(1)	-1(1)
C(5)	10(1)	13(1)	10(1)	-2(1)	1(1)	0(1)
C(6)	12(1)	11(1)	12(1)	-2(1)	2(1)	-2(1)
C(7)	12(1)	14(1)	23(1)	-2(1)	-2(1)	0(1)
C(8)	14(1)	24(1)	25(1)	-3(1)	-4(1)	-5(1)
C(9)	22(1)	20(1)	23(1)	-5(1)	-1(1)	-9(1)
C(10)	23(1)	11(1)	20(1)	-2(1)	4(1)	-1(1)
C(11)	11(1)	11(1)	8(1)	0(1)	1(1)	1(1)
C(12)	14(1)	13(1)	13(1)	0(1)	-2(1)	-1(1)
C(13)	12(1)	21(1)	18(1)	0(1)	-4(1)	-1(1)
C(14)	14(1)	22(1)	19(1)	4(1)	-2(1)	6(1)
C(15)	18(1)	12(1)	17(1)	2(1)	2(1)	4(1)
C(16)	16(1)	14(1)	18(1)	-1(1)	-3(1)	2(1)
C(17)	14(1)	12(1)	17(1)	-2(1)	-3(1)	-1(1)
C(18)	13(1)	11(1)	8(1)	-2(1)	1(1)	2(1)
C(19)	13(1)	12(1)	21(1)	-2(1)	-1(1)	0(1)
C(20)	14(1)	13(1)	20(1)	-1(1)	-1(1)	-1(1)
C(21)	24(1)	9(1)	30(1)	0(1)	-4(1)	4(1)
C(22)	10(1)	13(1)	8(1)	0(1)	-2(1)	1(1)
C(23)	11(1)	12(1)	11(1)	1(1)	1(1)	0(1)

C(24)	10(1)	12(1)	15(1)	1(1)	-2(1)	1(1)
C(25)	12(1)	12(1)	12(1)	-2(1)	2(1)	1(1)
C(26)	8(1)	11(1)	11(1)	-1(1)	1(1)	-1(1)
C(27)	10(1)	15(1)	9(1)	-1(1)	1(1)	1(1)
C(28)	24(1)	18(1)	14(1)	1(1)	4(1)	1(1)
C(29)	33(2)	32(1)	14(1)	-3(1)	12(1)	-2(1)
C(30)	28(1)	28(1)	20(1)	-12(1)	9(1)	0(1)
C(31)	17(1)	17(1)	23(1)	-9(1)	2(1)	0(1)
C(32)	9(1)	11(1)	12(1)	-1(1)	-1(1)	-2(1)
C(33)	14(1)	15(1)	13(1)	-1(1)	1(1)	-1(1)
C(34)	17(1)	26(1)	12(1)	2(1)	3(1)	-5(1)
C(35)	17(1)	21(1)	19(1)	9(1)	-1(1)	-8(1)
C(36)	14(1)	11(1)	24(1)	3(1)	-5(1)	-3(1)
C(37)	24(1)	14(1)	29(1)	2(1)	5(1)	0(1)
C(38)	18(1)	16(1)	24(1)	-1(1)	7(1)	2(1)
C(39)	16(1)	13(1)	10(1)	1(1)	0(1)	2(1)
C(40)	18(1)	16(1)	17(1)	1(1)	2(1)	3(1)
C(41)	20(1)	19(1)	16(1)	1(1)	3(1)	6(1)
C(42)	37(2)	10(1)	30(2)	-4(1)	1(1)	3(1)
Co(2)	10(1)	6(1)	10(1)	0(1)	0(1)	1(1)
N(9)	10(1)	9(1)	9(1)	0(1)	0(1)	0(1)
N(10)	14(1)	10(1)	11(1)	1(1)	1(1)	3(1)
N(11)	12(1)	7(1)	12(1)	-1(1)	1(1)	0(1)
N(12)	14(1)	7(1)	16(1)	1(1)	1(1)	-1(1)
N(13)	10(1)	8(1)	10(1)	0(1)	0(1)	1(1)
N(14)	12(1)	10(1)	13(1)	0(1)	1(1)	1(1)
N(15)	11(1)	9(1)	12(1)	1(1)	0(1)	1(1)

N(16)	26(1)	10(1)	14(1)	1(1)	-3(1)	-4(1)
C(43)	9(1)	11(1)	8(1)	0(1)	0(1)	1(1)
C(44)	11(1)	12(1)	12(1)	1(1)	-1(1)	-1(1)
C(45)	13(1)	7(1)	11(1)	1(1)	0(1)	0(1)
C(46)	12(1)	9(1)	9(1)	2(1)	1(1)	0(1)
C(47)	9(1)	11(1)	8(1)	1(1)	0(1)	1(1)
C(48)	11(1)	10(1)	10(1)	-1(1)	1(1)	1(1)
C(49)	12(1)	14(1)	20(1)	-1(1)	-3(1)	1(1)
C(50)	13(1)	22(1)	25(1)	-2(1)	-5(1)	4(1)
C(51)	21(1)	18(1)	20(1)	2(1)	-4(1)	8(1)
C(52)	18(1)	13(1)	17(1)	1(1)	1(1)	5(1)
C(53)	12(1)	11(1)	8(1)	0(1)	-1(1)	0(1)
C(54)	13(1)	12(1)	16(1)	1(1)	-3(1)	1(1)
C(55)	11(1)	21(1)	18(1)	-1(1)	-4(1)	1(1)
C(56)	13(1)	18(1)	18(1)	-2(1)	-2(1)	-3(1)
C(57)	16(1)	11(1)	15(1)	-2(1)	0(1)	-2(1)
C(58)	21(1)	13(1)	18(1)	-1(1)	-7(1)	0(1)
C(59)	18(1)	11(1)	18(1)	0(1)	-8(1)	0(1)
C(60)	10(1)	9(1)	14(1)	2(1)	1(1)	-2(1)
C(61)	19(1)	11(1)	12(1)	1(1)	-3(1)	-3(1)
C(62)	22(1)	10(1)	16(1)	4(1)	-4(1)	-1(1)
C(63)	27(1)	7(1)	24(1)	-2(1)	0(1)	-1(1)
C(64)	10(1)	9(1)	9(1)	0(1)	-2(1)	1(1)
C(65)	13(1)	8(1)	11(1)	0(1)	-1(1)	2(1)
C(66)	10(1)	8(1)	13(1)	0(1)	-2(1)	-1(1)
C(67)	11(1)	10(1)	13(1)	2(1)	2(1)	-2(1)
C(68)	8(1)	11(1)	11(1)	1(1)	-1(1)	1(1)

C(69)	12(1)	7(1)	13(1)	1(1)	0(1)	1(1)
C(70)	21(1)	11(1)	16(1)	-3(1)	5(1)	1(1)
C(71)	27(1)	20(1)	13(1)	-1(1)	10(1)	-2(1)
C(72)	29(1)	17(1)	17(1)	5(1)	6(1)	-6(1)
C(73)	23(1)	10(1)	16(1)	2(1)	0(1)	-1(1)
C(74)	10(1)	11(1)	11(1)	0(1)	-1(1)	1(1)
C(75)	17(1)	12(1)	12(1)	2(1)	2(1)	0(1)
C(76)	17(1)	22(1)	11(1)	-2(1)	4(1)	2(1)
C(77)	17(1)	16(1)	16(1)	-5(1)	-1(1)	4(1)
C(78)	13(1)	9(1)	18(1)	-3(1)	-2(1)	3(1)
C(79)	21(1)	13(1)	20(1)	-3(1)	0(1)	0(1)
C(80)	17(1)	11(1)	17(1)	1(1)	3(1)	-1(1)
C(81)	17(1)	9(1)	9(1)	0(1)	-1(1)	-1(1)
C(82)	19(1)	12(1)	18(1)	-3(1)	5(1)	-3(1)
C(83)	22(1)	16(1)	16(1)	-1(1)	4(1)	-6(1)
C(84)	38(2)	9(1)	24(1)	2(1)	-2(1)	-7(1)
P(1)	13(1)	22(1)	15(1)	-2(1)	-3(1)	2(1)
P(2)	14(1)	16(1)	16(1)	4(1)	4(1)	3(1)
P(3)	19(1)	46(1)	18(1)	-12(1)	-7(1)	15(1)
P(4)	19(1)	40(1)	18(1)	-1(1)	0(1)	9(1)
F(1)	33(1)	34(1)	32(1)	-14(1)	-8(1)	16(1)
F(2)	30(1)	59(1)	15(1)	2(1)	-5(1)	-3(1)
F(3)	17(1)	43(1)	25(1)	2(1)	-3(1)	-8(1)
F(4)	27(1)	21(1)	35(1)	0(1)	-10(1)	6(1)
F(5)	22(1)	25(1)	15(1)	0(1)	-2(1)	-1(1)
F(6)	21(1)	29(1)	29(1)	-4(1)	-6(1)	-7(1)
F(7)	32(1)	23(1)	34(1)	5(1)	6(1)	14(1)

F(8)	24(1)	69(1)	19(1)	2(1)	-2(1)	-9(1)
F(9)	29(1)	23(1)	37(1)	12(1)	5(1)	-3(1)
F(10)	33(1)	42(1)	55(1)	8(1)	10(1)	24(1)
F(11)	38(1)	43(1)	24(1)	-7(1)	-1(1)	-4(1)
F(12)	36(1)	37(1)	27(1)	5(1)	10(1)	-13(1)
F(13)	39(1)	39(1)	35(1)	-6(1)	-14(1)	8(1)
F(14)	25(1)	48(1)	18(1)	-9(1)	-3(1)	11(1)
F(15)	32(1)	49(1)	31(1)	-7(1)	-10(1)	-1(1)
F(16)	68(1)	65(1)	36(1)	-22(1)	-23(1)	49(1)
F(17)	31(1)	81(2)	19(1)	-16(1)	-9(1)	18(1)
F(18)	21(1)	110(2)	26(1)	-14(1)	-4(1)	2(1)
F(19)	42(1)	87(2)	37(1)	-34(1)	-10(1)	22(1)
F(20)	18(1)	48(1)	32(1)	-4(1)	0(1)	0(1)
F(21)	71(2)	77(2)	43(1)	36(1)	18(1)	29(1)
F(22)	39(1)	27(1)	38(1)	-6(1)	10(1)	4(1)
F(23)	24(1)	97(2)	63(2)	-21(1)	-11(1)	16(1)
F(24)	43(1)	33(1)	53(1)	5(1)	20(1)	3(1)
P(5)	17(1)	19(1)	16(1)	1(1)	2(1)	2(1)
P(6)	13(1)	16(1)	14(1)	-1(1)	-1(1)	2(1)
P(7)	16(1)	23(1)	18(1)	-2(1)	4(1)	0(1)
P(8)	26(1)	18(1)	26(1)	-6(1)	-9(1)	3(1)
F(25)	36(1)	37(1)	36(1)	-14(1)	-12(1)	2(1)
F(26)	19(1)	32(1)	21(1)	-2(1)	5(1)	3(1)
F(27)	52(1)	35(1)	22(1)	13(1)	7(1)	8(1)
F(28)	32(1)	27(1)	24(1)	-8(1)	4(1)	-1(1)
F(29)	22(1)	45(1)	36(1)	2(1)	1(1)	12(1)
F(30)	24(1)	29(1)	32(1)	12(1)	8(1)	0(1)

F(31)	25(1)	24(1)	29(1)	-2(1)	0(1)	12(1)
F(32)	29(1)	30(1)	17(1)	2(1)	-1(1)	10(1)
F(33)	19(1)	22(1)	40(1)	-6(1)	1(1)	-4(1)
F(34)	16(1)	32(1)	26(1)	-10(1)	2(1)	4(1)
F(35)	30(1)	43(1)	16(1)	5(1)	-6(1)	2(1)
F(36)	32(1)	21(1)	36(1)	0(1)	-6(1)	-9(1)
F(37)	32(1)	29(1)	24(1)	-7(1)	4(1)	0(1)
F(38)	18(1)	65(1)	48(1)	-18(1)	3(1)	7(1)
F(39)	53(1)	31(1)	46(1)	10(1)	30(1)	-4(1)
F(40)	32(1)	49(1)	48(1)	-28(1)	4(1)	-10(1)
F(41)	20(1)	31(1)	20(1)	5(1)	4(1)	7(1)
F(42)	41(1)	37(1)	24(1)	13(1)	0(1)	11(1)
F(43)	22(1)	30(1)	45(1)	4(1)	-12(1)	3(1)
F(44)	36(1)	40(1)	34(1)	12(1)	-16(1)	-1(1)
F(45)	53(1)	26(1)	85(2)	-17(1)	-37(1)	-2(1)
F(46)	37(1)	35(1)	71(2)	-26(1)	-2(1)	14(1)
F(47)	82(2)	72(2)	24(1)	-4(1)	-3(1)	5(1)
F(48)	25(1)	18(1)	50(1)	-4(1)	-2(1)	0(1)
N(17)	57(2)	25(1)	62(2)	-3(1)	-31(2)	0(1)
C(85)	28(2)	25(1)	35(2)	-11(1)	-12(1)	1(1)
C(86)	27(2)	32(2)	33(2)	2(1)	-6(1)	-2(1)
N(18)	99(3)	55(2)	55(2)	15(2)	-26(2)	-19(2)
C(87)	52(2)	45(2)	71(3)	32(2)	-23(2)	-19(2)
C(88)	61(3)	52(3)	141(5)	30(3)	23(3)	-14(2)

Table S5. Hydrogen coordinates (x 104) and isotropic displacement parameters ($\text{\AA}^2 \times 10^3$) for **1⁴⁺**.

	x	y	z	U(eq)
H(2)	1908	1080	6626	14
H(4)	-956	866	6005	14
H(7)	3058	1624	6831	20
H(8)	4037	2225	7098	26
H(9)	3274	2911	7076	26
H(10)	1584	2985	6775	21
H(12)	-2487	1208	5806	16
H(13)	-3954	1623	5590	20
H(14)	-3847	2375	5659	22
H(15)	-2315	2694	5942	19
H(16)	2430	-303	6653	19
H(17)	2215	435	6552	17
H(19)	-800	225	6189	18
H(20)	-520	-505	6299	19
H(21A)	840	-1075	6213	31
H(21B)	756	-1039	6839	31
H(21C)	1860	-999	6559	31
H(23)	72	3814	5623	14
H(25)	-1438	3721	7017	14
H(28)	758	3431	4961	23
H(29)	1351	2963	4294	32

H(30)	1384	2220	4454	31
H(31)	821	1961	5260	23
H(33)	-1726	3278	7697	17
H(34)	-1965	2762	8366	22
H(35)	-1462	2046	8216	23
H(36)	-760	1862	7405	20
H(37)	508	5194	6144	27
H(38)	642	4453	6067	23
H(40)	-2295	4346	6615	21
H(41)	-2375	5092	6667	22
H(42A)	-1444	5751	6761	39
H(42B)	-1281	5797	6140	39
H(42C)	-300	5792	6525	39
H(44)	2914	1322	3582	14
H(46)	5806	1144	4176	12
H(49)	1738	1811	3367	19
H(50)	678	2372	3049	24
H(51)	1321	3077	3034	23
H(52)	2994	3210	3346	19
H(54)	7269	1468	4384	16
H(55)	8749	1869	4614	20
H(56)	8660	2626	4594	20
H(57)	7122	2957	4348	17
H(58)	3284	-55	3044	21
H(59)	3358	687	3150	19
H(61)	5056	511	4474	17
H(62)	4959	-227	4340	19

H(63A)	4237	-818	3927	29
H(63B)	4600	-751	3331	29
H(63C)	3393	-752	3473	29
H(65)	4520	4104	4544	13
H(67)	6108	3984	3170	13
H(70)	3673	3689	5192	19
H(71)	3028	3204	5820	24
H(72)	3140	2462	5660	25
H(73)	3870	2221	4877	19
H(75)	6381	3497	2487	17
H(76)	6649	2944	1869	20
H(77)	6191	2234	2089	20
H(78)	5487	2094	2913	16
H(79)	4399	5519	4034	22
H(80)	4154	4786	4168	18
H(82)	6924	4567	3470	20
H(83)	7116	5303	3355	22
H(84A)	6085	5985	3211	36
H(84B)	6484	6040	3804	36
H(84C)	5278	6090	3670	36
H(86A)	1274	749	5235	46
H(86B)	1466	503	4691	46
H(86C)	324	528	4933	46
H(88A)	8228	4313	4284	127
H(88B)	9320	4297	4582	127
H(88C)	8322	4078	4842	127

Table S6. Torsion angles [°] for **1⁴⁺**.

N(3)-Co(1)-N(1)-C(5)	0.39(16)	C(10)-N(2)-C(6)-C(1)	178.1(2)
N(2)-Co(1)-N(1)-C(5)	179.30(18)	Co(1)-N(2)-C(6)-C(1)	-3.5(2)
N(6)-Co(1)-N(1)-C(5)	-91.12(17)	N(1)-C(1)-C(6)-N(2)	2.7(3)
N(7)-Co(1)-N(1)-C(5)	89.14(17)	C(2)-C(1)-C(6)-N(2)	-175.9(2)
N(3)-Co(1)-N(1)-C(1)	180.00(18)	N(1)-C(1)-C(6)-C(7)	-177.5(2)
N(2)-Co(1)-N(1)-C(1)	-1.08(16)	C(2)-C(1)-C(6)-C(7)	3.9(4)
N(6)-Co(1)-N(1)-C(1)	88.49(17)	N(2)-C(6)-C(7)-C(8)	1.2(4)
N(7)-Co(1)-N(1)-C(1)	-91.24(17)	C(1)-C(6)-C(7)-C(8)	-178.6(2)
C(5)-N(1)-C(1)-C(2)	-2.2(3)	C(6)-C(7)-C(8)-C(9)	0.1(4)
Co(1)-N(1)-C(1)-C(2)	178.20(16)	C(7)-C(8)-C(9)-C(10)	-0.9(4)
C(5)-N(1)-C(1)-C(6)	179.09(19)	C(6)-N(2)-C(10)-C(9)	0.9(4)
Co(1)-N(1)-C(1)-C(6)	-0.5(2)	Co(1)-N(2)-C(10)-C(9)	-177.19(19)
N(1)-C(1)-C(2)-C(3)	1.4(3)	C(8)-C(9)-C(10)-N(2)	0.3(4)
C(6)-C(1)-C(2)-C(3)	180.0(2)	C(15)-N(3)-C(11)-C(12)	-0.3(3)
C(1)-C(2)-C(3)-C(4)	0.9(3)	Co(1)-N(3)-C(11)-C(12)	176.55(17)
C(1)-C(2)-C(3)-C(18)	-176.3(2)	C(15)-N(3)-C(11)-C(5)	-179.34(19)
C(2)-C(3)-C(4)-C(5)	-2.4(3)	Co(1)-N(3)-C(11)-C(5)	-2.4(2)
C(18)-C(3)-C(4)-C(5)	174.7(2)	N(1)-C(5)-C(11)-N(3)	2.7(3)
C(1)-N(1)-C(5)-C(4)	0.6(3)	C(4)-C(5)-C(11)-N(3)	-179.4(2)
Co(1)-N(1)-C(5)-C(4)	-179.83(16)	N(1)-C(5)-C(11)-C(12)	-176.2(2)
C(1)-N(1)-C(5)-C(11)	178.60(19)	C(4)-C(5)-C(11)-C(12)	1.7(4)
Co(1)-N(1)-C(5)-C(11)	-1.8(2)	N(3)-C(11)-C(12)-C(13)	0.3(3)
C(3)-C(4)-C(5)-N(1)	1.8(3)	C(5)-C(11)-C(12)-C(13)	179.2(2)
C(3)-C(4)-C(5)-C(11)	-176.0(2)	C(11)-C(12)-C(13)-C(14)	0.0(4)
C(10)-N(2)-C(6)-C(7)	-1.7(3)	C(12)-C(13)-C(14)-C(15)	-0.2(4)
Co(1)-N(2)-C(6)-C(7)	176.70(18)	C(11)-N(3)-C(15)-C(14)	0.1(3)

Co(1)-N(3)-C(15)-C(14)	-176.27(18)	Co(1)-N(5)-C(26)-C(32)	3.1(3)
C(13)-C(14)-C(15)-N(3)	0.2(4)	C(24)-C(25)-C(26)-N(5)	-4.5(3)
C(20)-N(4)-C(16)-C(17)	-0.4(4)	C(24)-C(25)-C(26)-C(32)	172.9(2)
C(21)-N(4)-C(16)-C(17)	178.1(2)	C(31)-N(6)-C(27)-C(28)	-1.8(3)
N(4)-C(16)-C(17)-C(18)	0.8(4)	Co(1)-N(6)-C(27)-C(28)	178.67(18)
C(16)-C(17)-C(18)-C(19)	-1.1(3)	C(31)-N(6)-C(27)-C(22)	176.9(2)
C(16)-C(17)-C(18)-C(3)	177.0(2)	Co(1)-N(6)-C(27)-C(22)	-2.6(2)
C(2)-C(3)-C(18)-C(17)	-9.8(3)	N(5)-C(22)-C(27)-N(6)	-0.6(3)
C(4)-C(3)-C(18)-C(17)	173.1(2)	C(23)-C(22)-C(27)-N(6)	-179.4(2)
C(2)-C(3)-C(18)-C(19)	168.2(2)	N(5)-C(22)-C(27)-C(28)	178.0(2)
C(4)-C(3)-C(18)-C(19)	-8.9(3)	C(23)-C(22)-C(27)-C(28)	-0.7(4)
C(17)-C(18)-C(19)-C(20)	1.1(3)	N(6)-C(27)-C(28)-C(29)	2.7(4)
C(3)-C(18)-C(19)-C(20)	-177.0(2)	C(22)-C(27)-C(28)-C(29)	-175.9(2)
C(16)-N(4)-C(20)-C(19)	0.5(4)	C(27)-C(28)-C(29)-C(30)	-1.8(4)
C(21)-N(4)-C(20)-C(19)	-178.1(2)	C(28)-C(29)-C(30)-C(31)	0.1(4)
C(18)-C(19)-C(20)-N(4)	-0.9(4)	C(27)-N(6)-C(31)-C(30)	0.0(4)
C(26)-N(5)-C(22)-C(23)	1.4(3)	Co(1)-N(6)-C(31)-C(30)	179.4(2)
Co(1)-N(5)-C(22)-C(23)	-177.04(16)	C(29)-C(30)-C(31)-N(6)	0.8(4)
C(26)-N(5)-C(22)-C(27)	-177.42(19)	C(36)-N(7)-C(32)-C(33)	0.2(3)
Co(1)-N(5)-C(22)-C(27)	4.1(3)	Co(1)-N(7)-C(32)-C(33)	-178.87(17)
N(5)-C(22)-C(23)-C(24)	-2.9(3)	C(36)-N(7)-C(32)-C(26)	177.90(19)
C(27)-C(22)-C(23)-C(24)	175.7(2)	Co(1)-N(7)-C(32)-C(26)	-1.2(2)
C(22)-C(23)-C(24)-C(25)	0.8(3)	N(5)-C(26)-C(32)-N(7)	-1.0(3)
C(22)-C(23)-C(24)-C(39)	177.5(2)	C(25)-C(26)-C(32)-N(7)	-178.6(2)
C(23)-C(24)-C(25)-C(26)	2.9(3)	N(5)-C(26)-C(32)-C(33)	176.6(2)
C(39)-C(24)-C(25)-C(26)	-173.9(2)	C(25)-C(26)-C(32)-C(33)	-0.9(4)
C(22)-N(5)-C(26)-C(25)	2.4(3)	N(7)-C(32)-C(33)-C(34)	0.3(3)
Co(1)-N(5)-C(26)-C(25)	-179.20(16)	C(26)-C(32)-C(33)-C(34)	-177.2(2)
C(22)-N(5)-C(26)-C(32)	-175.30(19)	C(32)-C(33)-C(34)-C(35)	-0.2(4)

C(33)-C(34)-C(35)-C(36)	-0.4(4)	Co(2)-N(9)-C(43)-C(48)	0.4(2)
C(32)-N(7)-C(36)-C(35)	-0.9(3)	N(9)-C(43)-C(44)-C(45)	-0.2(3)
Co(1)-N(7)-C(36)-C(35)	178.07(17)	C(48)-C(43)-C(44)-C(45)	176.9(2)
C(34)-C(35)-C(36)-N(7)	0.9(4)	C(43)-C(44)-C(45)-C(46)	0.9(3)
C(41)-N(8)-C(37)-C(38)	-0.6(4)	C(43)-C(44)-C(45)-C(60)	-175.2(2)
C(42)-N(8)-C(37)-C(38)	179.3(2)	C(44)-C(45)-C(46)-C(47)	-1.1(3)
N(8)-C(37)-C(38)-C(39)	-0.6(4)	C(60)-C(45)-C(46)-C(47)	175.0(2)
C(37)-C(38)-C(39)-C(40)	1.2(4)	C(43)-N(9)-C(47)-C(46)	0.1(3)
C(37)-C(38)-C(39)-C(24)	-176.5(2)	Co(2)-N(9)-C(47)-C(46)	-177.93(16)
C(23)-C(24)-C(39)-C(38)	-41.2(3)	C(43)-N(9)-C(47)-C(53)	178.30(19)
C(25)-C(24)-C(39)-C(38)	135.5(2)	Co(2)-N(9)-C(47)-C(53)	0.3(2)
C(23)-C(24)-C(39)-C(40)	141.1(2)	C(45)-C(46)-C(47)-N(9)	0.6(3)
C(25)-C(24)-C(39)-C(40)	-42.1(3)	C(45)-C(46)-C(47)-C(53)	-177.4(2)
C(38)-C(39)-C(40)-C(41)	-0.7(4)	C(52)-N(10)-C(48)-C(49)	-1.7(3)
C(24)-C(39)-C(40)-C(41)	177.0(2)	Co(2)-N(10)-C(48)-C(49)	175.36(18)
C(37)-N(8)-C(41)-C(40)	1.2(4)	C(52)-N(10)-C(48)-C(43)	177.1(2)
C(42)-N(8)-C(41)-C(40)	-178.7(2)	Co(2)-N(10)-C(48)-C(43)	-5.9(2)
C(39)-C(40)-C(41)-N(8)	-0.5(4)	N(9)-C(43)-C(48)-N(10)	4.0(3)
N(14)-Co(2)-N(13)-C(64)	-3.04(16)	C(44)-C(43)-C(48)-N(10)	-173.2(2)
N(15)-Co(2)-N(13)-C(64)	175.53(17)	N(9)-C(43)-C(48)-C(49)	-177.3(2)
N(10)-Co(2)-N(13)-C(64)	86.08(17)	C(44)-C(43)-C(48)-C(49)	5.5(3)
N(11)-Co(2)-N(13)-C(64)	-96.54(17)	N(10)-C(48)-C(49)-C(50)	1.1(4)
N(14)-Co(2)-N(13)-C(68)	177.70(17)	C(43)-C(48)-C(49)-C(50)	-177.5(2)
N(15)-Co(2)-N(13)-C(68)	-3.73(16)	C(48)-C(49)-C(50)-C(51)	0.0(4)
N(10)-Co(2)-N(13)-C(68)	-93.17(17)	C(49)-C(50)-C(51)-C(52)	-0.6(4)
N(11)-Co(2)-N(13)-C(68)	84.21(17)	C(48)-N(10)-C(52)-C(51)	1.1(3)
C(47)-N(9)-C(43)-C(44)	-0.4(3)	Co(2)-N(10)-C(52)-C(51)	-175.37(18)
Co(2)-N(9)-C(43)-C(44)	177.69(16)	C(50)-C(51)-C(52)-N(10)	0.1(4)
C(47)-N(9)-C(43)-C(48)	-177.67(19)	C(57)-N(11)-C(53)-C(54)	-0.4(3)

Co(2)-N(11)-C(53)-C(54)	173.90(17)	Co(2)-N(13)-C(64)-C(65)	-179.43(16)
C(57)-N(11)-C(53)-C(47)	-178.87(19)	C(68)-N(13)-C(64)-C(69)	-179.24(19)
Co(2)-N(11)-C(53)-C(47)	-4.6(2)	Co(2)-N(13)-C(64)-C(69)	1.5(2)
N(9)-C(47)-C(53)-N(11)	3.1(3)	N(13)-C(64)-C(65)-C(66)	-2.3(3)
C(46)-C(47)-C(53)-N(11)	-178.8(2)	C(69)-C(64)-C(65)-C(66)	176.6(2)
N(9)-C(47)-C(53)-C(54)	-175.3(2)	C(64)-C(65)-C(66)-C(67)	1.9(3)
C(46)-C(47)-C(53)-C(54)	2.8(3)	C(64)-C(65)-C(66)-C(81)	178.7(2)
N(11)-C(53)-C(54)-C(55)	-0.1(3)	C(65)-C(66)-C(67)-C(68)	0.7(3)
C(47)-C(53)-C(54)-C(55)	178.2(2)	C(81)-C(66)-C(67)-C(68)	-176.2(2)
C(53)-C(54)-C(55)-C(56)	0.4(4)	C(64)-N(13)-C(68)-C(67)	3.0(3)
C(54)-C(55)-C(56)-C(57)	-0.1(4)	Co(2)-N(13)-C(68)-C(67)	-177.77(16)
C(53)-N(11)-C(57)-C(56)	0.6(3)	C(64)-N(13)-C(68)-C(74)	-174.29(19)
Co(2)-N(11)-C(57)-C(56)	-172.46(18)	Co(2)-N(13)-C(68)-C(74)	5.0(2)
C(55)-C(56)-C(57)-N(11)	-0.4(4)	C(66)-C(67)-C(68)-N(13)	-3.2(3)
C(62)-N(12)-C(58)-C(59)	0.7(4)	C(66)-C(67)-C(68)-C(74)	173.6(2)
C(63)-N(12)-C(58)-C(59)	-178.4(2)	C(73)-N(14)-C(69)-C(70)	-2.1(3)
N(12)-C(58)-C(59)-C(60)	0.1(4)	Co(2)-N(14)-C(69)-C(70)	177.12(18)
C(58)-C(59)-C(60)-C(61)	-1.1(4)	C(73)-N(14)-C(69)-C(64)	176.5(2)
C(58)-C(59)-C(60)-C(45)	175.8(2)	Co(2)-N(14)-C(69)-C(64)	-4.3(2)
C(46)-C(45)-C(60)-C(61)	35.0(3)	N(13)-C(64)-C(69)-N(14)	2.0(3)
C(44)-C(45)-C(60)-C(61)	-148.9(2)	C(65)-C(64)-C(69)-N(14)	-177.0(2)
C(46)-C(45)-C(60)-C(59)	-141.8(2)	N(13)-C(64)-C(69)-C(70)	-179.5(2)
C(44)-C(45)-C(60)-C(59)	34.3(3)	C(65)-C(64)-C(69)-C(70)	1.6(4)
C(59)-C(60)-C(61)-C(62)	1.3(4)	N(14)-C(69)-C(70)-C(71)	2.5(4)
C(45)-C(60)-C(61)-C(62)	-175.6(2)	C(64)-C(69)-C(70)-C(71)	-176.0(2)
C(58)-N(12)-C(62)-C(61)	-0.5(4)	C(69)-C(70)-C(71)-C(72)	-1.0(4)
C(63)-N(12)-C(62)-C(61)	178.6(2)	C(70)-C(71)-C(72)-C(73)	-0.6(4)
C(60)-C(61)-C(62)-N(12)	-0.5(4)	C(69)-N(14)-C(73)-C(72)	0.4(4)
C(68)-N(13)-C(64)-C(65)	-0.2(3)	Co(2)-N(14)-C(73)-C(72)	-178.72(19)

C(71)-C(72)-C(73)-N(14)	0.9(4)	C(81)-C(82)-C(83)-N(16)	0.0(4)
C(78)-N(15)-C(74)-C(75)	0.6(3)		
Co(2)-N(15)-C(74)-C(75)	-176.56(17)		
C(78)-N(15)-C(74)-C(68)	177.78(19)		
Co(2)-N(15)-C(74)-C(68)	0.6(2)		
N(13)-C(68)-C(74)-N(15)	-3.4(3)		
C(67)-C(68)-C(74)-N(15)	179.6(2)		
N(13)-C(68)-C(74)-C(75)	173.7(2)		
C(67)-C(68)-C(74)-C(75)	-3.3(4)		
N(15)-C(74)-C(75)-C(76)	-0.5(3)		
C(68)-C(74)-C(75)-C(76)	-177.4(2)		
C(74)-C(75)-C(76)-C(77)	0.2(4)		
C(75)-C(76)-C(77)-C(78)	0.0(4)		
C(74)-N(15)-C(78)-C(77)	-0.4(3)		
Co(2)-N(15)-C(78)-C(77)	176.28(17)		
C(76)-C(77)-C(78)-N(15)	0.1(4)		
C(83)-N(16)-C(79)-C(80)	-1.8(4)		
C(84)-N(16)-C(79)-C(80)	179.1(2)		
N(16)-C(79)-C(80)-C(81)	-0.4(4)		
C(79)-C(80)-C(81)-C(82)	2.3(3)		
C(79)-C(80)-C(81)-C(66)	-175.4(2)		
C(67)-C(66)-C(81)-C(80)	143.6(2)		
C(65)-C(66)-C(81)-C(80)	-33.2(3)		
C(67)-C(66)-C(81)-C(82)	-34.0(3)		
C(65)-C(66)-C(81)-C(82)	149.2(2)		
C(80)-C(81)-C(82)-C(83)	-2.1(4)		
C(66)-C(81)-C(82)-C(83)	175.6(2)		
C(79)-N(16)-C(83)-C(82)	2.0(4)		
C(84)-N(16)-C(83)-C(82)	-178.9(2)		

Symmetry transformations used to generate equivalent atoms:

```
#1 x,-y+1/2,z+1/2  #2 x-1,y,z  #3 -x+1,-y,-z+1  
#4 -x,-y,-z+1  #5 x-1,-y+1/2,z+1/2  #6 -x,-y+1,-z+1  
#7 -x+1,y-1/2,-z+1/2  #8 -x+1,-y+1,-z+1  #9 -x+1,y+1/2,-z+1/2  #10 x+1,y,z
```

Table S7. Crystal data and structure refinement for **1³⁺·3PF₆**.

Identification code	1_3plus	
Empirical formula	C46 H40 Co F18 N10 P3	
Formula weight	1226.72	
Temperature	120(2) K	
Wavelength	0.71073 Å	
Crystal system	Monoclinic	
Space group	C2/c	
Unit cell dimensions	a = 15.050(2) Å	α= 90°.
	b = 15.460(2) Å	β= 108.853(3)°.
	c = 22.031(3) Å	γ = 90°.
Volume	4851.0(13) Å ³	
Z	4	
Density (calculated)	1.680 Mg/m ³	
Absorption coefficient	0.570 mm ⁻¹	
F(000)	2480	
Crystal size	.24 x .13 x .08 mm ³	
Theta range for data collection	1.944 to 27.859°.	
Index ranges	-19<=h<=19, -20<=k<=17, -28<=l<=26	
Reflections collected	16648	
Independent reflections	5744 [R(int) = 0.0543]	
Completeness to theta = 25.242°	99.9 %	
Absorption correction	Semi-empirical from equivalents	
Max. and min. transmission	0.7456 and 0.5790	
Refinement method	Full-matrix least-squares on F ²	
Data / restraints / parameters	5744 / 612 / 358	
Goodness-of-fit on F ²	1.067	
Final R indices [I>2sigma(I)]	R1 = 0.0782, wR2 = 0.1953	
R indices (all data)	R1 = 0.1128, wR2 = 0.2195	
Extinction coefficient	n/a	
Largest diff. peak and hole	0.720 and -1.074 e.Å ⁻³	

Table S8. Atomic coordinates ($x \times 10^4$) and equivalent isotropic displacement parameters ($\text{\AA}^2 \times 10^3$) for $\mathbf{1}^{3+}$. U(eq) is defined as one third of the trace of the orthogonalized U^{ij} tensor.

	x	y	z	U(eq)
Co(1)	0	2034(1)	2500	29(1)
P(1)	7206(1)	4901(1)	4611(1)	29(1)
P(2)	0	5632(1)	2500	59(1)
F(1)	6131(2)	4827(2)	4576(2)	44(1)
F(2)	7492(2)	4958(2)	5375(1)	44(1)
F(3)	7119(3)	5923(2)	4568(2)	51(1)
F(4)	8282(2)	4966(2)	4659(2)	55(1)
F(5)	6912(2)	4839(2)	3851(1)	43(1)
F(6)	7291(2)	3871(2)	4658(2)	50(1)
F(7)	-752(3)	4911(2)	2181(2)	59(1)
F(8)	-356(3)	5636(3)	3105(2)	80(1)
F(9A)	800(9)	6257(7)	2932(5)	84(3)
F(9B)	674(10)	6455(7)	2674(6)	84(3)
N(1)	-188(2)	2949(2)	3129(2)	21(1)
N(2)	1250(2)	2108(2)	3123(2)	20(1)
N(3)	717(2)	1110(2)	2177(2)	23(1)
N(4)	5860(3)	2759(3)	5230(2)	30(1)
N(5)	1755(5)	8242(5)	2659(4)	85(2)
C(2)	-1005(3)	3336(3)	3096(2)	26(1)
C(3)	-1073(3)	3927(3)	3544(2)	30(1)
C(4)	-272(3)	4132(3)	4052(2)	30(1)
C(5)	570(3)	3748(3)	4091(2)	28(1)
C(6)	601(3)	3157(3)	3626(2)	22(1)
C(7)	1443(3)	2703(3)	3605(2)	21(1)
C(8)	2337(3)	2838(3)	4007(2)	22(1)
C(9)	3103(3)	2372(3)	3933(2)	22(1)
C(10)	2888(3)	1764(3)	3427(2)	23(1)
C(11)	1980(3)	1649(3)	3036(2)	21(1)
C(12)	1661(3)	1063(3)	2492(2)	22(1)
C(13)	2237(3)	489(3)	2302(2)	28(1)
C(14)	1844(3)	-46(3)	1783(2)	35(1)

C(15)	879(3)	-11(3)	1469(2)	34(1)
C(16)	348(3)	566(3)	1678(2)	28(1)
C(17)	5165(3)	3314(3)	5207(2)	32(1)
C(18)	4281(3)	3212(3)	4789(2)	30(1)
C(19)	4045(3)	2508(3)	4362(2)	24(1)
C(20)	4800(3)	1951(3)	4385(2)	36(1)
C(21)	5676(3)	2084(4)	4816(3)	40(1)
C(22)	6791(3)	2884(4)	5717(3)	40(1)
C(23)	1259(6)	8205(6)	2944(5)	86(3)
C(24)	654(7)	8125(8)	3348(6)	116(4)

—

Table S9. Bond lengths [Å] and angles [°] for **1³⁺**.

Co(1)-N(2)#1	1.941(3)	N(3)-C(12)	1.366(5)
Co(1)-N(2)	1.941(3)	N(4)-C(17)	1.340(6)
Co(1)-N(3)#1	2.052(4)	N(4)-C(21)	1.355(6)
Co(1)-N(3)	2.052(4)	N(4)-C(22)	1.477(6)
Co(1)-N(1)#1	2.062(4)	N(5)-C(23)	1.121(10)
Co(1)-N(1)	2.062(4)	C(2)-C(3)	1.373(7)
P(1)-F(3)	1.586(3)	C(3)-C(4)	1.391(6)
P(1)-F(5)	1.591(3)	C(4)-C(5)	1.376(6)
P(1)-F(4)	1.593(3)	C(5)-C(6)	1.386(6)
P(1)-F(6)	1.598(3)	C(6)-C(7)	1.462(6)
P(1)-F(2)	1.598(3)	C(7)-C(8)	1.367(5)
P(1)-F(1)	1.599(3)	C(8)-C(9)	1.414(6)
P(2)-F(7)	1.583(4)	C(9)-C(10)	1.412(6)
P(2)-F(7)#1	1.583(4)	C(9)-C(19)	1.442(6)
P(2)-F(8)	1.589(4)	C(10)-C(11)	1.371(6)
P(2)-F(8)#1	1.589(4)	C(11)-C(12)	1.455(6)
P(2)-F(9B)	1.595(2)	C(12)-C(13)	1.397(6)
P(2)-F(9B)#1	1.595(2)	C(13)-C(14)	1.379(7)
P(2)-F(9A)	1.597(2)	C(14)-C(15)	1.393(7)
P(2)-F(9A)#1	1.597(2)	C(15)-C(16)	1.372(7)
F(9A)-F(9B)	0.619(19)	C(17)-C(18)	1.361(6)
N(1)-C(2)	1.348(5)	C(18)-C(19)	1.409(6)
N(1)-C(6)	1.368(5)	C(19)-C(20)	1.414(6)
N(2)-C(7)	1.364(5)	C(20)-C(21)	1.369(6)
N(2)-C(11)	1.371(5)	C(23)-C(24)	1.469(13)
N(3)-C(16)	1.353(6)		
N(2)#1-Co(1)-N(2)	173.3(2)	N(2)-Co(1)-N(1)#1	97.05(14)
N(2)#1-Co(1)-N(3)#1	77.74(14)	N(3)#1-Co(1)-N(1)#1	155.84(13)
N(2)-Co(1)-N(3)#1	107.09(14)	N(3)-Co(1)-N(1)#1	92.45(14)
N(2)#1-Co(1)-N(3)	107.10(14)	N(2)#1-Co(1)-N(1)	97.05(14)
N(2)-Co(1)-N(3)	77.74(14)	N(2)-Co(1)-N(1)	78.28(14)
N(3)#1-Co(1)-N(3)	91.7(2)	N(3)#1-Co(1)-N(1)	92.45(14)
N(2)#1-Co(1)-N(1)#1	78.28(14)	N(3)-Co(1)-N(1)	155.84(13)

N(1)#1-Co(1)-N(1)	93.40(19)	F(9B)#1-P(2)-F(9A)	87.6(5)
F(3)-P(1)-F(5)	90.45(18)	F(7)-P(2)-F(9A)#1	82.5(6)
F(3)-P(1)-F(4)	90.2(2)	F(7)#1-P(2)-F(9A)#1	169.9(4)
F(5)-P(1)-F(4)	90.22(18)	F(8)-P(2)-F(9A)#1	96.0(6)
F(3)-P(1)-F(6)	179.7(2)	F(8)#1-P(2)-F(9A)#1	83.8(6)
F(5)-P(1)-F(6)	89.78(18)	F(9B)-P(2)-F(9A)#1	87.6(5)
F(4)-P(1)-F(6)	90.0(2)	F(9B)#1-P(2)-F(9A)#1	22.4(7)
F(3)-P(1)-F(2)	89.89(18)	F(9A)-P(2)-F(9A)#1	105.5(11)
F(5)-P(1)-F(2)	179.4(2)	F(9B)-F(9A)-P(2)	78.6(4)
F(4)-P(1)-F(2)	90.27(18)	F(9A)-F(9B)-P(2)	79.0(4)
F(6)-P(1)-F(2)	89.89(18)	C(2)-N(1)-C(6)	118.6(4)
F(3)-P(1)-F(1)	90.39(18)	C(2)-N(1)-Co(1)	126.1(3)
F(5)-P(1)-F(1)	90.67(17)	C(6)-N(1)-Co(1)	115.3(3)
F(4)-P(1)-F(1)	178.9(2)	C(7)-N(2)-C(11)	118.6(3)
F(6)-P(1)-F(1)	89.47(19)	C(7)-N(2)-Co(1)	120.2(3)
F(2)-P(1)-F(1)	88.84(17)	C(11)-N(2)-Co(1)	120.5(3)
F(7)-P(2)-F(7)#1	90.3(3)	C(16)-N(3)-C(12)	117.9(4)
F(7)-P(2)-F(8)	89.3(2)	C(16)-N(3)-Co(1)	126.2(3)
F(7)#1-P(2)-F(8)	91.0(2)	C(12)-N(3)-Co(1)	115.9(3)
F(7)-P(2)-F(8)#1	91.0(2)	C(17)-N(4)-C(21)	118.8(4)
F(7)#1-P(2)-F(8)#1	89.3(2)	C(17)-N(4)-C(22)	119.3(4)
F(8)-P(2)-F(8)#1	179.5(4)	C(21)-N(4)-C(22)	121.9(4)
F(7)-P(2)-F(9B)	167.7(5)	N(1)-C(2)-C(3)	122.4(4)
F(7)#1-P(2)-F(9B)	98.5(6)	C(2)-C(3)-C(4)	118.9(4)
F(8)-P(2)-F(9B)	99.0(6)	C(5)-C(4)-C(3)	119.6(4)
F(8)#1-P(2)-F(9B)	80.7(6)	C(4)-C(5)-C(6)	119.2(4)
F(7)-P(2)-F(9B)#1	98.5(6)	N(1)-C(6)-C(5)	121.3(4)
F(7)#1-P(2)-F(9B)#1	167.7(5)	N(1)-C(6)-C(7)	113.5(4)
F(8)-P(2)-F(9B)#1	80.7(6)	C(5)-C(6)-C(7)	125.2(4)
F(8)#1-P(2)-F(9B)#1	99.0(6)	N(2)-C(7)-C(8)	121.7(4)
F(9B)-P(2)-F(9B)#1	74.1(12)	N(2)-C(7)-C(6)	112.3(3)
F(7)-P(2)-F(9A)	169.9(4)	C(8)-C(7)-C(6)	126.0(4)
F(7)#1-P(2)-F(9A)	82.5(6)	C(7)-C(8)-C(9)	121.0(4)
F(8)-P(2)-F(9A)	83.8(6)	C(10)-C(9)-C(8)	116.3(4)
F(8)#1-P(2)-F(9A)	96.0(6)	C(10)-C(9)-C(19)	122.7(4)
F(9B)-P(2)-F(9A)	22.4(7)	C(8)-C(9)-C(19)	121.0(4)

C(11)-C(10)-C(9)	120.6(4)	N(3)-C(16)-C(15)	123.0(4)
N(2)-C(11)-C(10)	121.7(4)	N(4)-C(17)-C(18)	122.1(5)
N(2)-C(11)-C(12)	111.8(3)	C(17)-C(18)-C(19)	121.5(4)
C(10)-C(11)-C(12)	126.5(4)	C(18)-C(19)-C(20)	114.8(4)
N(3)-C(12)-C(13)	121.6(4)	C(18)-C(19)-C(9)	122.2(4)
N(3)-C(12)-C(11)	113.5(4)	C(20)-C(19)-C(9)	122.9(4)
C(13)-C(12)-C(11)	124.9(4)	C(21)-C(20)-C(19)	121.2(5)
C(14)-C(13)-C(12)	119.2(4)	N(4)-C(21)-C(20)	121.5(5)
C(13)-C(14)-C(15)	119.2(4)	N(5)-C(23)-C(24)	176.4(12)
C(16)-C(15)-C(14)	119.1(4)		

Symmetry transformations used to generate equivalent atoms: #1 -x,y,-z+1/2

Table S10. Anisotropic displacement parameters ($\text{\AA}^2 \times 10^3$) for $\mathbf{1}^{3+}$. The anisotropic displacement factor exponent takes the form: $-2\pi^2 [h^2 a^* U_{11} + \dots + 2 h k a^* b^* U_{12}]$

	U ₁₁	U ₂₂	U ₃₃	U ₂₃	U ₁₃	U ₁₂
Co(1)	26(1)	35(1)	26(1)	0	8(1)	0
P(1)	24(1)	31(1)	32(1)	-1(1)	8(1)	4(1)
P(2)	59(1)	36(1)	99(2)	0	51(2)	0
F(1)	24(1)	64(2)	43(2)	9(2)	8(1)	-3(1)
F(2)	41(2)	54(2)	33(2)	-6(1)	8(1)	-6(1)
F(3)	76(2)	30(2)	69(2)	3(2)	52(2)	5(2)
F(4)	26(2)	81(3)	61(2)	-29(2)	19(2)	-5(2)
F(5)	42(2)	54(2)	33(2)	2(1)	12(1)	3(1)
F(6)	59(2)	31(2)	50(2)	1(1)	1(2)	11(1)
F(7)	57(2)	59(2)	71(3)	-3(2)	34(2)	-3(2)
F(8)	79(3)	81(3)	100(3)	-37(3)	59(3)	-11(2)
F(9A)	91(4)	40(4)	140(7)	-10(4)	65(5)	-18(4)
F(9B)	91(4)	40(4)	140(7)	-10(4)	65(5)	-18(4)
N(1)	19(2)	25(2)	19(2)	1(1)	7(1)	0(1)
N(2)	16(2)	28(2)	16(2)	-1(1)	6(1)	0(1)
N(3)	21(2)	28(2)	19(2)	-2(1)	4(1)	2(1)
N(4)	22(2)	37(2)	27(2)	1(2)	3(2)	-2(2)

N(5)	57(4)	100(5)	94(5)	-4(4)	21(4)	-16(4)
C(2)	16(2)	31(2)	30(2)	2(2)	7(2)	1(2)
C(3)	23(2)	37(3)	36(2)	-5(2)	15(2)	1(2)
C(4)	27(2)	34(2)	33(2)	-11(2)	15(2)	0(2)
C(5)	22(2)	35(2)	29(2)	-9(2)	11(2)	-4(2)
C(6)	21(2)	28(2)	20(2)	1(2)	9(2)	0(2)
C(7)	19(2)	26(2)	19(2)	2(2)	7(2)	-1(2)
C(8)	21(2)	25(2)	20(2)	-2(2)	5(2)	-1(2)
C(9)	19(2)	27(2)	20(2)	1(2)	7(2)	-2(2)
C(10)	18(2)	27(2)	23(2)	1(2)	7(2)	4(2)
C(11)	22(2)	23(2)	18(2)	2(2)	7(2)	3(2)
C(12)	21(2)	26(2)	18(2)	2(2)	4(2)	2(2)
C(13)	26(2)	30(2)	27(2)	-2(2)	7(2)	5(2)
C(14)	34(2)	35(3)	33(3)	-8(2)	8(2)	8(2)
C(15)	35(2)	34(2)	27(2)	-11(2)	2(2)	2(2)
C(16)	25(2)	33(2)	23(2)	-2(2)	2(2)	2(2)
C(17)	27(2)	35(2)	33(2)	-5(2)	8(2)	-1(2)
C(18)	23(2)	33(2)	33(2)	-6(2)	7(2)	-2(2)
C(19)	22(2)	31(2)	19(2)	4(2)	7(2)	0(2)
C(20)	24(2)	41(3)	35(3)	-10(2)	-1(2)	6(2)
C(21)	22(2)	47(3)	43(3)	-8(2)	-1(2)	9(2)
C(22)	24(2)	47(3)	38(3)	-1(2)	-3(2)	-5(2)
C(23)	65(5)	79(5)	120(7)	-8(5)	41(5)	-13(4)
C(24)	93(7)	140(9)	129(9)	-36(7)	55(6)	-31(6)

Table S11. Hydrogen coordinates ($\times 10^4$) and isotropic displacement parameters ($\text{\AA}^2 \times 10^3$) for $\mathbf{1}^{3+}$.

	x	y	z	U(eq)
H(2)	-1553	3195	2750	31
H(3)	-1657	4191	3508	37
H(4)	-305	4534	4370	36

H(5)	1124	3887	4433	34
H(8)	2445	3251	4342	27
H(10)	3377	1431	3358	27
H(13)	2892	468	2526	34
H(14)	2226	-434	1642	42
H(15)	593	-382	1116	41
H(16)	-310	583	1462	34
H(17)	5295	3794	5492	39
H(18)	3812	3626	4786	36
H(20)	4698	1477	4096	43
H(21)	6168	1692	4825	48
H(22A)	7236	2467	5644	59
H(22B)	6742	2793	6146	59
H(22C)	7011	3473	5686	59
H(24A)	25	8341	3112	174
H(24B)	920	8464	3741	174
H(24C)	614	7515	3459	174

Table S12. Torsion angles [°] for **1³⁺**.

F(7)-P(2)-F(9A)-F(9B)	-179.6(14)	N(1)-C(2)-C(3)-C(4)	-0.2(7)
F(7)#1-P(2)-F(9A)-F(9B)	136(3)	C(2)-C(3)-C(4)-C(5)	0.7(7)
F(8)-P(2)-F(9A)-F(9B)	-133(3)	C(3)-C(4)-C(5)-C(6)	-0.6(7)
F(8)#1-P(2)-F(9A)-F(9B)	47(3)	C(2)-N(1)-C(6)-C(5)	0.4(6)
F(9B)#1-P(2)-F(9A)-F(9B)	-52(4)	Co(1)-N(1)-C(6)-C(5)	-178.5(3)
F(9A)#1-P(2)-F(9A)-F(9B)	-38(3)	C(2)-N(1)-C(6)-C(7)	-179.3(4)
F(7)-P(2)-F(9B)-F(9A)	179.7(11)	Co(1)-N(1)-C(6)-C(7)	1.7(5)
F(7)#1-P(2)-F(9B)-F(9A)	-45(3)	C(4)-C(5)-C(6)-N(1)	0.1(7)
F(8)-P(2)-F(9B)-F(9A)	48(3)	C(4)-C(5)-C(6)-C(7)	179.8(4)
F(8)#1-P(2)-F(9B)-F(9A)	-133(3)	C(11)-N(2)-C(7)-C(8)	-1.3(6)
F(9B)#1-P(2)-F(9B)-F(9A)	125(4)	Co(1)-N(2)-C(7)-C(8)	-172.6(3)
F(9A)#1-P(2)-F(9B)-F(9A)	143(3)	C(11)-N(2)-C(7)-C(6)	178.4(4)
C(6)-N(1)-C(2)-C(3)	-0.3(7)	Co(1)-N(2)-C(7)-C(6)	7.1(5)
Co(1)-N(1)-C(2)-C(3)	178.5(3)	N(1)-C(6)-C(7)-N(2)	-5.4(5)

C(5)-C(6)-C(7)-N(2)	174.9(4)	C(8)-C(9)-C(19)-C(18)	-12.6(7)
N(1)-C(6)-C(7)-C(8)	174.3(4)	C(10)-C(9)-C(19)-C(20)	-11.1(7)
C(5)-C(6)-C(7)-C(8)	-5.4(7)	C(8)-C(9)-C(19)-C(20)	167.7(4)
N(2)-C(7)-C(8)-C(9)	1.0(6)	C(18)-C(19)-C(20)-C(21)	2.8(7)
C(6)-C(7)-C(8)-C(9)	-178.6(4)	C(9)-C(19)-C(20)-C(21)	-177.4(5)
C(7)-C(8)-C(9)-C(10)	-0.5(6)	C(17)-N(4)-C(21)-C(20)	-0.9(8)
C(7)-C(8)-C(9)-C(19)	-179.4(4)	C(22)-N(4)-C(21)-C(20)	177.1(5)
C(8)-C(9)-C(10)-C(11)	0.3(6)	C(19)-C(20)-C(21)-N(4)	-1.2(9)
C(19)-C(9)-C(10)-C(11)	179.1(4)		
C(7)-N(2)-C(11)-C(10)	1.1(6)		
Co(1)-N(2)-C(11)-C(10)	172.4(3)		
C(7)-N(2)-C(11)-C(12)	-178.2(4)		
Co(1)-N(2)-C(11)-C(12)	-7.0(5)		
C(9)-C(10)-C(11)-N(2)	-0.6(7)		
C(9)-C(10)-C(11)-C(12)	178.6(4)		
C(16)-N(3)-C(12)-C(13)	1.6(6)		
Co(1)-N(3)-C(12)-C(13)	-177.0(3)		
C(16)-N(3)-C(12)-C(11)	-177.6(4)		
Co(1)-N(3)-C(12)-C(11)	3.8(5)		
N(2)-C(11)-C(12)-N(3)	1.6(5)		
C(10)-C(11)-C(12)-N(3)	-177.7(4)		
N(2)-C(11)-C(12)-C(13)	-177.5(4)		
C(10)-C(11)-C(12)-C(13)	3.2(7)		
N(3)-C(12)-C(13)-C(14)	-0.3(7)		
C(11)-C(12)-C(13)-C(14)	178.7(5)		
C(12)-C(13)-C(14)-C(15)	-1.0(8)		
C(13)-C(14)-C(15)-C(16)	1.1(8)		
C(12)-N(3)-C(16)-C(15)	-1.6(7)		
Co(1)-N(3)-C(16)-C(15)	176.9(4)		
C(14)-C(15)-C(16)-N(3)	0.2(8)		
C(21)-N(4)-C(17)-C(18)	1.1(8)		
C(22)-N(4)-C(17)-C(18)	-176.9(5)		
N(4)-C(17)-C(18)-C(19)	0.8(8)		
C(17)-C(18)-C(19)-C(20)	-2.7(7)		
C(17)-C(18)-C(19)-C(9)	177.6(4)		
C(10)-C(9)-C(19)-C(18)	168.6(4)		

Symmetry transformations used to generate equivalent atoms: #1 -x,y,-z+1/2

8. DFT Calculations

All density functional theory analyses were performed using Gaussian 16 revision A.03. All calculations employed the unrestricted b3lyp functional, a triple ζ basis set for Co and N (def2tzvpp), and a double ζ basis set for C and H (def2svp). A full structural model of **1³⁺** was analyzed along with a truncated model in which the flanking pyridyl groups were replaced by aminomethyls (H_2NCH_2^-). Both models provided similar results, so the **1²⁺** and **1⁺** states were analyzed only as truncated models. The metal-ligand antiferromagnetic coupling in **1³⁺** and **1²⁺** was evaluated by first optimizing these structures in higher spin-states than indicated experimentally, followed by locating lower-spin wavefunctions starting from an initial guess featuring a localized ligand π^* electron of opposite spin to that of the metal. The resulting broken symmetry wavefunctions lower the electronic energy of the DFT models and provide good agreement with experimental data, supporting the accuracy of these results. Mulliken and NBO population analyses were performed to evaluate the spin state and 3d orbital occupancies of cobalt. Details specific to each structure are provided here:

1³⁺-DFT. Starting from the solid-state geometry of **1⁴⁺**, the structure of **1³⁺** was optimized in S = 1 and S = 2 states, finding electronic configurations consisting of a ligand-centered radical that is spin-aligned with either a low-spin (for S = 1) or high-spin (for S = 2) Co^{II} center. Analytical frequency calculations confirmed that both structures are local minima. The S = 2 state has Co—N distances, pyridine-pyridinium C—C distances, and pyridine-pyridinium torsion angles that are consistent with those of the solid-state structure of **1³⁺•3PF₆**. In contrast, low-spin Co^{II} imparts a Jahn-Teller distortion on the Co—N distances calculated for the S = 1 state, which is inconsistent with experimental observations. The S = 2 state was found to be 4.27 kcal/mol lower in energy than the S = 1 state. A new S = 1 wavefunction was then calculated at the S = 2 geometry, in this case with the ligand π^* electron coupled antiferromagnetically to the high spin Co^{II} center, lowering the electronic energy by 2.52 kcal/mol relative to the S = 2 state. In this final wavefunction determined for **1³⁺-DFT**, a Mulliken spin-density of 2.658 was determined for cobalt, and NPA analysis found a valance 3d occupancy of 7.33 e⁻, both corresponding to a Co^{II} description. This antiferromagnetically-coupled S = 1 model provides good agreement with the solid-state structure and solution-phase characterization of **1³⁺**, though the π^* electron is fully delocalized in **1³⁺-DFT**, suggesting electronic coupling is slightly overestimated relative to that determined by spectral analysis of **1³⁺** in MeCN. Thus, the model **1³⁺-DFT** corresponds best to the symmetric solid-state structure of **1³⁺**. A truncated model with the flanking pyridyl groups of the ligands replaced by aminomethyl groups was also examined, finding a geometry and electronic structure in good agreement with the full model.

1²⁺-DFT. A truncated model structure for **1²⁺** was constructed by replacing the flanking pyridyl groups of the optimized **1³⁺-DFT** structure with aminomethyl groups. This structure was then optimized in an $S = 2.5$ state, resulting in the flattening of the pyridine-pyridinium dihedral angles and a symmetric shortening of the pyridine-pyridinium C—C bonds to a length consistent with reduction by 1e⁻ each. Analytical frequency calculations confirmed that the resulting geometry is a local minimum. An $S = 1.5$ wavefunction was then located in which π^* electrons on each ligand have opposite spins to each other, allowing one to couple antiferromagnetically to the high-spin Co^{II} center. This wavefunction was found to be 2.33 kcal/mol more stable than the optimized $S = 2.5$ state. A Mulliken spin-density of 2.689 was determined for cobalt, and NPA analysis found a valance 3d occupancy of 7.32 e⁻, thus maintaining a Co^{II} description essentially identical to that of **1³⁺-DFT**. Notably, the final $S = 1.5$ state of **1²⁺-DFT** has closely spaced LUMO and LUMO+1 orbitals (see Figure S34 below), consistent with the two distinct NIR absorptions observed experimentally for **1²⁺** (see Figure S17). Thus, this DFT model appears to provide an accurate electronic depiction of **1²⁺**.

1⁺-DFT. The optimized structure of **1²⁺-DFT** was used as a starting point for a truncated model of **1⁺**. Optimization of **1⁺** in an $S = 2$ state provided a geometry in which the ligands feature symmetrically shortened pyridine-pyridinium C—C bonds. Analytical frequency calculations confirmed that the resulting geometry is a local minimum. There are two π^* electrons located entirely on the ligands with their spins aligned with cobalt, while an electron of the opposite spin is delocalized fully across ligand π^* and cobalt 3d orbitals (see Figure S35 below). A large 3d contribution to this latter orbital provides considerable Co^I character to **1^{+-DFT}**. Likewise, a Mulliken spin-density of 2.383 on cobalt and a valance 3d occupancy of 7.62 e⁻ (the latter from NPA analysis) show reduction of the cobalt center in **1^{+-DFT}** relative to **1^{3+-DFT}** and **1^{2+-DFT}**, providing considerable Co^I character in **1^{+-DFT}**. These findings were validated by comparison with a solid-state structure determined for **1^{+-PF₆}**. The experimentally determined structure will be disclosed fully in a future report, but the salient features are its similarly shortened pyridine-pyridinium C—C bonds (1.412(2) and 1.424(2) Å) indicating nearly symmetric reduction of the ligands. Furthermore, these bonds are shortened only a small amount relative to those in **1^{3+-3PF₆}**, indicating that the metal must accept some electron density upon reduction to the **1⁺** state. Thus, like the models **1^{3+-DFT}** and **1^{2+-DFT}**, the accuracy of **1^{+-DFT}** is supported experimentally.

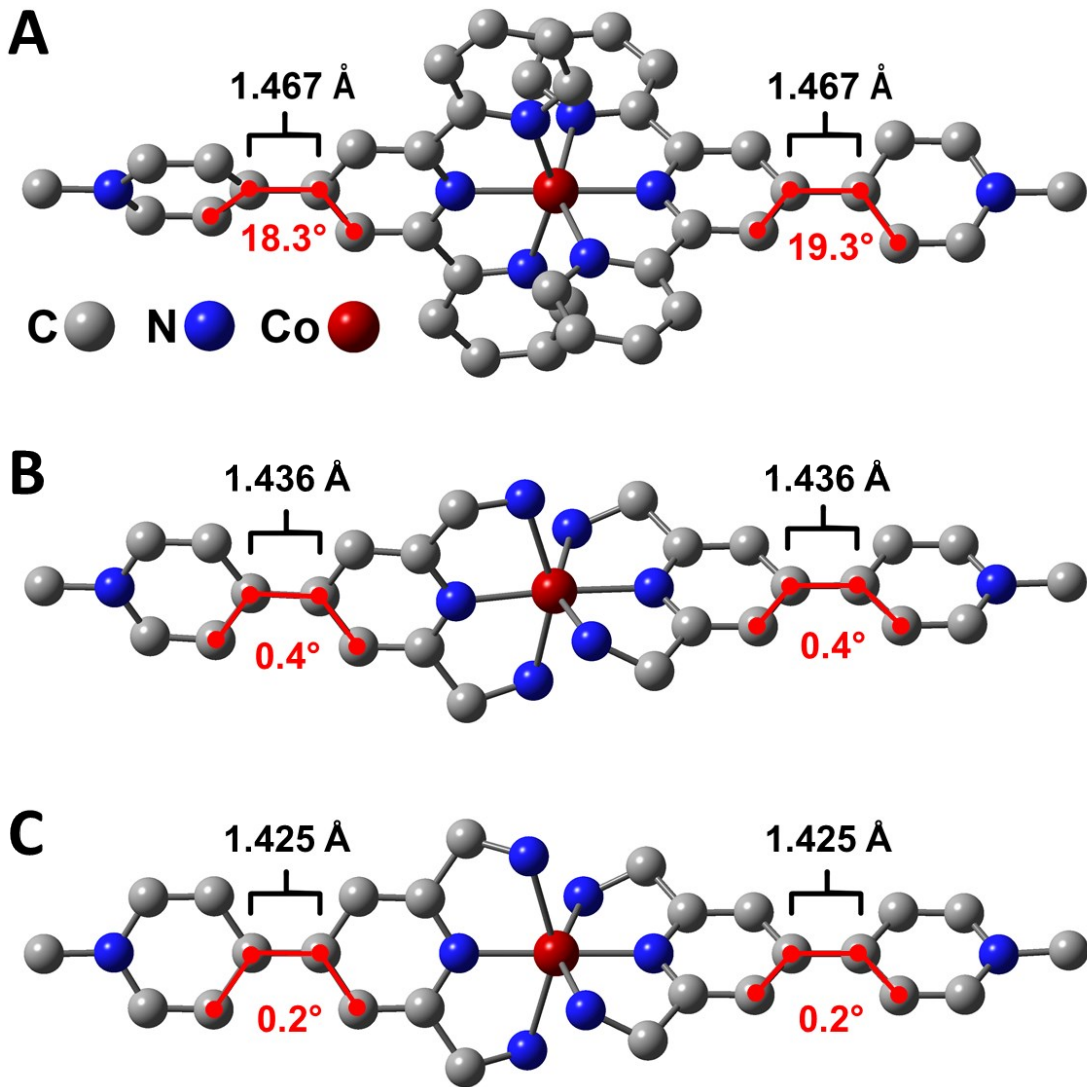


Figure S32. Computationally optimized structures of **1ⁿ⁺-DFT** with the pyridine-pyridinium C—C bond distances and dihedral angles labeled to illustrate the degree of reduction of the ligands. (A) **1³⁺-DFT**. The bond distances and dihedral angles in this model structure are consistent with symmetric partial reduction of the ligands as indicated experimentally in the solid state. However, the bond lengths and dihedral angles in the computational model are somewhat larger than those found in the solid-state of **1³⁺•3PF₆**, which is attributed to packing forces in the solid state. (B) **1²⁺-DFT**. The shortened C—C distances and flattened dihedral angles indicate symmetric reduction of the ligands by 1e⁻ each, as expected in this non-mixed valent state. (C) **1⁺-DFT**. The C—C distances are not shortened much relative to the 2+ state because the metal center accepts considerable electron density upon reduction to the 1+ state. These structural features are validated in an experimentally determined solid-state structure of **1⁺•PF₆**, which will be described in detail in a future report.

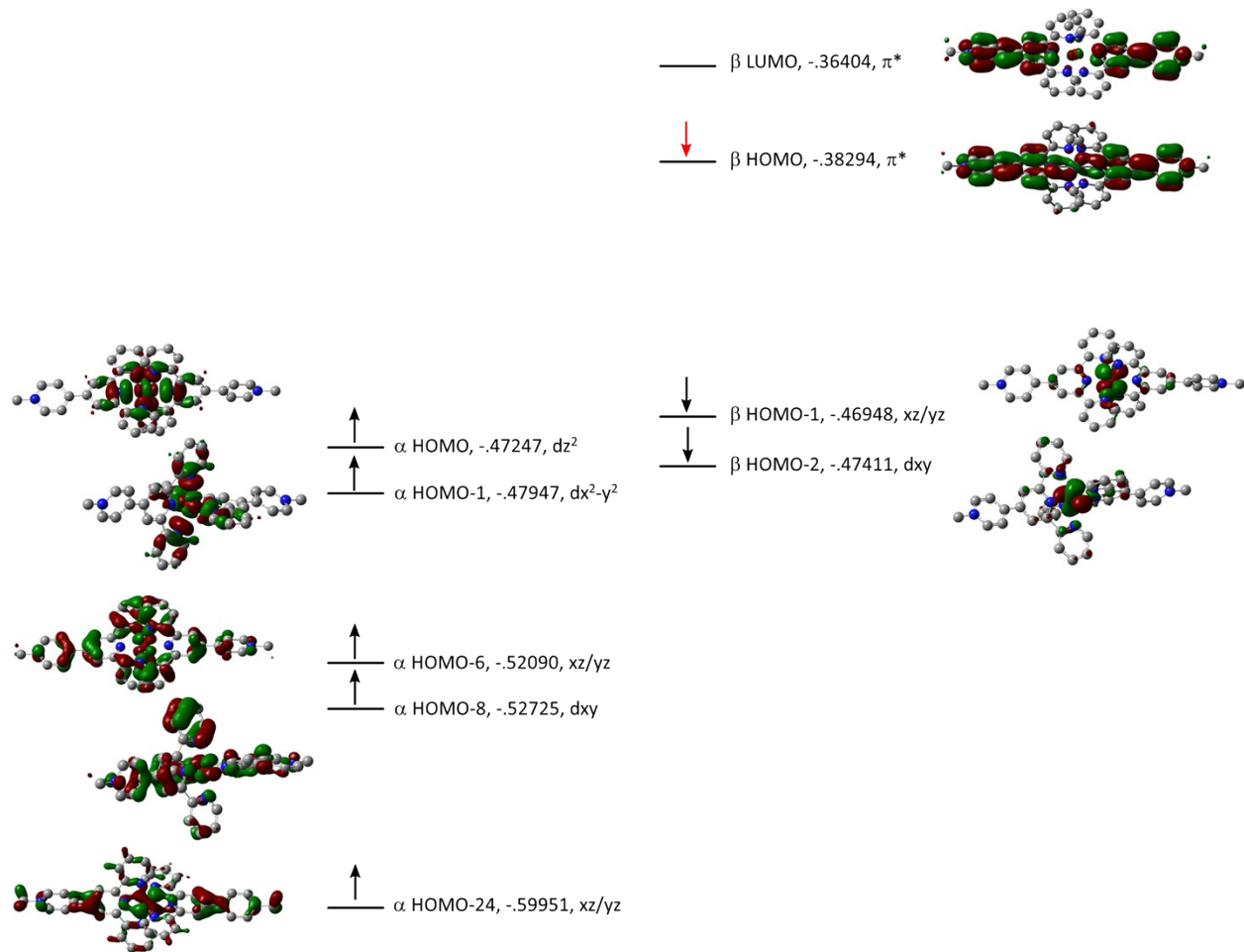


Figure S33. Representative canonical orbitals of **1³⁺-DFT** illustrating the cobalt 3d and ligand π^* orbital occupancies. Orbitals are plotted with a surface isovalue of 0.025, and orbital energies are provided in Hartrees. The labels dz^2 , dx^2-y^2 , dxy , and xz/yz indicate the main 3d contribution to the orbitals with significant cobalt 3d parentage (note: xz/yz indicates a substantial mix of both dxz and dyz character). The label π^* is used to indicate orbitals of net π -antibonding character within the ligands. Electrons indicated with red arrows are not present in the **1⁴⁺** state. The β HOMO is a singly occupied π^* orbital that is delocalized across both ligands with a small contribution from a cobalt 3d orbital. The β LUMO is a π^* orbital with a small energy separation from the β HOMO, consistent with the observation of a low energy IVCT band in the electronic absorption spectrum of **1³⁺**.

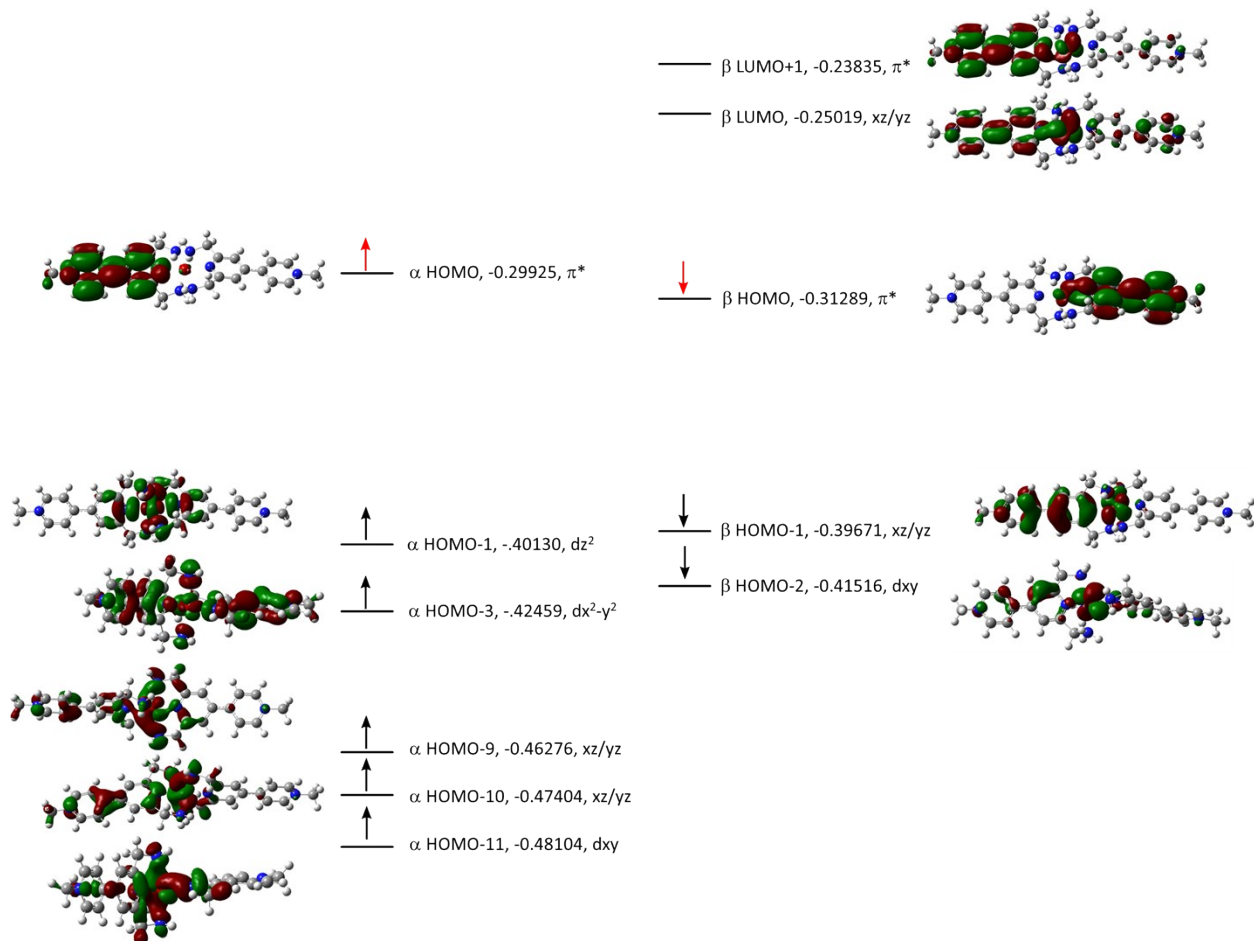


Figure S34. Representative canonical orbitals of **1²⁺-DFT** illustrating the cobalt 3d and ligand π^* orbital occupancies. Orbitals are plotted with a surface isovalue of 0.025, and orbital energies are provided in Hartrees. The labels dz^2 , dx^2-y^2 , dxy , and xz/yz indicate the main 3d contribution to the orbitals with significant cobalt 3d parentage (note: xz/yz indicates a substantial mix of both dxz and dyz character). The label π^* is used to indicate orbitals of net π -antibonding character within the ligands. Electrons indicated with red arrows are not present in the **1⁴⁺** state. The highest occupied α and β molecular orbitals are π^* orbitals that are each localized on a different ligand, with the β HOMO including a small cobalt 3d contribution. The β LUMO and β LUMO+1 both comprise mixtures of π^* and cobalt 3d character. These two orbitals are similar in energy, consistent with the observation of two overlapping NIR bands in the electronic absorption spectra of **1²⁺**.

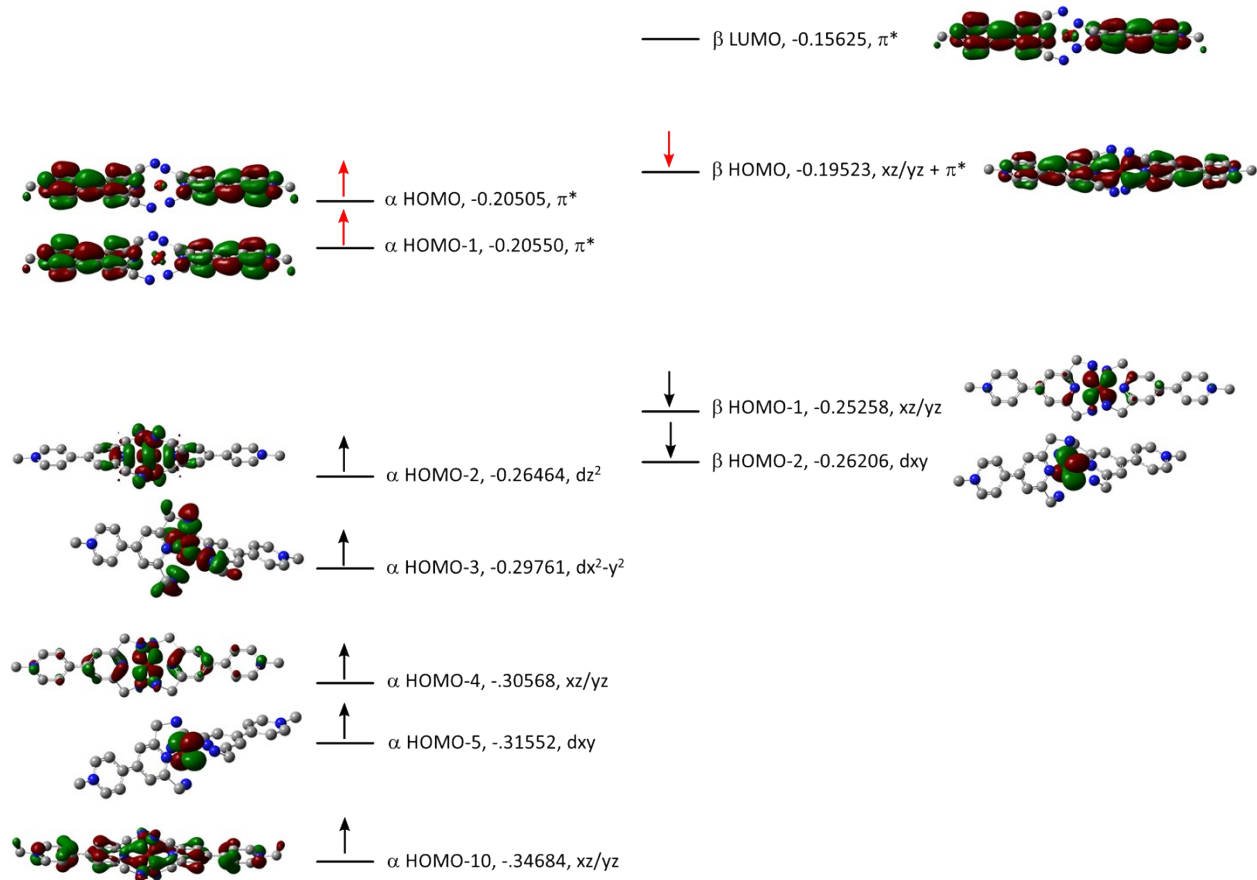


Figure S35. Representative canonical orbitals of **1⁺-DFT** illustrating the cobalt 3d and ligand π^* orbital occupancies. Orbitals are plotted with a surface isovalue of 0.025, and orbital energies are provided in Hartrees. The labels dz^2 , dx^2-y^2 , dxy , and xz/yz indicate the main 3d contribution to orbitals of significant cobalt 3d parentage (note: xz/yz indicates a substantial mix of both dxz and dyz character). The label π^* is used to indicate orbitals of net π -antibonding character within the ligands. Electrons indicated with red arrows are not present in the **1⁴⁺** state. The α HOMO is a π^* orbital, but the β HOMO mixes considerable cobalt 3d character with the ligand π^* orbitals, providing increased Co^l character to **1^{+-DFT}**. The β LUMO is a ligand π^* orbital, suggesting that the experimentally observed NIR absorption has metal-to-ligand charge-transfer character.

9. References

- (1) M. Kobayashi, S. Masaoka and K. Sakai, *Dalton Trans.*, 2012, **41**, 4903–4911.
- (2) J. Wang, G. S. Hanan, *Synlett*, 2005, **8**, 1251–1254.
- (3) E. C. Constable,; C.E. Housecroft, M. Neuburger, D. Phillips, P.R. Raithby, E. Schofield, E. Sparr, D.A Tocher, M. Zehnder, and Y. Zimmermann, *J. Chem. Soc., Dalton Trans.* 2000, **13**, 2219–2228.
- (4) E.C. Constable, C.E. Housecroft, T. Kulke, C. Lazzarini, E.R. Schofield, and Y. Zimmermann, *J. Chem. Soc., Dalton Trans.*, 2001, 2864–2871.
- (5) R. Nicholson, *Anal. Chem.*, 1965, **37**, 1351-1355.
- (6) H. J. Paul and J. Leddy, *Anal. Chem.*, 1995, **67**, 1661–1668.
- (7) T. M. Powers, JoVE Science Education Database. Inorganic Chemistry. J. Vis. Exp. 2017
- (8) D.G. Kurth, J.P Lopez, and W.F. Dong, *Chem. Commun.* 2005, 2119-2121.
- (9) G. M. Sheldrick, *SADABS*. Version 2.03., University of Göttingen, Germany, 1997.
- (10) G. M. Sheldrick, *SHELXL97*., University of Göttingen, Germany, 1997.
- (11) G. M. Sheldrick, *SHELXTL*. Version 6.10., Bruker AXS Inc., Madison, WI, 2000.